NASA CONTRACTOR REPORT

NASA CR-505

NASA CR-505

STUDIES IN PRESTRESSED AND SEGMENTED BRITTLE STRUCTURES

by Ralph L. Barnett and Paul C. Hermann

Prepared by
IIT RESEARCH INSTITUTE
Chicago, Ill.
for

NATIONAL AERONAUTICS AND SPACE ADMINISTRATION • WASHINGTON, D. C. • JUNE 1966

NASA CR-505

STUDIES IN PRESTRESSED AND SEGMENTED BRITTLE STRUCTURES

By Ralph L. Barnett and Paul C. Hermann

Prepared under Contract No. NASr-65(04) by
IIT RESEARCH INSTITUTE
Chicago, Ill.

for

NATIONAL AERONAUTICS AND SPACE ADMINISTRATION

For sale by the Clearinghouse for Federal Scientific and Technical Information
Springfield, Virginia 22151 – Price $4.00

CONTENTS

CONTENTS (CONT'D)

ILLUSTRATIONS

ILLUSTRATIONS (Cont'd)

TABLES

STUDIES IN PRESTRESSED AND SEGMENTED BRITTLE STRUCTURES

by Ralph L. Barnett and Paul C. Hermann

SUMMARY

A nonlinear theory describing the response of rectangular prestressed segmented beams is verified experimentally. The applicability of the theory is extended to beam-columns and to I-beams with multiple tendons. The methods of limit analysis are used to predict the ultimate load carrying capacity of prestressed and segmented beams and plates. A statistical hypothesis is developed and verified for scaling the behavior of different height nonflat segmented columns. Finally, the feasibility of prestressing cylindrical and ogive shells is investigated and evidence is obtained which demonstrates the practicality of overwinding as a prestressing technique.

I. INTRODUCTION

To realize the considerable potential of ceramics and cermets in high performance structures it is necessary to circumvent the problems which attend brittleness and small section size. One approach to this problem utilizes the techniques of prestressing and segmenting, and indeed, the principal objective of this program is to study these techniques for their possible employment in aerospace applications. Specifically, our goal has been the development of an analytical capability for predicting the behavior of prestressed monolithic and segmented brittle structures from a knowledge of the behavior of their component elements.

In the first phase of the program, three fundamental problems were considered (ref. 1)*. The first of these dealt with the development of transverse tensile stress in a segmented column under axial compressive loading. The second, involved the prediction of the nonlinear response of a prestressed segmented beam.

*References listed at the end of text.

The last concerned itself with the benefits which accrue from prestressing a monolithic brittle element. We shall briefly review the highlights of this first effort.

A. Summary of Previous efforts

1. Transverse cracking phenomenon. - Cracking in a direction transverse to a uniaxial compressive load was first recognized by F. R. Shanley to be a major deterrent to the application of prestressing to segmented members. In 1957, the authors conducted a study of minimum weight deflection design for prestressed segmented beams in which the roughness of the segment interfaces played a predominant role. Based on this background, it was hypothesized that the interface roughness causes transverse cracking. To support this view the following evidence was established.

(1) The slope of the compressive stress-strain diagram of a segmented column increases with increasing stress. This is caused by the fact that the contact area increases with axial load and hence the stiffness correspondingly increases.

(2) Column strength increases with increasing flatness.

(3) Specimens increase in compressive strength with decreasing cross sectional area.

(4) Internal transverse crack lenses can be observed in glass columns (2x4x1/2 inches).

(5) Photoelastic and two-dimensional elasticity results indicate that an uneven load distribution on a segment will cause internal tensile stresses in directions parallel to the interfaces.

(6) Triaxial compressive tests indicate a very substantial increase in axial strength when a lateral prestress is imposed.

2. Load-deflection characteristics of prestressed segmented beams. - Two quite different mathematical models were developed to describe the nonlinear response of prestressed segmented beams with perfectly flat interfaces. The statistical nature of the nonflat interface problem was identified and its implication to both bending and column behavior was described. Load-deflection diagrams were experimentally obtained for segmented glass beams using several levels of prestress. The general characteristics of these diagrams are illustrated in Figure 1-a where we can identify a linear and a nonlinear region. The rough interfaces of the glass segments precluded a deterministic prediction of the linear portion of the curve; however, when our "perfect interface" models were modified to reflect the proper linear behavior, the nonlinear region was predicted with remarkable precision.

3. Strength of prestressed monolithic brittle beams. - Applying Weibull's statistical fracture theory, it was possible to theoretically establish for simple beams a relationship among prestress level, reliability, loading, member geometry, and material properties. A specific example was treated in which the prestress results in a 25-fold increase in ultimate capacity over a conventional beam of equal weight and reliability. The general characteristics of the load-deflection diagrams for such members are illustrated in Figure 1-b where we observe the influence of both deterministic and statistical phenomena.

B. Summary of Current Accomplishments

The bending theory previously formulated for prestressed segmented beams with perfectly flat interfaces was verified by carefully performed experiments on a segmented tungsten carbide beam. The segment interfaces for this rectangular member were no more than one half lightband out of flat. Having placed the theory on a solid foundation, a computer program was written to extend our analysis capability to I-beams and box beams with multiple tendon arrangements. The applicability of limit analysis theory for predicting the ultimate load carrying capacity of prestressed segmented beams was demonstrated by tests conducted on a 16-foot tubular alumina beam with a thin wall circular cross section.

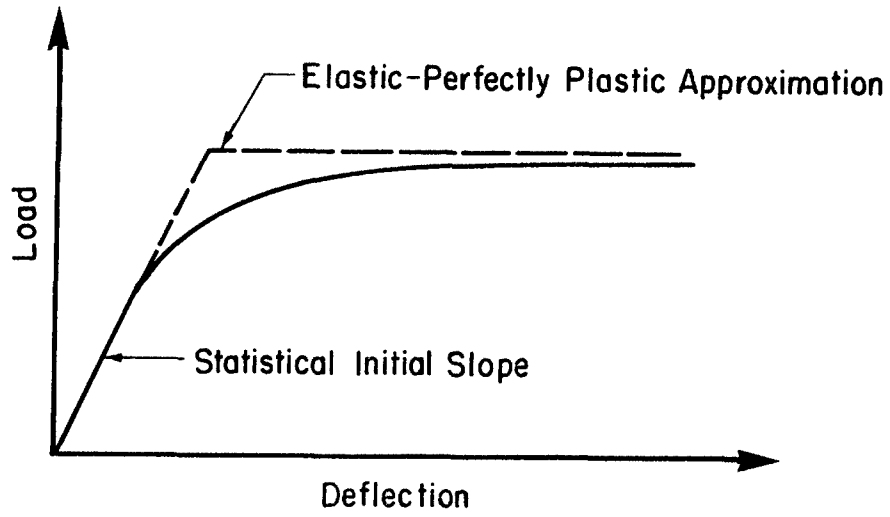

Figure 1-a Prestressed Segmented Bending Behavior

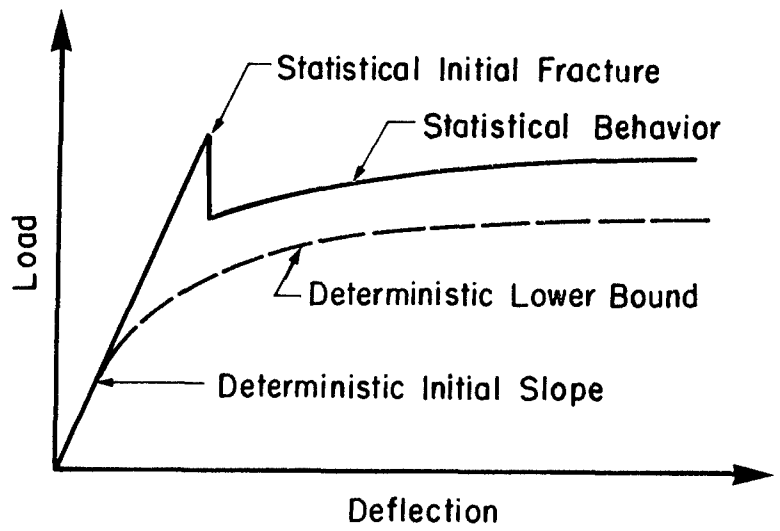

Figure 1-b Prestressed Monolithic Bending Behavior

Monolithic Hydrostone plaster beams were used to accumulate statistical data on the "initial fracture" strength of beam-columns. Weibull's statistical fracture theory provided a satisfactory description of the measured behavior.

Starting with the bending theory for perfectly flat segmented beams, it was possible to describe the behavior of perfect segmented beam-columns under eccentric axial loads. The buckling load of a perfect segmented column was shown to be equal to the classical Euler load. A statistical theory was proposed for scaling the compressive stress-strain diagrams of different height segmented columns with nonflat interfaces. Data obtained for various size segmented glass columns supported our hypothesis that the stiffness distribution is normal and scales as the "distribution of the mean". A brief investigation into the behavior of nonprismatic segmented columns indicated that cracks are not necessarily arrested at segment interfaces. Furthermore, the results of tests on short plaster backbone columns suggest that nature may prefer the prismatic column.

The theory of limit analysis was applied to prestressed segmented circular plates and the resulting predictions agreed closely with results obtained from preliminary experiments performed on Hydrostone plaster disks. Theoretically, this theory provides a lower bound to the strength of monolithic prestressed brittle plates and tests conducted on such elements support this prediction.

Finally, preliminary studies were conducted with prestressed cylindrical and ogive shells. The technique of overwinding was shown to be an effective method for applying a prestressing force over an extended area. The first experiments with segmented plaster ogive shells seemed to indicate that the interface roughness problem may be of critical concern.

C. Acknowledgments

The diversified nature of this program required the specialized talents of many people. The authors would like to acknowledge the important technical contributions made by K. E. Hofer and J. R. Wingfield in the area of experimental mechanics, by J. F. Costello in the field of statistical fracture theory, L. A. Bertram in the area of computer technology, and by K. L. Cole in the area of filament winding.

II. PRESTRESSED BEAMS

A number of fundamental investigations involving prestressed monolithic and segmented beams are described in this section. Specifically, the theory of perfect segmented beams (absolutely flat interfaces) presented in our first report is verified experimentally. This theory is applied to prismatic I-beams or box beams with multiple elastic tendons and a computer program is presented for establishing the load-deflection diagrams for such members. The possibility of using limit analysis methods to establish the load-carrying capacity of segmented beams is briefly exploited with the aid of a 16-foot aluminum oxide segmented circular tube. Finally, the ultimate capacities of prestressed monolithic hydrostone plaster beams are measured and compared to predictions derived from a statistical formulation of the problem that uses a beam-column analysis together with the Weibull distribution function.

A. Nonlinear Bending Theory

1. Theory of perfect segmented beams. - In our first report two different mathematical models were developed to account for the segment separation which occurs during the bending of a segmented beam (ref. 1). The first of these, the incremental model shown in Figure 2a considers the beam at some instant during the loading process. At this instant the beam is in equilibrium with the applied moment $M(x)$, and in general, cracks will have penetrated into the beam section for some distance along the segment interfaces. The relationship between crack penetration and the bending moment at a station along the beam is established in a straightforward manner from moment equilibrium. If an additional infinitesimal moment $\delta M(x)$ is added to this beam, the resulting infinitesimal response can be calculated as the linear response of the uncracked beam section. The total live load deflection is then found by summing all such infinitesimal responses which occur between $M(x) = 0$ and $M(x) = M(x)\big|_{\text{final}}$.

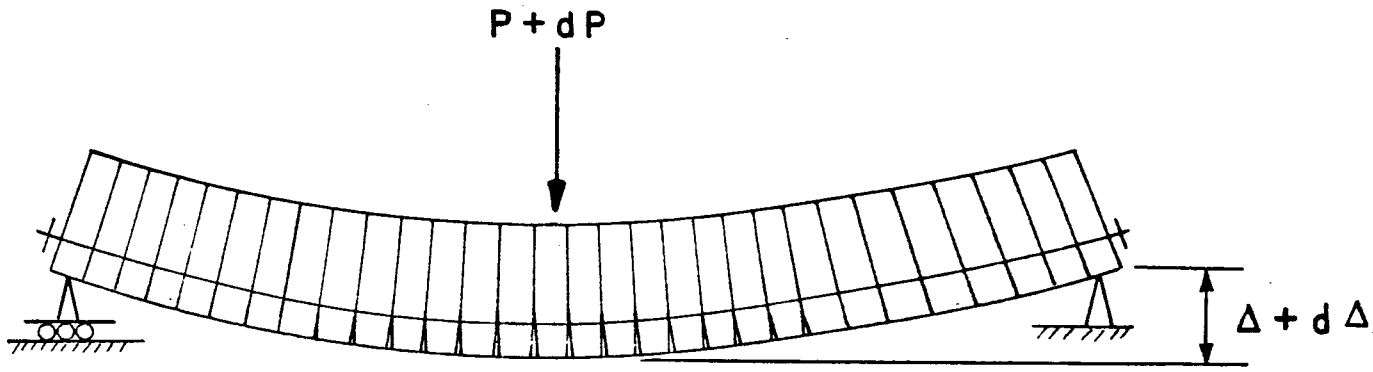

(a) Incremental Model

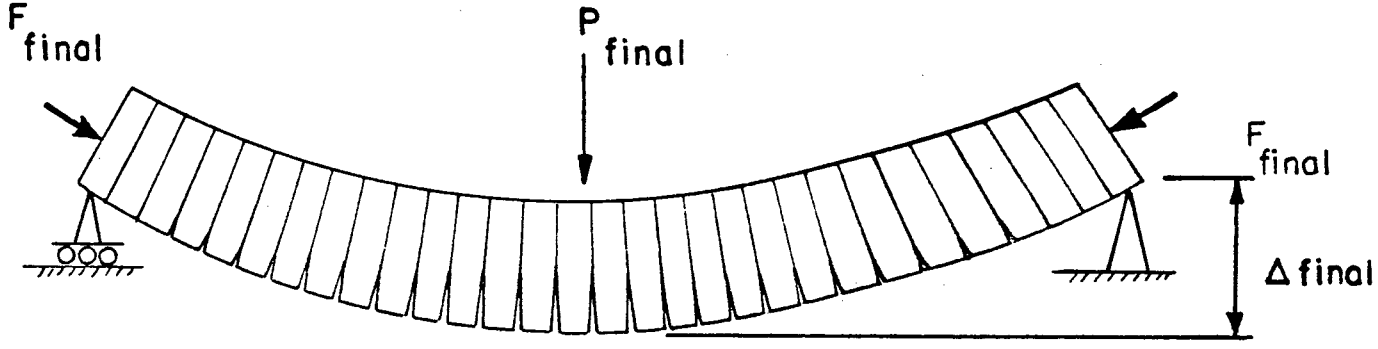

(b) Equilibrium Model

Figure 2 Mathematical Models for Bending Response

In the second model, the equilibrium model shown in Figure 2b, the beam is considered in its final loading state. The portion of the beam which is uncracked is considered to be an elastic beam under the external loading $M(x)$ and the internal loading caused by the prestressing. Since the deflection of an elastic beam can be uniquely determined for every loading, the deflection of the entire beam can be viewed as the deflection of the uncracked portion.

Since the general demonstration of the equivalence of these models was not attempted in our previous study, we shall deal with this problem here.

2. Equivalence of the two models. - In the postulation of both the "incremental" and "equilibrium" models, it was assumed that: (1) the segment material is linearly elastic up to its ultimate compressive strength, (2) the interfaces are absolutely flat, (3) the tendons are constrained to deflect with the segments (eliminating any beam-column action), (4) the number of segments is infinite, and (5) the resultant prestressing force is located within the section kern (precluding the existence of tensile bending stresses and hence, cracking under zero external load). Also, for the sake of simplicity, the equivalence of the two models will be demonstrated for the case of rectangular cross section and zero stiffness tendons.

Both models are identical as long as the beam is completely uncracked. In the cracked region, the incremental method leads to the following expression for the deflection

$$\Delta = \Delta_c + \int_{P_c}^{P} \frac{d\Delta_k}{dP} \, dP \qquad (1)$$

where the applied bending moment distribution, $M(x)$, has been represented by $Pg(x)$, P being the maximum applied bending moment,

and where Δ_c is the cracking deflection, P_c is the cracking moment, and

$$\frac{d\Delta_k}{dP} = \int_S \frac{mg(x)}{EI} dx + \int_{S_c} \frac{mg(x)}{EI_c} dx \qquad (2)$$

and where S and S_c are respectively uncracked and cracked portions of the beam and are functions of P. In the cracked region, the equilibrium model leads to following expression

$$\Delta = \int_S \frac{Tm}{EI} dx + \int_{S_c} \frac{Tm}{EI_c} dx \qquad (3)$$

where T is the resulting moment acting on a cross section.

The fact that these two models are indentical will be demonstrated by showing that

$$\frac{d\Delta}{dP} = \frac{d\Delta_k}{dP} \qquad (4)$$

Without loss of generality, temporarily assume that $S(P)$ is the interval 0 to $a(P)$ and that $S_c(P)$ is the interval $a(P)$ to L.

Then for Equation (3)

$$\frac{d\Delta}{dP} = \frac{d}{dP}\int_0^{a(P)} \frac{Tm}{EI} dx + \frac{d}{dP} \int_{a(P)}^{L} \frac{Tm}{EI_c} dx \qquad (5)$$

Thus

$$\frac{d\Delta}{dP} = \int_0^{a(P)} \frac{m}{EI}\frac{dT}{dP}\,dx - \left|\frac{Tm}{EI}\right|_{x=0}\cdot 0 + \left|\frac{Tm}{EI}\right|_{x=a(P)}\frac{da}{dP}$$

$$+ \int_{a(P)}^{0} \frac{m}{E}\frac{d}{dP}\left(\frac{T}{I_c}\right)dx - \left|\frac{Tm}{EI_c}\right|_{x=a(P)}\frac{da}{dP} + \left|\frac{Tm}{EI_c}\right|_{x=L}\cdot 0$$

and since at $x = a(P)$, $I_c = I$, we have

$$\frac{d\Delta}{dP} = \int_0^{a(P)} \frac{m}{EI}\frac{dT}{dP}\,dx + \int_{a(P)}^{L} \frac{m}{E}\frac{d}{dP}\left(\frac{T}{I_c}\right)dx$$

or more generally

$$\frac{d\Delta}{dP} = \int_S \frac{m}{EI}\frac{dT}{dP}\,dx + \int_{S_c} \frac{m}{E}\frac{d}{dP}\left(\frac{T}{I_c}\right)dx \qquad (6)$$

For rectangular cross section we have

$$I = \frac{bd^3}{12}$$

$$I_c = 18\,b\left(\frac{T}{F}\right)^3 \qquad (7)$$

$$T = Pg(x) - Fe \text{ in } S$$

$$T = \frac{1}{2}\left[F\left(e+\frac{d}{2}\right) - Pg(x)\right] \text{ in } S_c$$

Thus, using Equation (7),

$$\text{in } S: \quad \frac{dT}{dP} = g(x)$$
$$\text{in } S_c: \quad \frac{d}{dP}\left(\frac{T}{I_c}\right) = \frac{g(x)}{I_c} \qquad (8)$$

Inserting Equation (8) into Equation (6) we have completed the proof, i.e.

$$\frac{d\Delta}{dP} = \frac{d\Delta_k}{dP} = \int_S \frac{mg(x)}{EI}\,dx + \int_{S_c} \frac{mg(x)}{EI_c}\,dx \qquad (9)$$

3. General relationships for multiple tendons. -

a. Arbitrary cross section: The most general relationships holding for any cross sectional geometry and/or any number of elastic tendons, will now be described. If F^i is the force in the i^{th} tendon located e_i from the uncracked neutral axis, Figure 3 , and M is the applied moment, then the resultant moment acting upon the cross section is

$$T = M - \sum_{i=1}^{n} F^i Q_i \qquad (10)$$

where

$$Q_i = e_i + f - q + \bar{x} \qquad (11)$$

and where n is the total number of tendons.

Define

$$F = \sum_{i=1}^{n} F^i \qquad (12)$$

and

$$e = \frac{\sum_{i=1}^{n} F_o{}^i e_i}{F_o} \qquad (13)$$

Using Equations (11), (12), and (13), Equation (10) may be written as

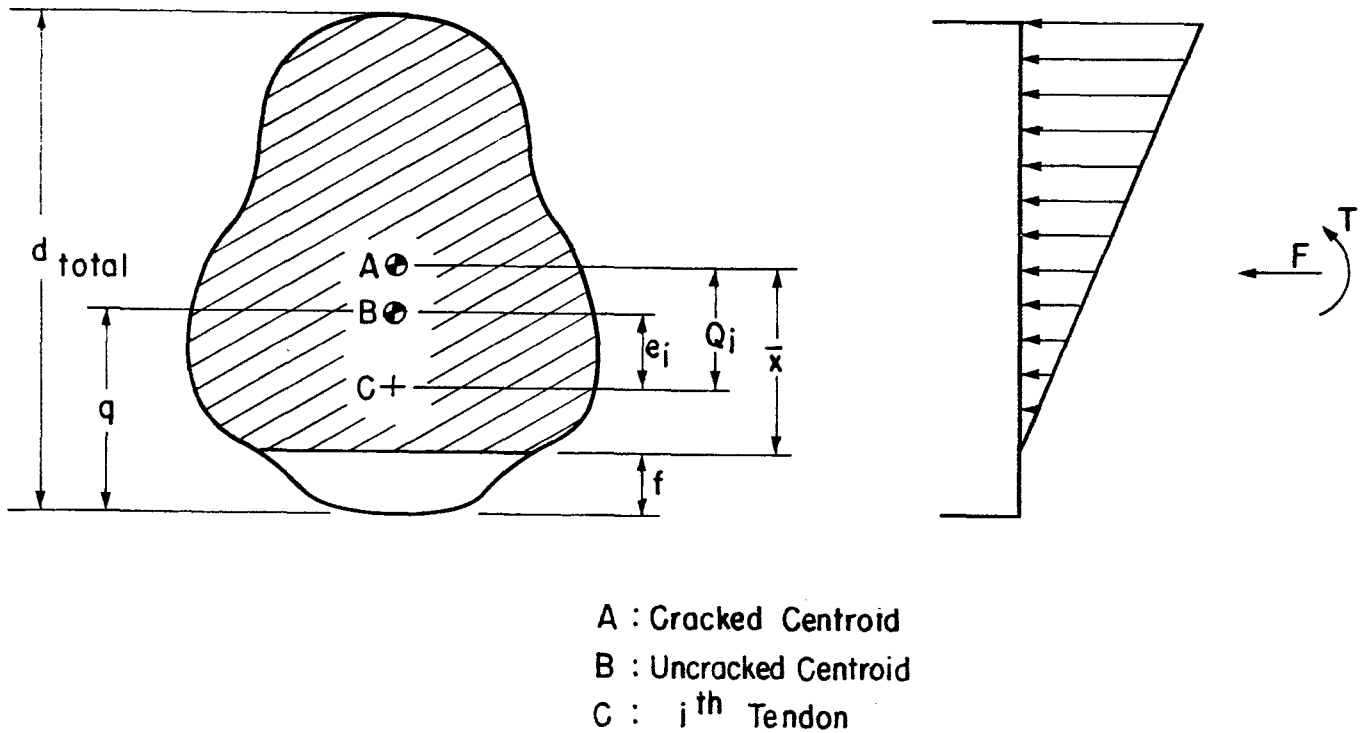

Figure 3 Geometry of Arbitrary Cross Section

$$T = M - F\,(e + f - q + \bar{x}) - \sum_{i=1}^{n} F^i\,(e_i - e) \qquad (14)$$

If we further define

$$M_T = \sum_{i=1}^{n} F^i\,(e_i - e) \qquad (15)$$

Then the expression for the resultant moment becomes

$$T = M - F\,(e + f - q + \bar{x}) - M_T \qquad (16)$$

As they have been defined, e represents the effective eccentricity of the initial total prestress F_o and M_T represents the resultant moment due to the effective bending stiffness of the tendons. We note that $M_T = 0$ when $F = F_o$ and also that $M_T = 0$ for the case when all the tendons have the same e_i (equivalent to a single elastic tendon).

In order to determine the crack penetration f we use the fact that the stress is equal to zero at the top of the crack.

$$\sigma_{crack} = 0 = -\frac{F}{A} + \frac{T\,\bar{x}}{I} \qquad (17)$$

Combining Equations (16) and (17) yields

$$\frac{M - M_T}{F} = e + f - q + \bar{x} + \frac{I}{A\bar{x}} \qquad (18)$$

where

$$I = I(f),\ \bar{x} = \bar{x}(f) \quad \text{and} \quad A = A(f).$$

In general (except for the case of rectangular cross section), Equation (18) cannot be solved explicitly for f . In the I-beam computer program it is convenient to define $W = (M - M_T)/F$, tabulate W vs f, and use the table to accomplish inversion and thus obtain $f = f(W)$.

The expressions for deflection and slope are simply

$$\Delta = \int_0^L \frac{Tm_\Delta}{EI}\, dx$$

$$\theta_L = \int_0^L \frac{Tm_L}{EI}\, dx \qquad (19)$$

$$\theta_R = \int_0^L \frac{Tm_R}{EI}\, dx$$

where the virtual moments are

$$m_\Delta = (1 - \frac{x_\Delta}{L})\, x \ , \text{ for } \ 0 \le x \le x_\Delta$$

$$m_\Delta = \frac{x_\Delta}{L}\, (L - x) \ , \text{ for } x_\Delta \le x \le L \qquad (20)$$

$$m_L = (1 - \frac{x}{L})$$

$$m_R = \frac{x}{L}$$

Now

$$\theta_o = \theta_{Lo} = \theta_{Ro} = - \frac{F_o eL}{2EI_o} \qquad (21)$$

where I_o is the uncracked moment of inertia.

The equations for determining the tendon forces are now, for the i^{th} tendon

$$\frac{(F^i - F_o^{\,i})L}{A_t E_t} = \left| Q_i\, (\theta - \theta_o) \right|_{x=0} + \left| Q_i\, (\theta - \theta_o) \right|_{x=L} - \frac{F - F_o}{E} \int_0^L \frac{dx}{A} \qquad (22)$$

where it has been assumed that all the tendons have area A_t and modulus E_t. There are n such relationships, all coupled explicitly by the $F-F_o$ term and implicitly by the other terms, to be solved simultaneously. However, due to the fact that all the tendons

have the same $A_t E_t$, these n equations may be added and solved for $F - F_o$ (although transcendentally):

$$F - F_o = \frac{\left|Q(\theta-\theta_o)\right|_{x=0} + \left|Q(\theta-\theta_o)\right|_{x=L}}{\frac{L}{A_t E_t} + \frac{n}{E}\int_0^L \frac{dx}{A}} \tag{23}$$

where

$$Q = \sum_{i=1}^{n} Q_i \tag{24}$$

Having used Equation (23) to determine $F - F_o$, the individual tendon forces may be found directly from Equation (22).

b. Rectangular cross section: Several of the expressions that were derived in the previous section simplify for the special case of rectangular cross section. In this case, taking $d_{total} = d$ and taking b to be the width, we have the following:

$$\begin{aligned} q &= \frac{d}{2} \\ \bar{x} &= \frac{d-f}{2} \\ A &= b(d-f) \\ I &= \frac{b(d-f)^3}{12} \end{aligned} \tag{25}$$

When these relationships are substituted into Equations (16) and (17) we find that the uncracked portion of the beam, S, corresponds to the condition $M - M_T \leq F(e+d/6)$ and the cracked portion, S_c, to the condition $M - M_T \geq F(e+d/6)$. Furthermore it is determined that

$$\begin{aligned} \text{in S:}\quad F &= 0 \\ T &= M - Fe - M_T \\ A &= A_o = bd \\ I &= I_o = bd^3/12 \end{aligned} \tag{26}$$

and in

$$S_c: \quad f = d - 6\left(\frac{T}{F}\right)$$

$$T = \frac{1}{2}\left[F\left(e + \frac{d}{2}\right) + M_T - M\right]$$

$$A = 6\ b\ \left(\frac{T}{F}\right) \qquad (27)$$

$$I = 18\ b\ \left(\frac{T}{F}\right)^3$$

4. Verification of theory. -

a. Design of experiments: Of the various assumptions entering into the deflection analysis of segmented beams, the most difficult to realize physically is that the segmented interfaces be perfectly flat. The glass beam used in our previous study did not approach this condition and, consequently, it could not be used to verify our proposed theory. In the present investigation we were fortunate to obtain a set of 100 tungsten carbide gage blocks with interfaces that were no more than one-half light band out of flat. As shown in Figure 4, the compression load-deflection diagram for a 18.75-inch column of 1-inch x 2-inch x 1/4-inch blocks is linear down to very low loads and has a slope equal to that of a monolithic tungsten carbide bar, that is, the modulus of elasticity is about 92×10^6 psi.

The selection of extremely flat blocks was the first consideration in the design of our experimental program. To minimize the influence of the small range of nonlinearity in the compression load-deflection diagram at low loads, a high prestressing level (7,000 psi) was chosen for the tungsten carbide beam. Our previous work on glass never exceeded the 1500 psi level. Further, to preclude the possibility that one or several segments exert a disproportionate influence on the overall beam behavior, a terminal couple-end rotation relationship was selected for the response comparisons.

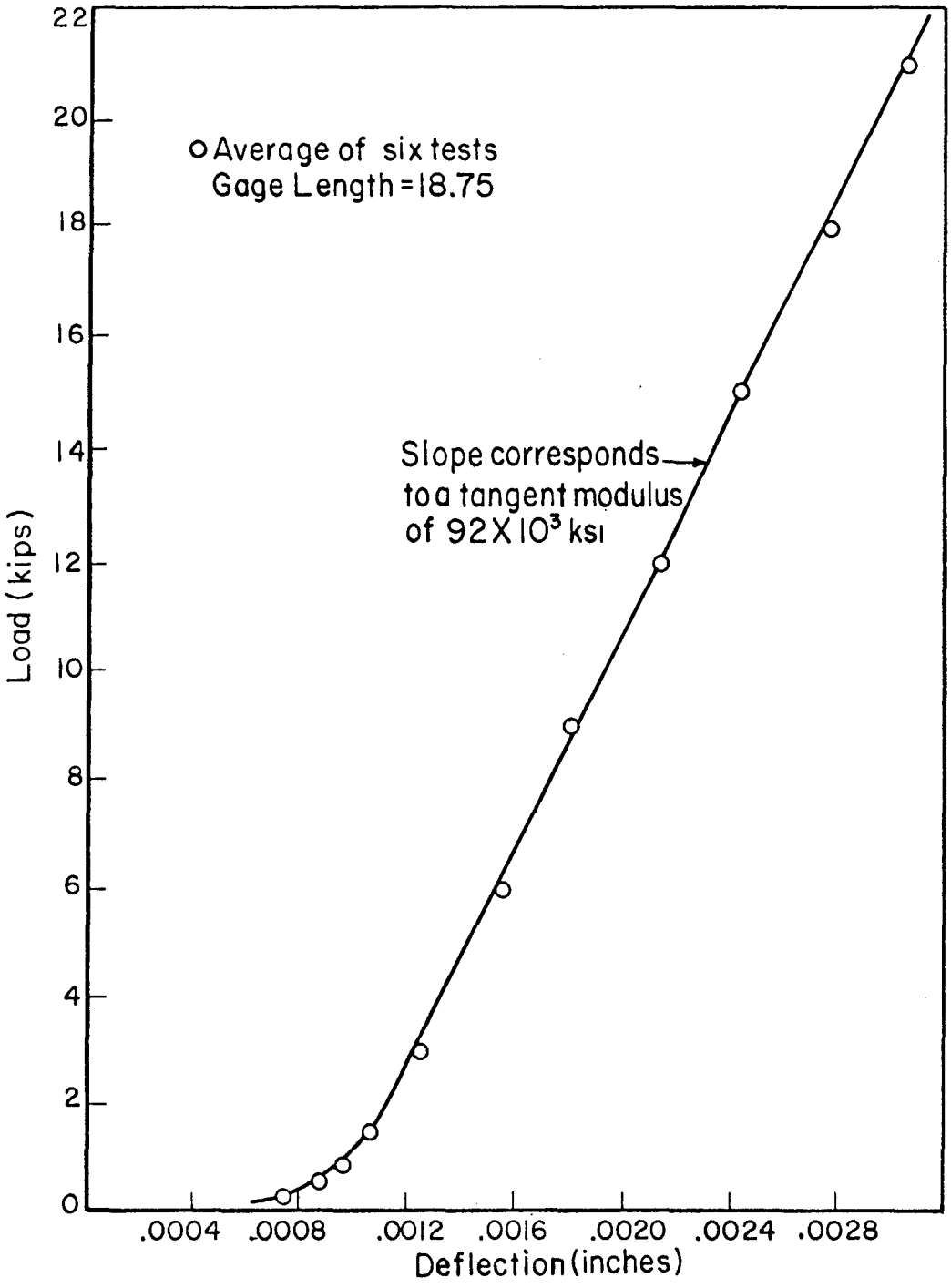

Figure 4 Compression Load-Deflection Diagram for a 18.75 inch Segmented Tungsten Carbide Column

b. Test description: The experimental setup for testing the prestressed and segmented WC beam is illustrated in Figure 5. In order to apply terminal couples to the WC beam, it was necessary to utilize steel extensions at the ends of the beam. Thus, by employing four point loading (all points located on the steel ends) a uniform bending moment distribution was produced in the beam.

The true (tangent) end rotations were not measured. Instead a secant approximation to the end rotations was obtained by measuring the relative deflection of a point 1.06 inches from the assumed end of the beam. In order to measure these deflections, transducers (DCDT's) were suspended from the beam and located on a freely swinging rack, Figure 5. The purpose of the rack was to automatically compensate for any rigid body rotations the beam might experience. The beam was loaded such that it bent concave downwards and thus produced extensions for the DCDT's to measure. The experimental setup was calibrated using a monolithic steel beam.

Pairs of strain gages were attached to each of the tendons to eliminate bending strains. The assembly of the steel ends and the tendons was calibrated in tension to verify the accuracy of the tendon strain gages. Tendon strain gage readings were also recorded during the bending tests for correlation with our elastic tendon theory.

Two slightly different beam configurations were used to obtain data. Details of these two configurations are presented in Figures 6 and 7. Configuration no. 2 is the better one from the point of view of the theory due to its simplicity. However, it has the significant drawback that the amount of preload that could be generated by tightening the nuts on the tendons is limited by the relatively poor threads that were cut on the tendons. Consequently, for all the higher preload levels, resort had to be made to configuration no. 1 which generated the preload by extending the jack screws.

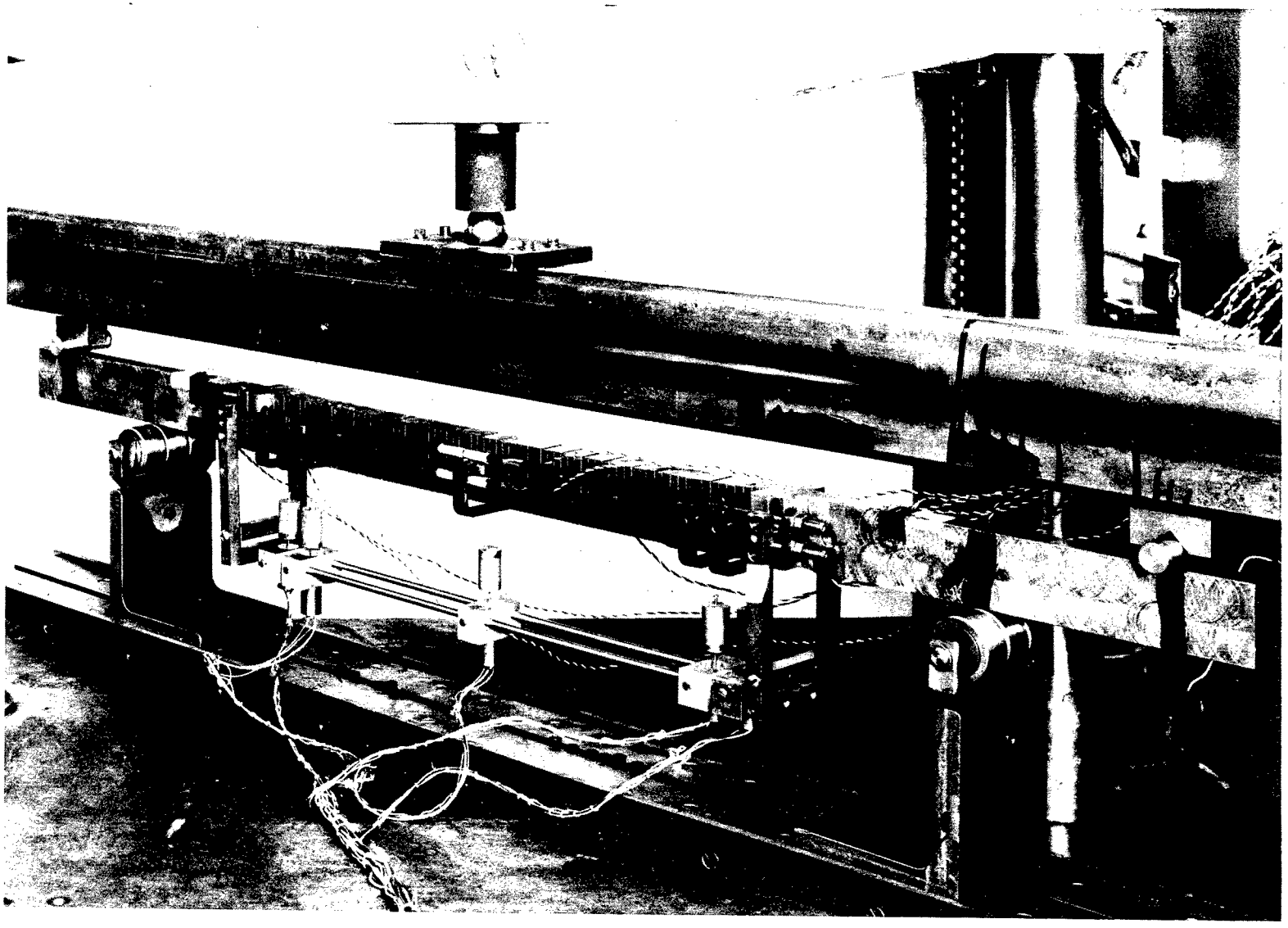

Figure 5 Tungsten Carbide Beam Experimental Setup

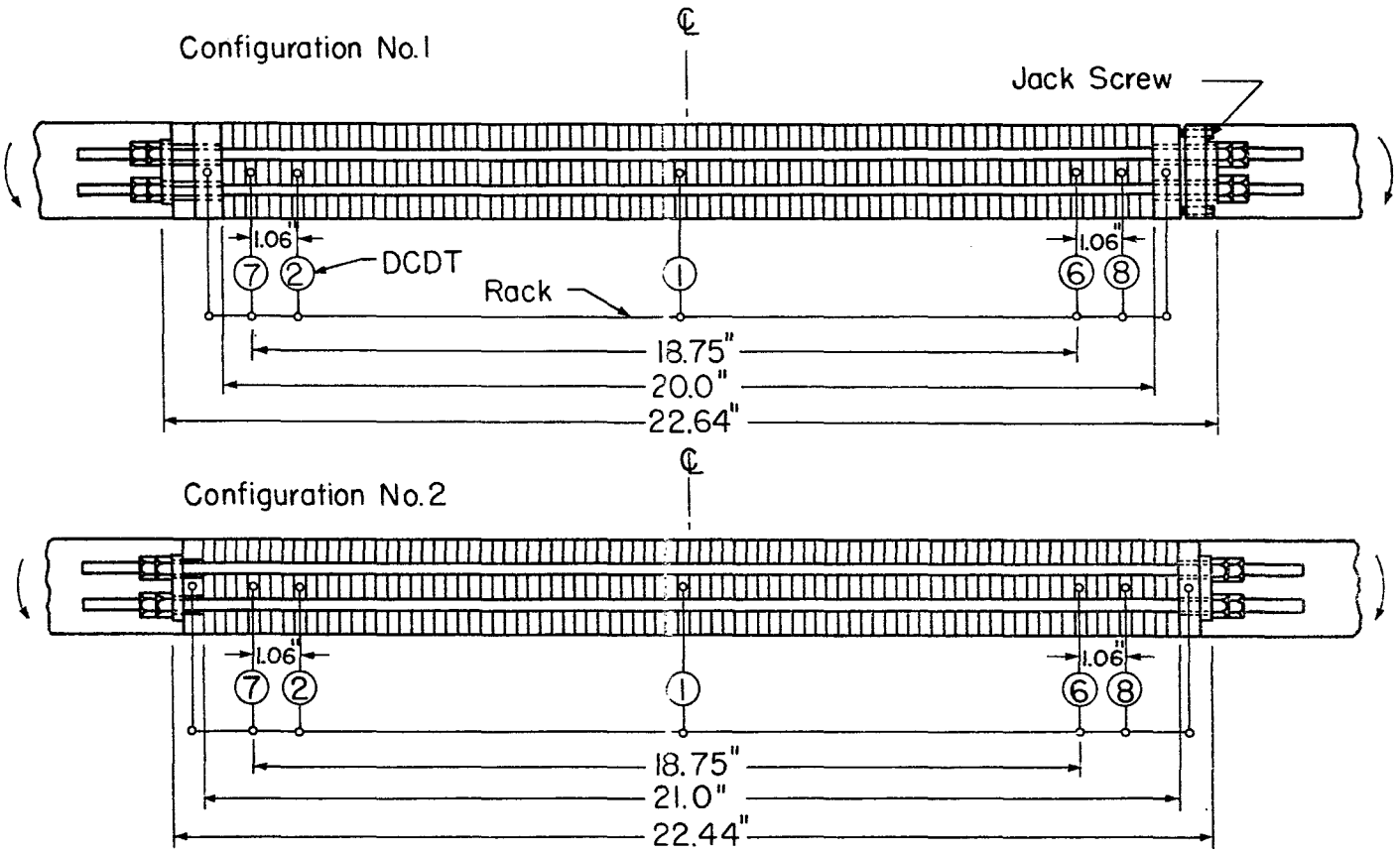

Figure 6 Tungsten Carbide Beam Configurations

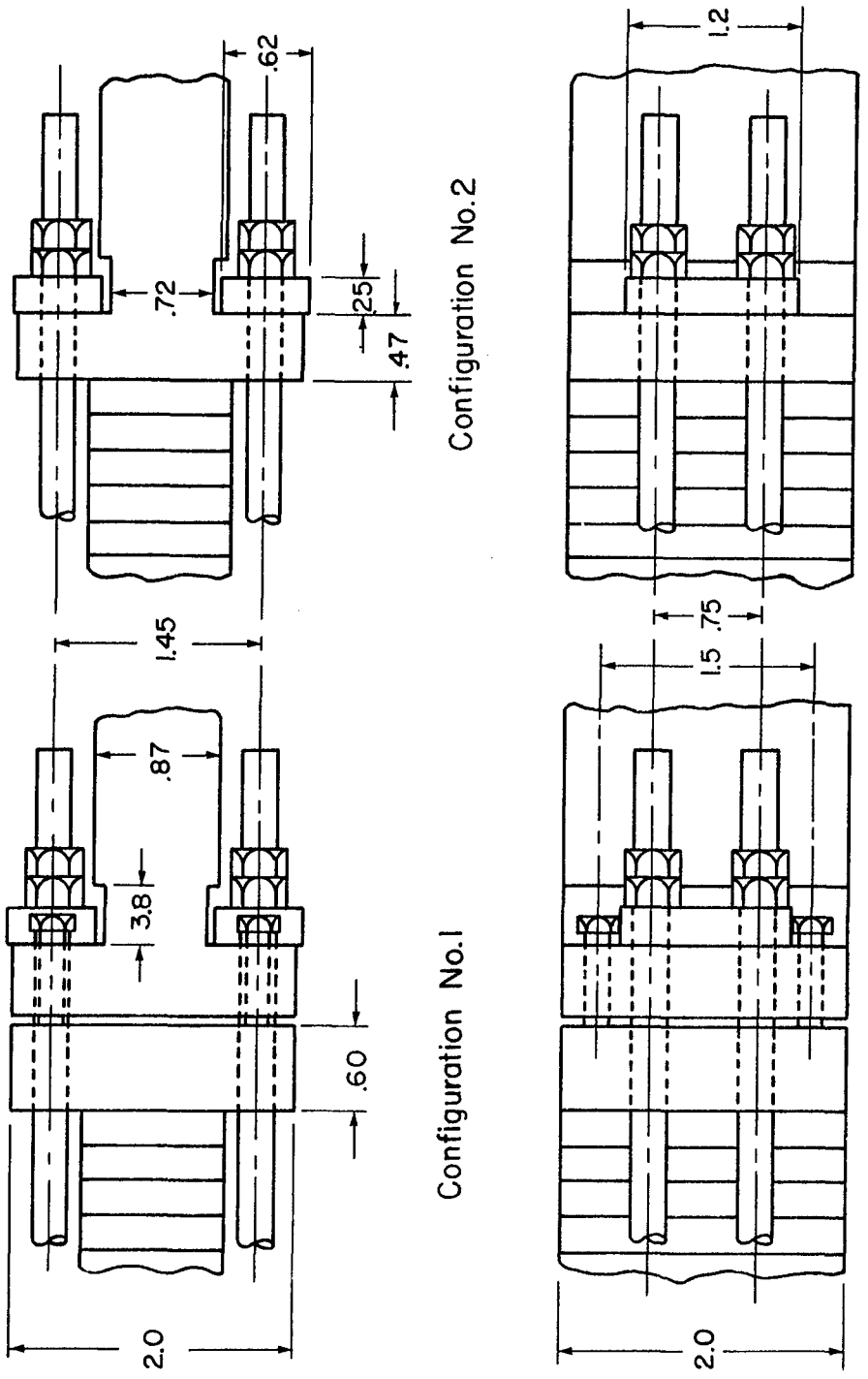

Figure 7 Details of Beam End Configurations

Preliminary bending tests were conducted using configuration no. 1. Preload levels of 5, 8, 11 and 14 kips were selected which were in the monolithic stiffness range according to Figure 4 for the column test. The tests were run in the sequence 14, 11, 8, 5, 5, 8, 11 and 14 without ever bringing the preload to zero. The results of these tests are presented in Figure 8.

Two final terminal couple-end rotation diagrams were determined for the WC beam where exceptional attention was devoted to the testing details. In each test, the preload was gradually increased from zero to the desired level and many load precycles were applied to the beam to completely stabilize the system. The first test was conducted with configuration no. 1 and a 14 kip preload. The preload in the second test was 4 kips which enabled us to use the configuration no. 2 and avoid the complications introduced by the jack screws. The results of these tests are presented in Figures 9 and 10.

c. Comparison of theory and experiment: The theory, with which the experiments will be compared, is in the form of a computer program which was developed under the first phase of this contract (ref. 1). In order to take into account the effect of multiple elastic tendons and also to attempt to compensate for the structural complications (especially in configuration no. 1) that were introduced between the end of the WC beam and tendons, the original computer program was significantly modified.

Recalling the elastic tendon equation for the case of multiple tendons, we have

$$\frac{(F^i - F_o^i)\, L}{A_t\, E_t} = \left| Q_i\, (\theta-\theta_o) \right|_{x=0} + \left| Q_i\, (\theta-\theta_o) \right|_{x=L} - \frac{F-F_o}{E} \int_0^L \frac{dx}{A} \qquad (22)$$

where $$\theta = \int_0^L \frac{Tm_L}{E\,I}\, dx \qquad (28)$$

and where the interval (0,L) represents the assumed length of

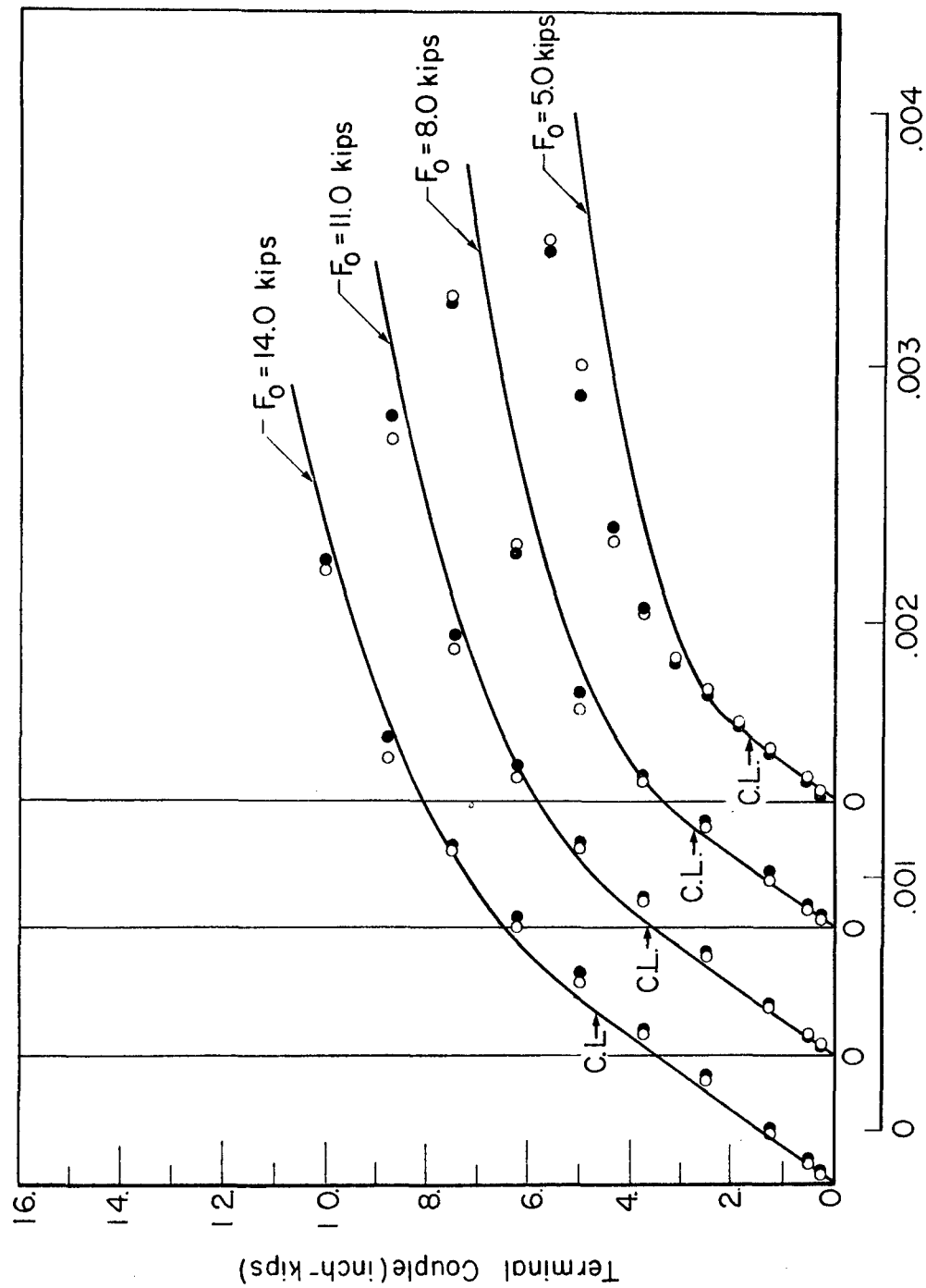

Figure 8 Preliminary Terminal Couple - End Rotation Diagrams for a Prestressed Segmented WC Beam

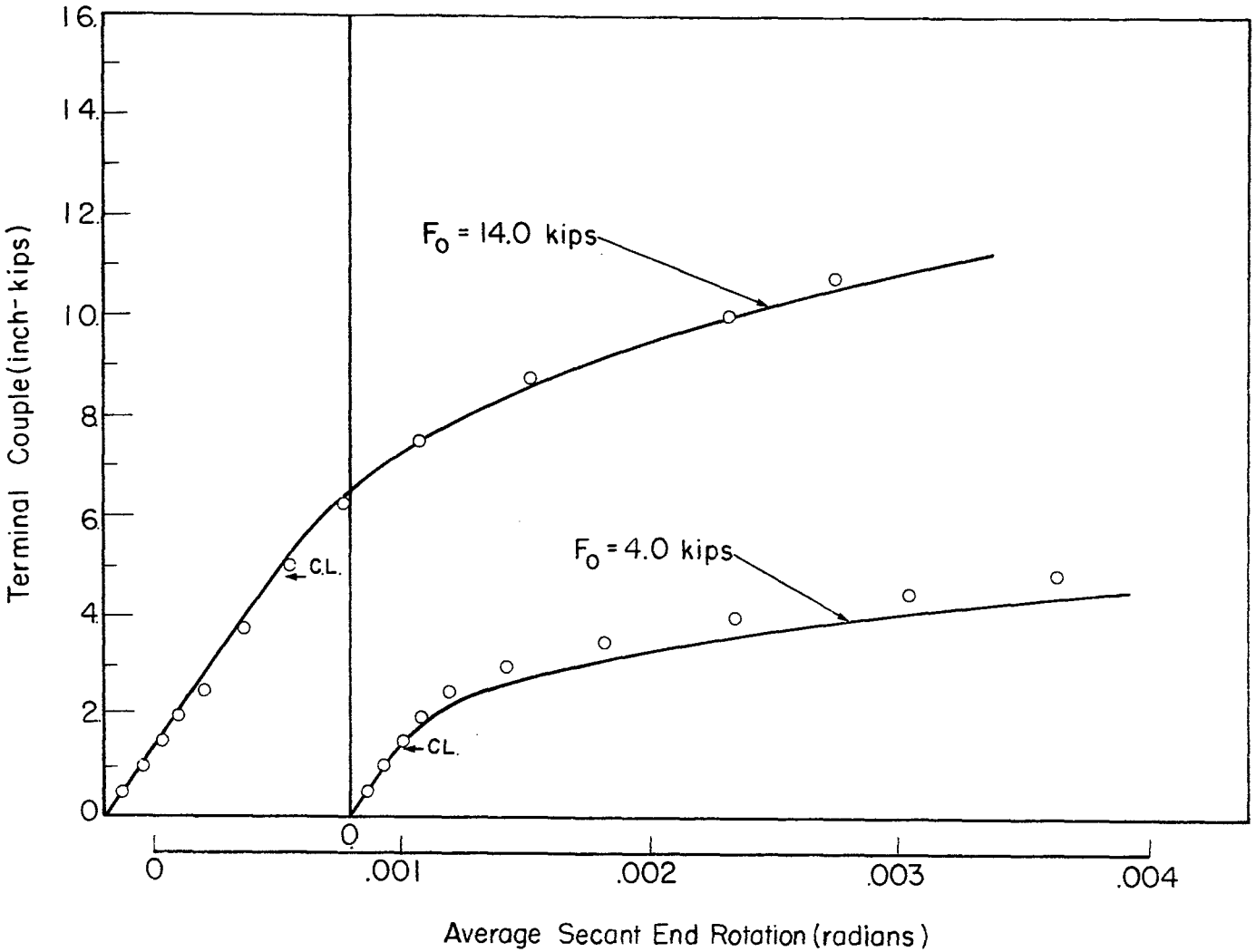

Figure 9 Final Terminal Couple - End Rotation Diagrams for a Prestressed Segmented WC Beam

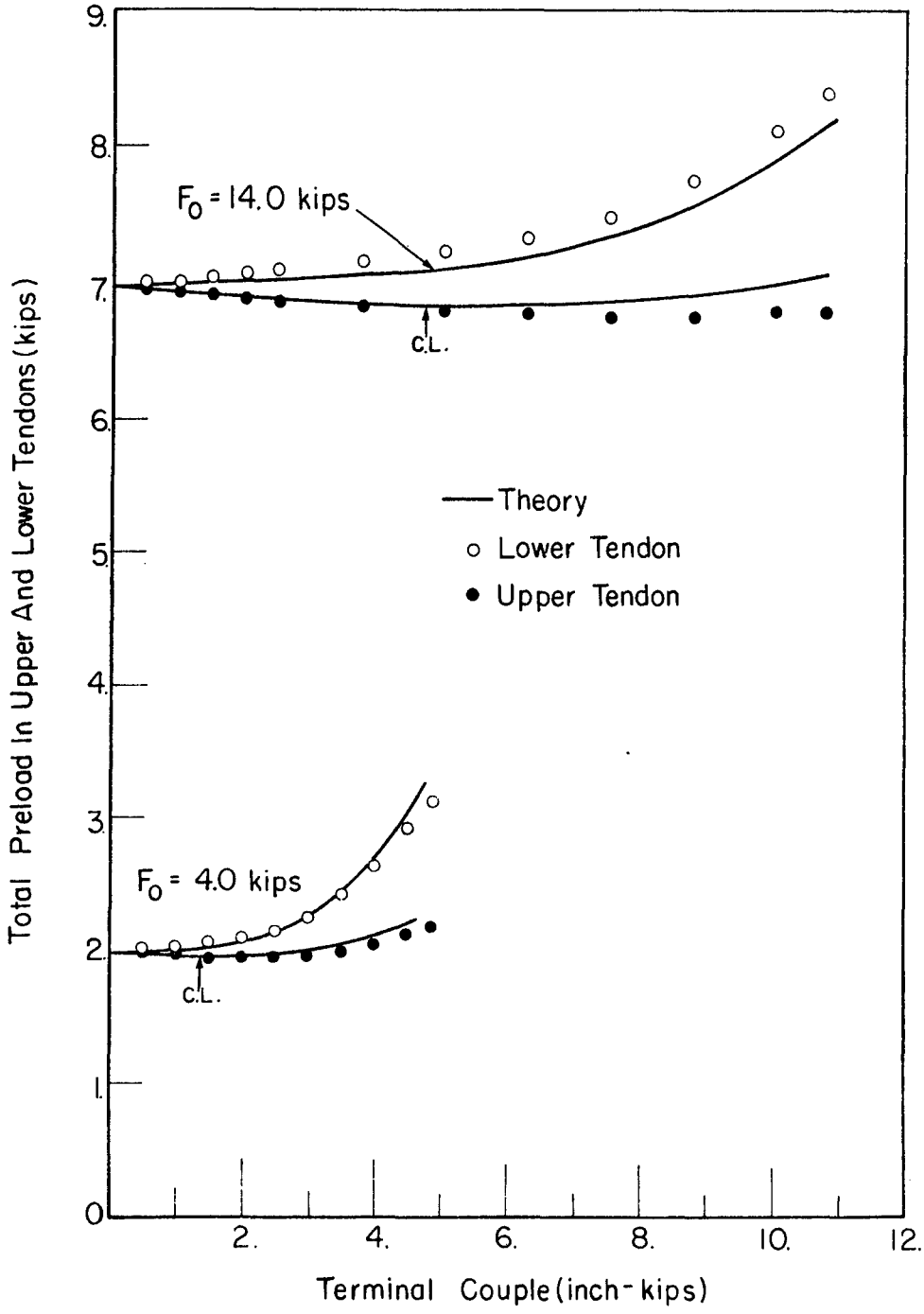

Figure 10 Tendon Stress - Terminal Couple Diagram for a Prestressed Segmented WC Beam

the WC beam. In order to account for the steel ends and (in configuration no. 1) the jack screws in Equation (22), the end rotation should be expressed as

$$\theta = K_1 \int_0^L \frac{Tm_L}{EI}\, dx + K_2\,(M - F_e - M_T) + K_3\,\left(\frac{T}{I}\right) \qquad (29)$$

and the beam compression term, $\frac{F - F_o}{E} \int_0^L \frac{dx}{A}$, should be modified to

$$(F - F_o)\left[\frac{K_1}{E}\int_0^L \frac{dx}{A} + K_4 + \frac{K_5}{A}\right] \qquad (30)$$

where

$$\begin{aligned} K_1 &= \frac{L_{WC}}{\text{Assumed Length}} \\ K_2 &= \frac{1}{4w^2}\left(\frac{\ell^\circ}{AE}\right)_{JS} \\ K_3 &= \frac{1}{2}\left(\frac{L}{E}\right)_{ST} \\ K_4 &= \frac{1}{4}\left(\frac{\ell^\circ}{AE}\right)_{JS} \\ K_5 &= \left(\frac{L}{E}\right)_{ST} \end{aligned} \qquad (31)$$

These correction terms and factors were derived with the following assumptions: (1) M(x) = constant; (2) the steel ends have the same width and depth as the WC beam and are infinitely segmented so that their area and moment of inertia depend upon the loading in the same manner assumed for the WC beam; and (3) that the jack screws act simply as two force members. The subscripts ST and JS refer to the steel ends and the jack screws respectively, 2w is the vertical distance between jack screws and ℓ°_{JS} is the extended length of the jack screws.

TABLE I

LENGTHS OF JACK SCREW CORRESPONDING TO THE VARIOUS PRESTRESS LEVELS

F_o(kips)	ℓ°_{JS} (inches)
14	0.0559
11	0.0439
8	0.0319
5	0.0200

In configuration no. 1, L_{ST} = 2.64 inch, w = .75 inch, A_{JS} = .0227 sq. in., and L_{wc} = 20.0 inch. In configuration no. 2, L_{ST} = 1.44 inch and L_{wc} = 21.0 inch. Also, in both configurations $E_{ST} = E_{JS} = 30 \times 10^3$ ksi, and the assumed length = 18.75 inch. Insertion of these values into Equations (31) yields Table II.

TABLE II

VARIOUS CONSTANTS USED IN THE ROTATION COMPUTATIONS FOR THE WC BEAM

F_o kips	Configuration No.	K_1	K_2 x10^{-6}	K_3 x10^{-6}	K_4 x10^{-6}	K_5 x10^{-6}
14	1	20/18.75	36	44	21	88
11	1	20/18.75	29	44	16	88
8	1	20/18.75	21	44	12	88
5	1	20/18.75	13	44	7	88
4	2	21/18.75	0	24	0	48

As mentioned previously, the experiments yielded average (of both ends) secant end rotations corresponding to vertical deflection measurements taken at stations 1.06 inches apart at both ends of the beam. Thus, the computer program was adjusted to compute the same secant end rotation.

Figure 8 illustrates the comparison of the theory and the preliminary experiments. It is observed that generally, the higher the preload, the better the agreement. There are a number of reasons why this is expected; higher preloads provide a

tighter system with greater contact area between segments, the influence of the low stress nonlinearity is suppressed, and the relative errors in preload determination are reduced. It should be noted that a rough analysis of the jack screws indicated that they tend to open up in the nonlinear ranges for the cases F_o = 5 and 8 kips.

The comparison of the theory and the final experiments is illustrated in Figures 9 and 10. The agreement is much better than in the case of the preliminary experiments, both in the linear and in the nonlinear ranges. This is due to the extra care used in performing the final experiments and possibly to the fact that the jack screws were eliminated in the case F_o = 4 kips. The jack screws behaved as predicted in the 14 kip case.

5. Segmented beams with nonflat interfaces. - When the segment interfaces are not flat, the contact area between any two segments may vary from almost full contact to almost no contact. Furthermore, the actual contact area cannot be predicted for particular segments since it varies randomly from interface to interface. However, when all the interfaces have been drawn from the same population, which usually happens when the same manufacturing technique is used for all the blocks, we can predict the behavior of groups of segments in a statistical sense. The compression test, for example, furnishes a measure of the average or effective contact area at every level of compression. For a given segmented column the effective area is computed by multiplying its nominal area by the ratio of its tangent stiffness to the equivalent monolithic stiffness.

The statistical nature of the interface contact gives rise to a number of important implications. First, a description of the compressive stress-strain diagram will be statistical and will depend on both the column area and the length. This problem will be studied more thoroughly in Section III. Second, the moment of inertia, like the area, will be random with a

lower bound equal to zero and an upper bound equal to the full moment of inertia. It follows that beam behavior will be statistical in nature and that the variability experienced will depend on the length and area of the beam, the number of segments, and on the loading.

Because the effective stress-strain curve of a segmented column is area and length dependent, it is clear that an equivalent nonlinear material cannot be defined which is useful for response calculations. For example, in a segmented beam under sufficiently high loads, the nominal "uncracked" area diminishes continually as the load is increased. Consequently, the stiffness of the section tends to increase as a result of increasing axial stress and decreasing nominal area; it tends to decrease because of a reduced moment of inertia. The theory of perfect segmented beams accounts only for variations in the moment of inertia. An exact solution for the response will require, in addition, that we describe the bending stiffness of any "uncracked" area subjected to a linear strain field that varies from zero at one end to some arbitrary maximum value at the other. It does not appear that an exact bending stiffness relationship can be derived from column tests. The desired relationship can be obtained from terminal couple-end rotation tests; however, the authors doubt whether the end result justifies the effort involved.

An approximate description of a load-deflection diagram can be obtained through a slight modification of the perfect interface theory. If the modulus of elasticity of the segment material entering into the theory is replaced by the tangent modulus of the beam associated with the initial prestress level, the perfect interface theory will predict the average load deflection diagram. In our first report we demonstrated that this procedure predicted the nonlinear behavior of segmented beams when the initial straight line portion of the curve was matched to the data. The necessity of matching up the initial slope rather than inferring it from the tangent modulus taken from the associated column tests strikes at the core of the statistical problem. The tangent modulus prediction

describes only the average behavior of a group of segmented beams and not the response of a single member.

To use the suggested approximate technique for predicting beam response, we require a description of the compressive stress-strain curve for the nominal cross-sectional area of the beam. There is every reason to believe that the statistical description of a single typical size column will enable one to describe any other column of different area and length. This problem is studied in Section III.

As a final observation concerning nonflat interfaces, we recall from our last report that the initial portion of the central load-central deflection diagrams for the glass beam were all straight. On the other hand, the compression stress-strain diagram for the glass is curvilinear with a monotonically increasing slope. This apparent anomaly can be explained by considering an axial prestressed beam that is free from lateral loads. The initial bending stiffness of this member is proportional to the tangent modulus of a compression curve at the given prestress level. Now, when a bending moment is applied to this member the compression fibers will tend to get stiffer and the tension fibers will tend to become more flexible. The two effects neutralize each other and mitigate the influence of the compression nonlinearity.

B. I-Beam or Box Beam with Multiple Tendons

The analysis of I (or equivalently box) beams proceeds exactly as outlined in the section on general relationships. Referring to Figure 11, we obtain the following cross sectional properties:

Uncracked section properties ($f \equiv 0$)

$$A = 2\,bt_f + dt_w$$

$$\bar{x} = q = \frac{d_{total}}{2} = d + \frac{t_f}{2} \tag{32}$$

$$I = \frac{t_w d^3}{12} + \frac{bt_f^3}{6} + \frac{bt_f}{2}(d + t_f)^2$$

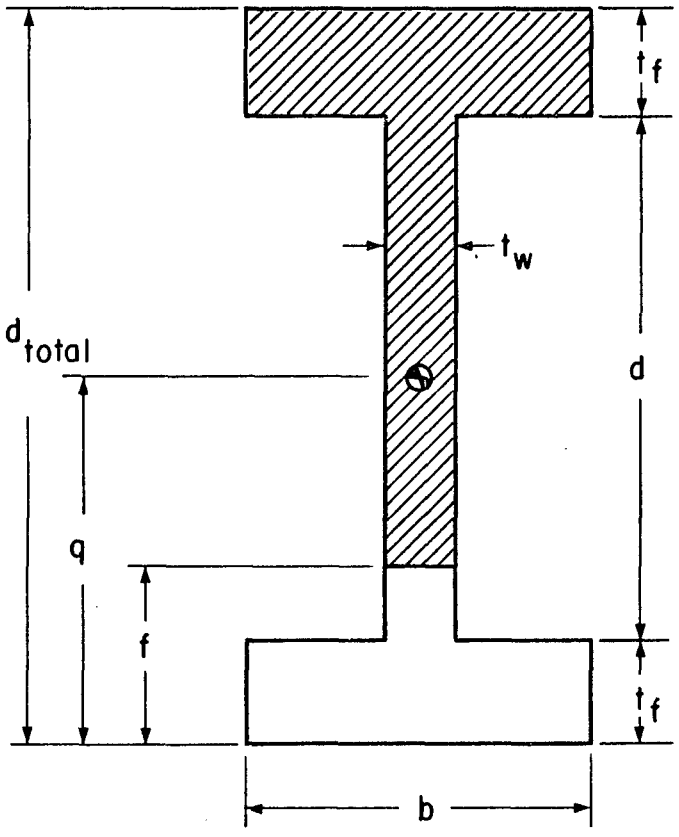

Figure 11 Geometry of Cracked I-Beam Cross Section

Cracked section properties

Case I $(0 \leq f \leq t_f)$

$$A = b(t_f - f) + dt_w + bt_f$$

$$\bar{x} = \frac{1}{A}\left[\frac{b}{2}(t_f - f)^2 + dt_w\left(t_f + \frac{d}{2} - f\right) + bt_f\left(\frac{3}{2}t_f + d - f\right)\right] \quad (33)$$

$$I = \frac{1}{12}\left[b(t_f - f)^3 + t_w d^3 + bt_f{}^3\right] + b(t_f - f)\left(\bar{x} - \frac{t_f}{2} + \frac{f}{2}\right)^2$$

$$+ dt_w\left(\bar{x} - \frac{d}{2} - t_f + f\right)^2 + bt_f\left(\frac{3}{2}t_f + d - \bar{x} - f\right)^2$$

Case II $(t_f \leq f \leq t_f + d)$

$$A = (t_f + d - f)\, t_w + bt_f$$

$$\bar{x} = \frac{1}{A}\left[\frac{t_w}{2}(t_f + d - f)^2 + bt_f\left(\frac{3}{2}t_f + d - f\right)\right] \quad (34)$$

$$I = \frac{1}{12}\left[t_w(t_f + d - f)^3 + bt_f{}^3\right] + t_w(t_f + d - f)\left(\bar{x} - \frac{t_f}{2} - \frac{d}{2} + \frac{f}{2}\right)^2$$

$$+ bt_f\left(\frac{3}{2}t_f + d - \bar{x} - f\right)^2$$

Case III $(t_f + d \leq f \leq 2t_f + d)$

$$A = b(2t_f + d - f)$$

$$\bar{x} = t_f + \frac{d}{2} - \frac{f}{2} \quad (35)$$

$$I = \frac{b}{12}(2t_f + d - f)^3$$

Due to the algebraic complexity of the above expressions for $A(f)$, $\bar{x}(f)$ and $I(f)$, the equation for the crack penetration

$$W = e + f - q + \bar{x} + \frac{I(f)}{A(f)\bar{x}(f)} \quad (36)$$

where

$$W \equiv \frac{M - M_T}{F}$$

cannot in general be inverted to find f=f(W). In order to be able to handle this new complication, a new computer program has been developed. A listing of the program (in Fortran II for the IBM 7094) plus sample input-output is presented in Appendix A. This program is currently set up to handle I-beams with multiple elastic tendons. Each of the cross section properties A(f), $\bar{x}(f)$ and I(f) are programmed as function subprograms and, consequently any other cross section geometry may be investigated by merely changing these three subprograms.

The inversion of Equation (32) is accomplished in the computer program through the vehicle of a table of W vs f. This table is constructed in increments according to input specifications. The inversion is easily effected by a function subprogram which merely searches the table using W and linearly interpolates between the bracketing values.

Prestressed segmented glass beams with the cross sectional geometries shown in Figure 12 and with $E = 10.5 \times 10^6$ psi, $E_t = 30 \times 10^6$ psi, and $L = L_t = 38$ inches have been selected to illustrate and compare the behavior of I-beams, webless I-beams, and rectangular beams of the same overall dimensions. Figure 13 illustrates the behavior of these beams under terminal couples for the case of zero stiffness tendons (E_t=0). We observe that the rectangular beam is the stiffest (least deflection) member in the initial load range, the I-beam in the middle range, and finally the webless I-beam in the final range.

It is interesting to note that, for a load of 18 inch kips, the rectangular beam has a crack penetration of 2.5 inches, the I-beam has 1.7 inches, and the webless I-beam is still uncracked. Thus, the webless I-beam, which has only 25 percent of the area and weight of the rectangular beam, is unquestionably the most efficient cross section for prestressed beams in terms of stiffness per unit weight.

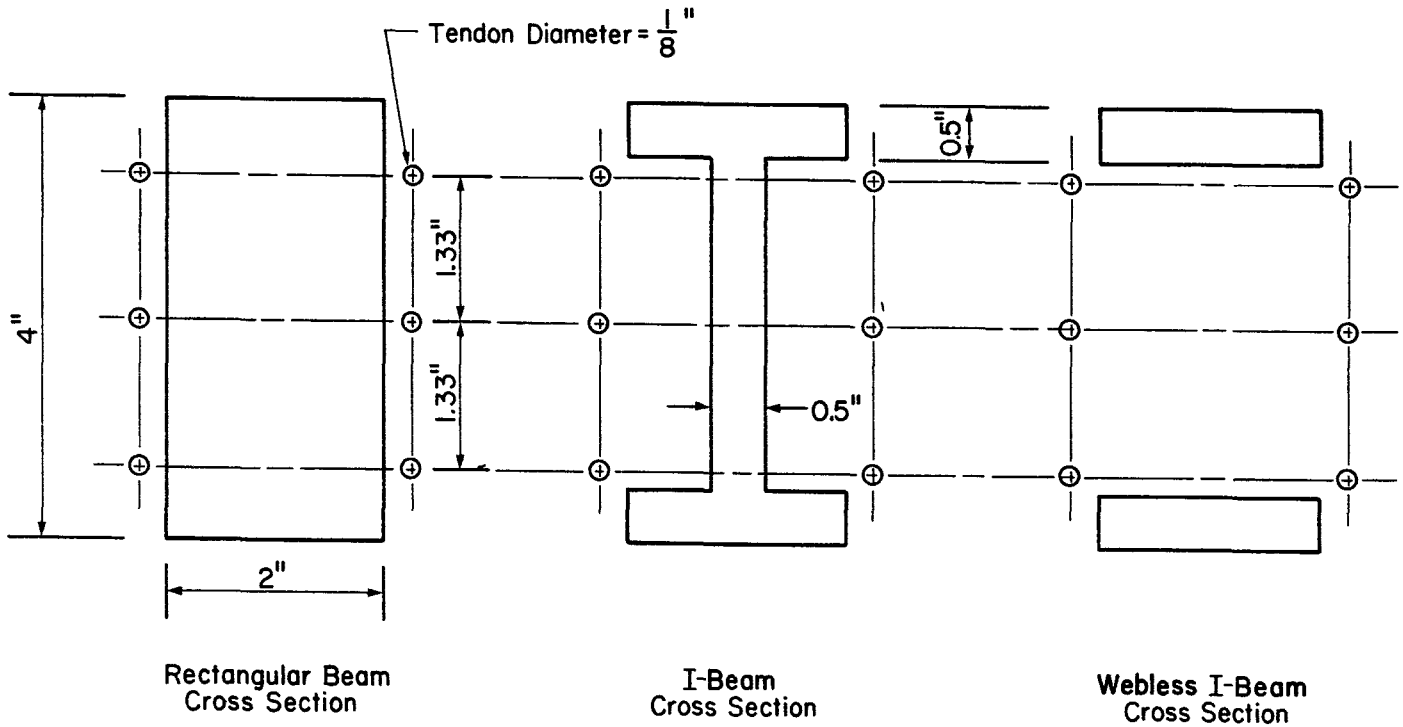

Figure 12 Beam and Tendon Geometries

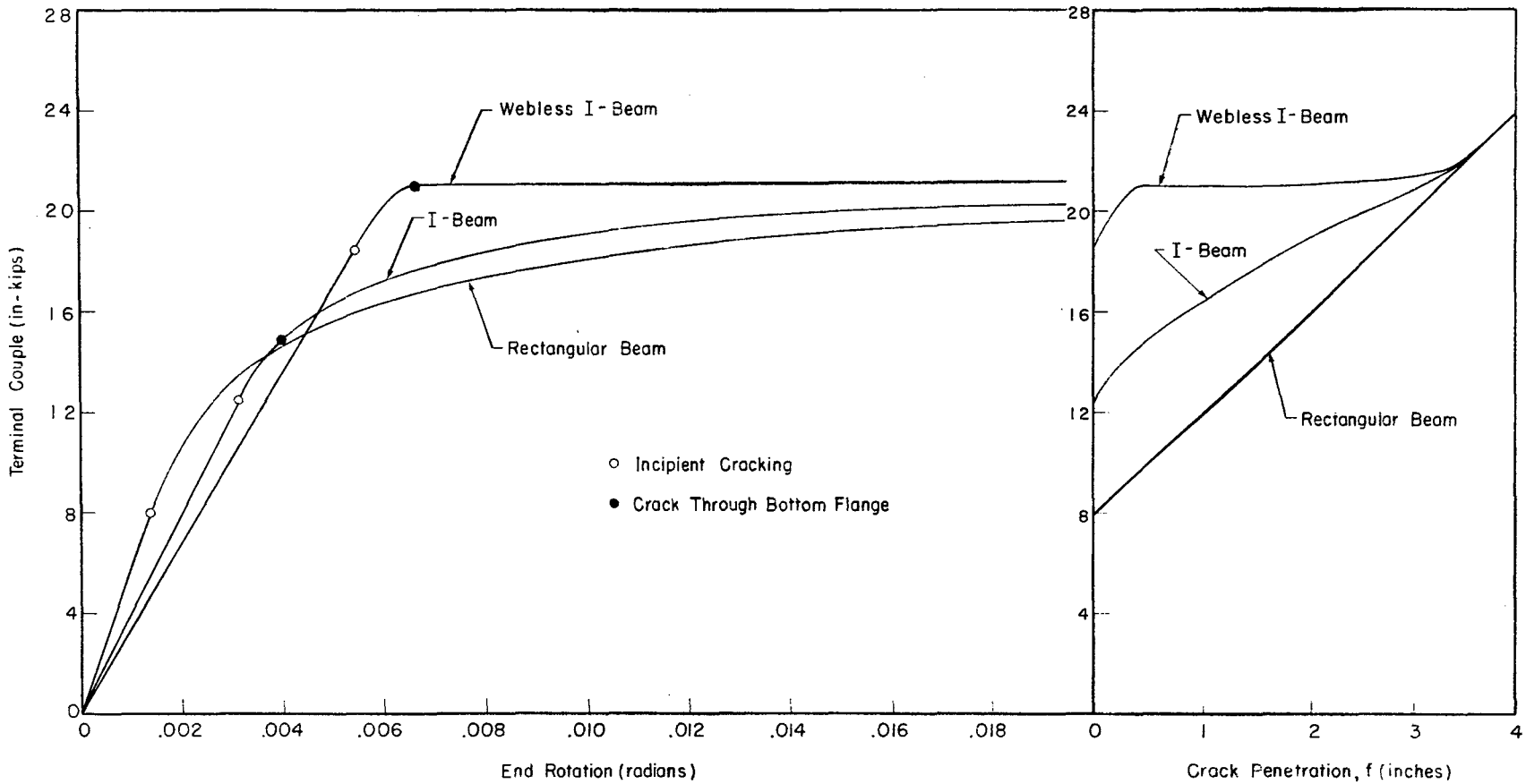

Figure 13 Load-Deflection Diagrams and Crack Penetration Diagrams for I-Beams with Zero Stiffness Tendons

We also observe for the case of the webless I-beam that although abrupt changes in character occur in the terminal couple vs. end rotation curve and the terminal couple vs. crack penetration curve as the crack passes through the bottom flange, that there is in fact no discontinuity in slope in either of these curves. One additional noteworthy item for the case of zero stiffness tendons is the fact that, as the cracks penetrate the cross sections, eventually ($f > t_f + d$) the uncracked sections become identical and hence the behavior of the three beams coincide in this range.

The behavior of the three beams for the case of elastic tendons is shown in Figure 14 and 15. In general, the effect of the tendon elasticity is to increase the stiffness and the slope of the terminal couple vs. end rotation curve and to limit its minimum slope as the load increases to infinity. There are no discontinuities in the slope of the curves for end rotation, prestress force, prestress moment, or crack penetration as the crack passes through the bottom flange for the case of the webless I-beam.

As in the case of terminal couples on a rectangular beam with a single elastic tendon (ref. 1) it is expected that the cracks will never pass completely through the section. This fact is verified by the crack penetration curves in Figure 15 which seem to be approaching asymptotic values other than $d_{total} = 4$. Whether all three curves will have the same asymptote depends upon the relative stiffnesses of the beams to the tendons. Thus, in general, it cannot be expected that the behavior of the rectangular beam, I-beam, and webless I-beam will become coincident as the applied load becomes unbounded.

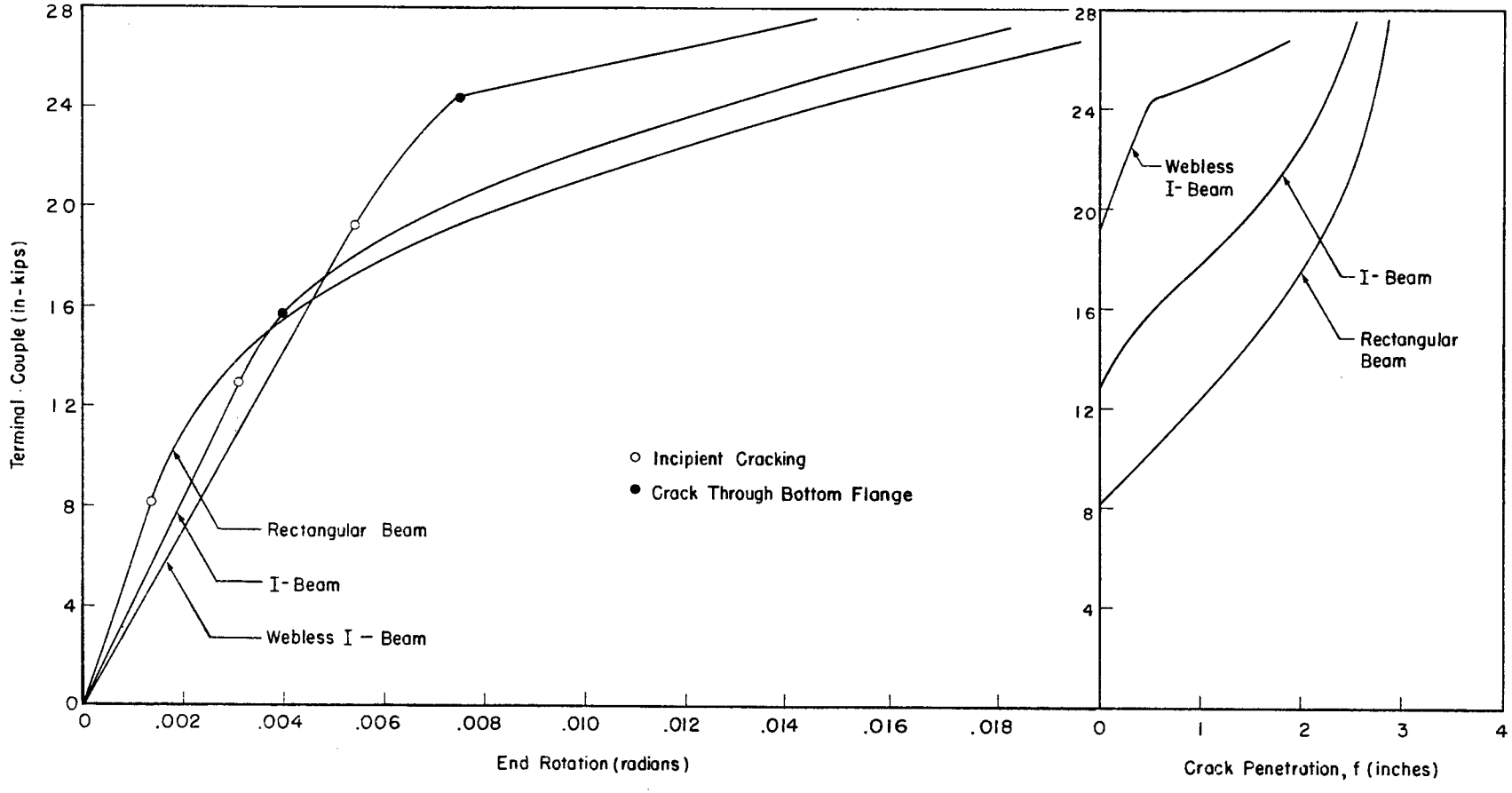

Figure 14 Load-Deflection Diagrams and Crack Penetration Diagrams for I-Beams with Elastic Tendons

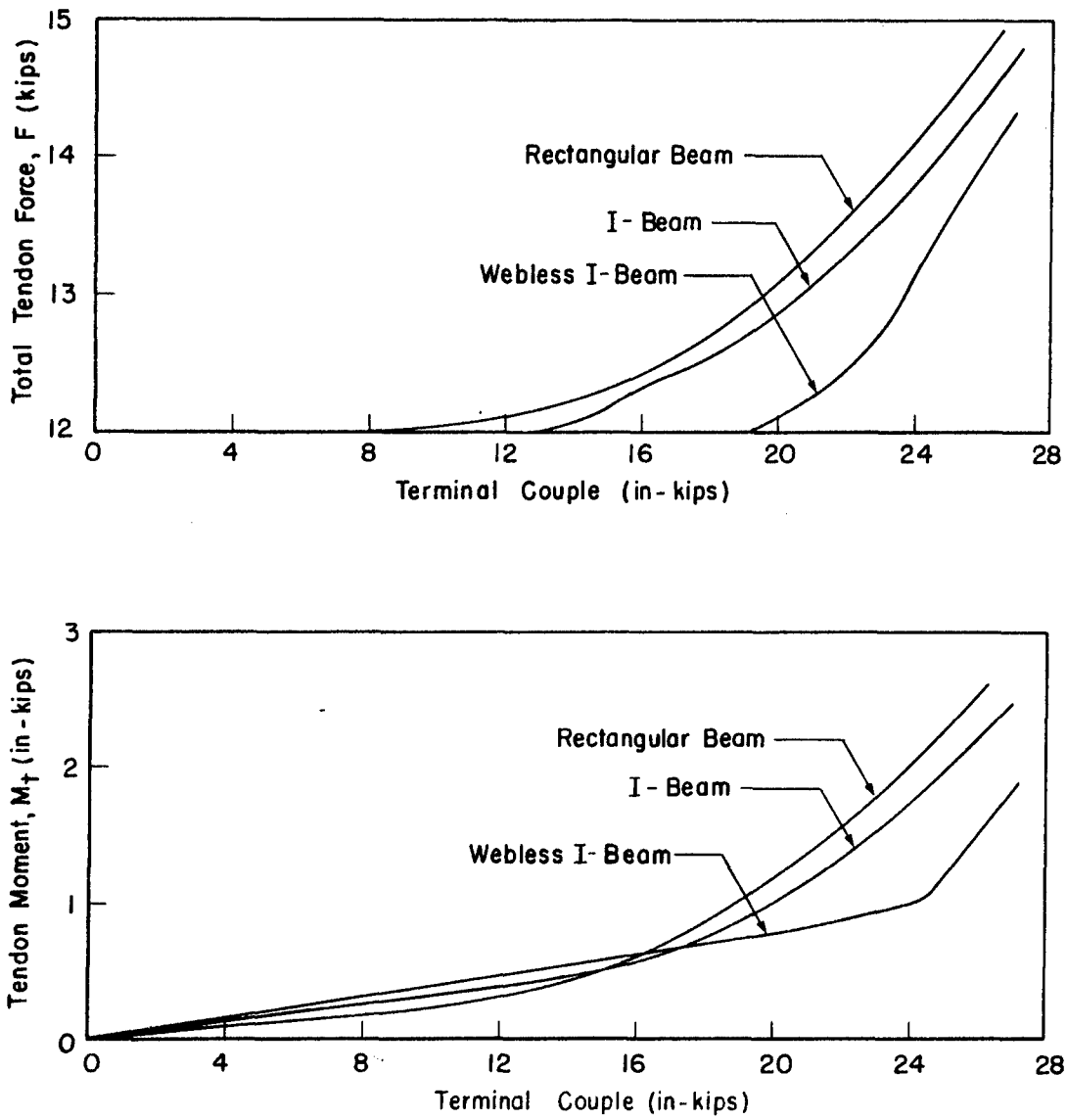

Figure 15 Tendon Force and Moment vs. Terminal Couple

C. Limit Analysis

The possibility of approximating the load-deflection diagram of a prestressed segmented beam by one which is elastic-perfectly plastic was suggested in our previous report (ref. 1). Indeed, this possibility was exploited in 1952 by Kooharian in his study of segmented concrete arches (ref. 2). In these arches, the compressive forces acting normal to the segment interfaces were not provided by prestressed tendons, but rather by the arches' reaction to live and dead loading.

The applicability of limit analysis for predicting the ultimate load-carrying capacity of prestressed segmented beams is investigated in this section with the aid of the 16-foot segmented aluminum oxide beam shown in Figure 16 . Each segment in this member was four-inches in both length and outside diameter with a wall thickness of 3/16-inch. The beam was composed of 48 such segments and the prestressing was accomplished by pretensioning a 1/4-inch steel prestressing tendon that passed along the axes of the cylinders and was secured to steel end plates. To preclude the presence of secondary bending effects (beam-column behavior), the tendon was constrained to the centroid of the sections by five closely fitting wooden spacer inserts on three-foot centers. Two strain gages on opposite sides of the tendon were used to monitor the prestress level. Simple end supports were provided by two saw horses as shown in Figure 17a . The beam was loaded with dead weights and the finest load increment was five pounds.

The beam was tested under the three types of loading shown in Figure 18 . In all cases, the loading was continually increased until a 0.005-inch thick feeler gage could be inserted between the separated segments to a depth of two-inches. The load associated with this condition is recorded in Figure 18 as $P_{Measured}$. The first test run was the central loading configuration. It was noted at the conclusion of this test that longitudinal cracks had appeared on the compressive side of several segments that were close to the beam's center. For the

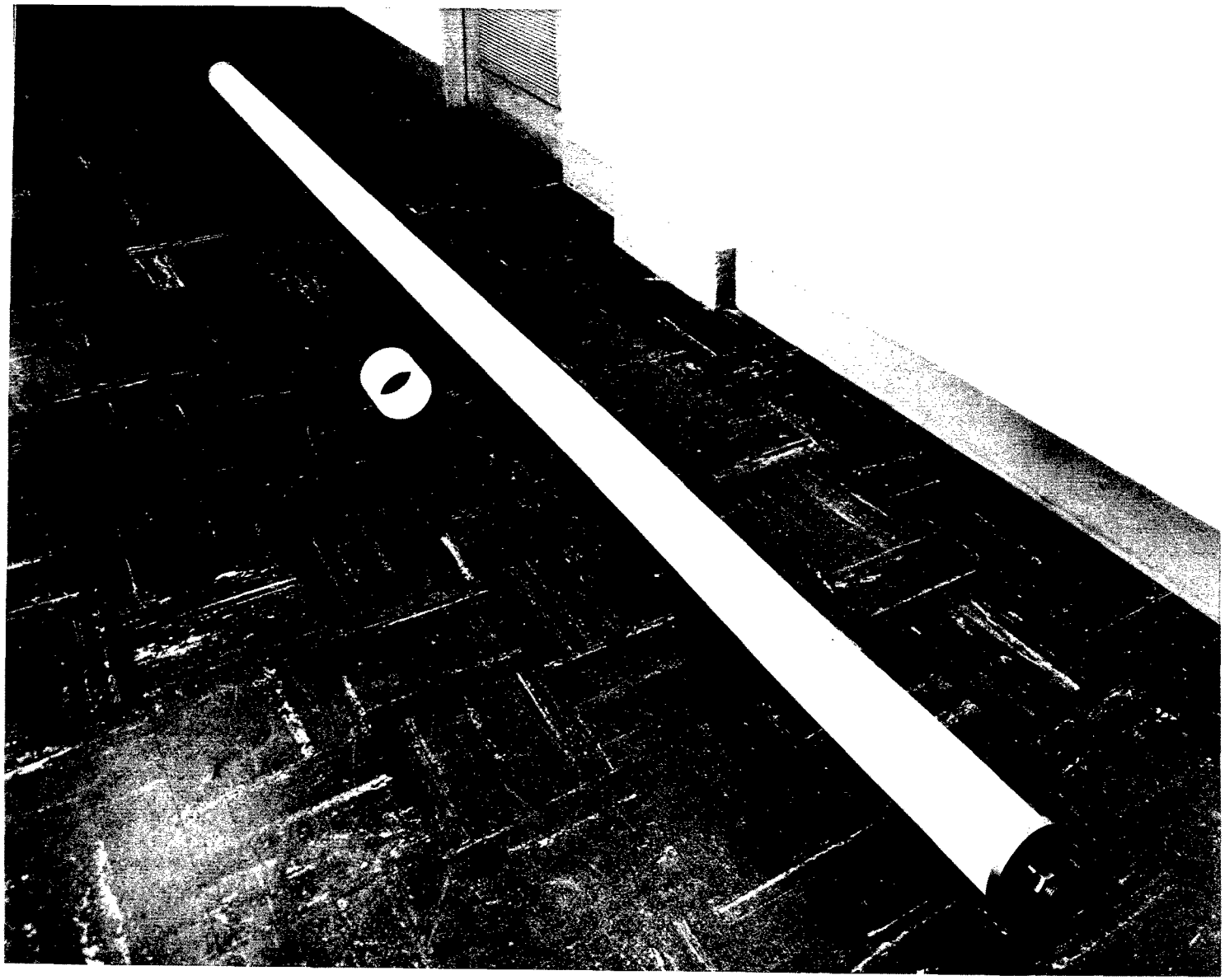

Figure 16 Alumina Hollow Circular Prestressed Segmented Beam

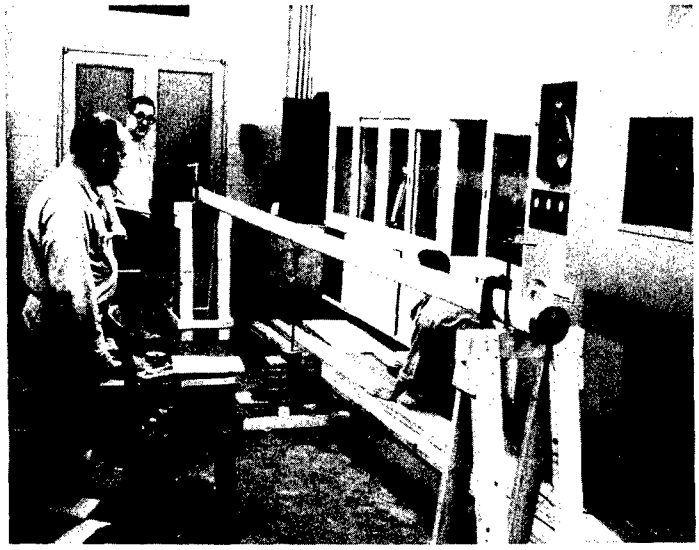

a. Support Conditions

b. Beam Fracture

Figure 17 Segmented Alumina Beam Tests

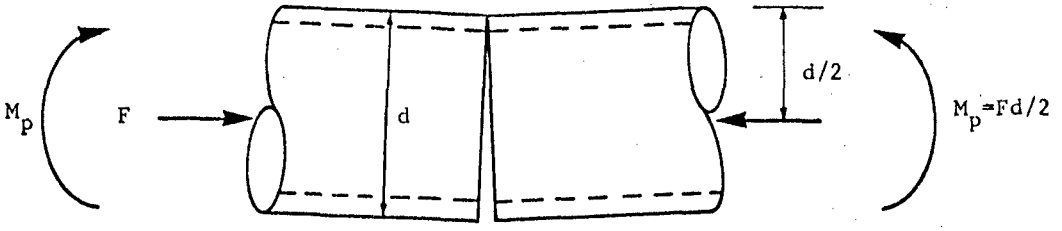

a) Plastic Moment: M_p

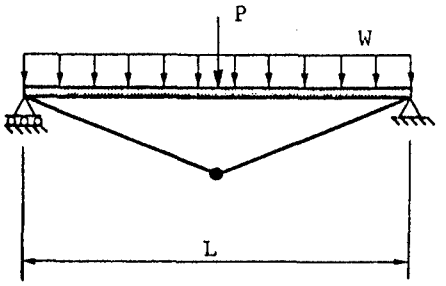

$P_{Theory} = \frac{4M_p}{L} - \frac{W}{2} = 174$ lb

$P_{Measured} = 180$ lb

b) Central Loading

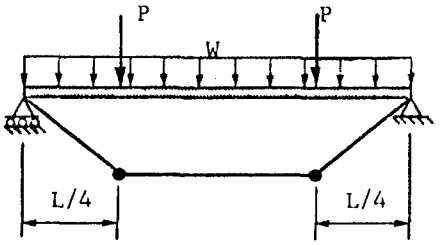

$P_{Theory} = \frac{4M_p}{L} - \frac{W}{2} = 174$ lb

$P_{Measured} = 185$ lb

c) Quarter Point Loading

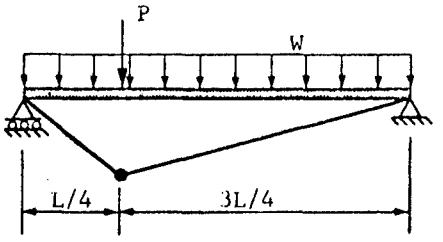

$P_{Theory} = \frac{16M_p}{3L} - \frac{2W}{3} = 233$ lb

$P_{Measured} = 240$ lb

d) Single Quarter Point Loading

Figure 18 Limit Analysis of Prestressed Segmented $A\ell_2O_3$ Beam

remaining two tests the beam was rotated such that the final bearing area was away from the cracks. During the final loading, two concentrated loads at the quarter points, horizontal cracks developed under the loads which resulted in the catastrophic failure shown in Figure 17b. The failure modes shown in Figure 19 are typical of the primary segment fractures.

The prediction of the ultimate loading of the alumina beam follows precisely the methods of limit analysis for simple beams. Here, we take the plastic moment to be the prestressing force times half the beam depth as shown in Figure 18a . The formulas and predictions for the limit loads are given in Figure 18b, c, and d where we reflect the following physical data:

(1) Prestress level, F = 5000 lb
(2) Weight density of tendon - 0.167 lb/ft
(3) Span length, L = 182.5 in.
(4) Weight of entire beam, W = 90 lb
(5) Weight of loading fixture - 10 lb
(6) Plastic moment, M_p = (2) (5000) = 10,000 in.-lb

We observe from this figure that the predicted loads are from 2.92 percent to 5.41 percent lower than the measured loads.

D. Prestressed Monolithic Beams

Our previous work (ref. 1) was directed toward application of Weibull's statistical fracture theory to monolithic prestressed brittle beams, neglecting the effect of beam-column action. That effort was devoted to developing the relationships among prestress level, load, geometry and the reliability of a structural member. We then proposed to demonstrate those results by means of an experimental program using Hydrostone plaster beams. In this year's effort, the additional moment due to the eccentricity of a straight tendon when the beam is laterally loaded has been considered. This may well not be of major significance in a real-life application where the prestressing tendon should be constrained to deflect with the beam, but it

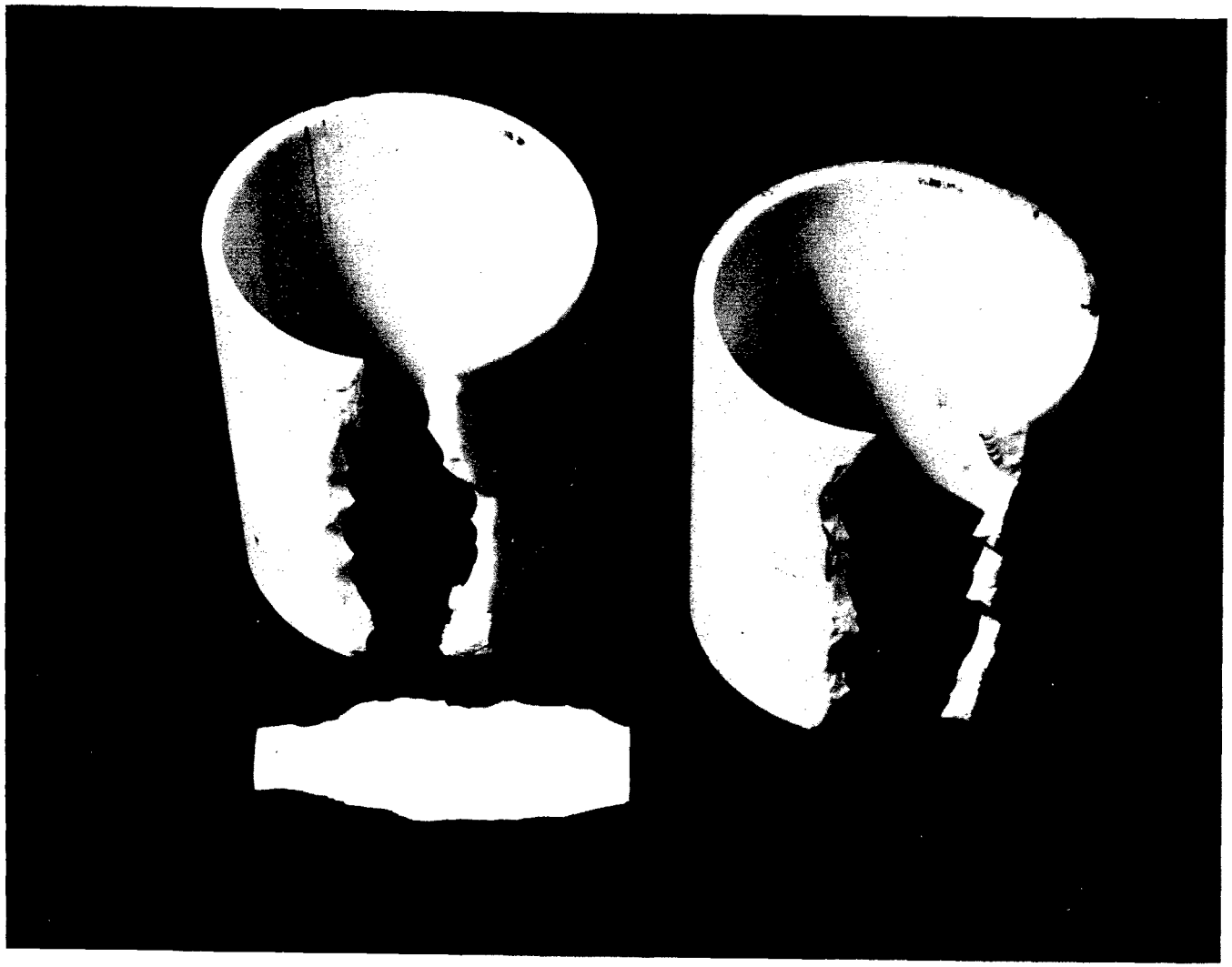

Figure 19 Typical Failure Modes of Alumina Beam Segments

is necessary explain the experimental results reported in this section. The experiments which were carried out involved four-point bending tests on the hydrostone beams described in Appendix B. The dimensions are shown in Figure 20, and the loading fixture in Figure 21. Since all specimens failed between the loads, the experiment can be considered as a pure bending test with a gage length L.

According to Weibull's theory, the failure probability F will be:

$$F(\sigma) = 1 - \exp\left[-\iiint g \, d\xi_1 \, d\xi_2 \, d\xi_3\right]$$

$$g = \frac{1}{\bar{v}} \left[\frac{\sigma\phi(\xi_1, \xi_2, \xi_3) - \sigma_u}{\sigma_o}\right]^m ; \quad \sigma\phi \geq \sigma_u \geq 0 \qquad (37)$$

$$g = 0 ; \quad \sigma\phi < \sigma_u$$

where σ is an intensity level; $\sigma\phi$ is the actual stress distribution in the body; ξ_1, ξ_2, and ξ_3 are space coordinates; $\bar{v}$ is a unit volume; and m, σ_u, and σ_o are statistical distribution parameters. For convenience, the notation

$$F = 1 - \exp[-B] \qquad (38)$$

is used, where the definite integral B is called the risk of rupture.

For the case of a rectangular beam subjected to a pure couple, the risk of rupture is

$$B = \int_{\frac{\sigma_u d}{2\sigma}}^{d/2} \left(\frac{\frac{2\sigma}{d} y - \sigma_u}{\sigma_o}\right)^m L \, b \, dy = \frac{V}{2(m+1)} \frac{(\sigma-\sigma_u)^{m+1}}{\sigma \, \sigma_o^m} \qquad (39)$$

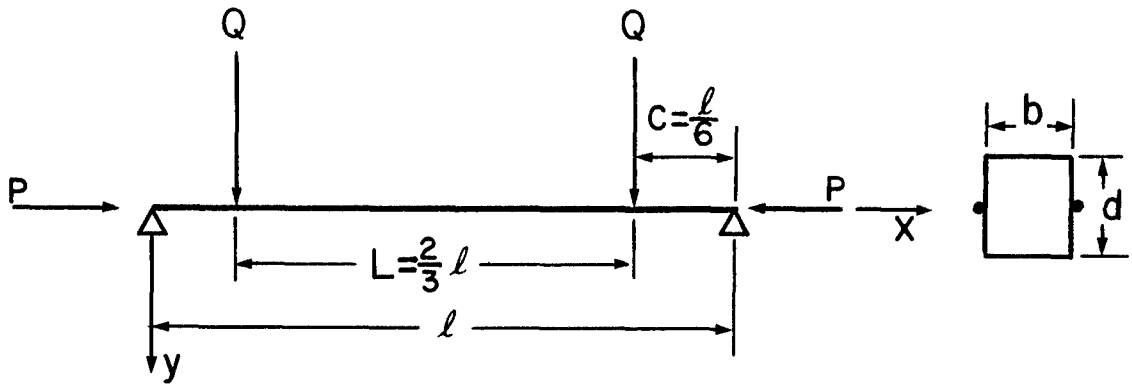

Dimension: ℓ = 45 inch
b = d = 2.5 inch

Unprestressed Case: P = 0
Number of Tests, N = 130

Prestressed Case: P = 10,000 Pounds

Prestress $\sigma_p = \frac{P}{bd}$ = 1,600 Psi

Number of Tests, N = 26

Figure 20 Schematic of Four-Point Bending Test

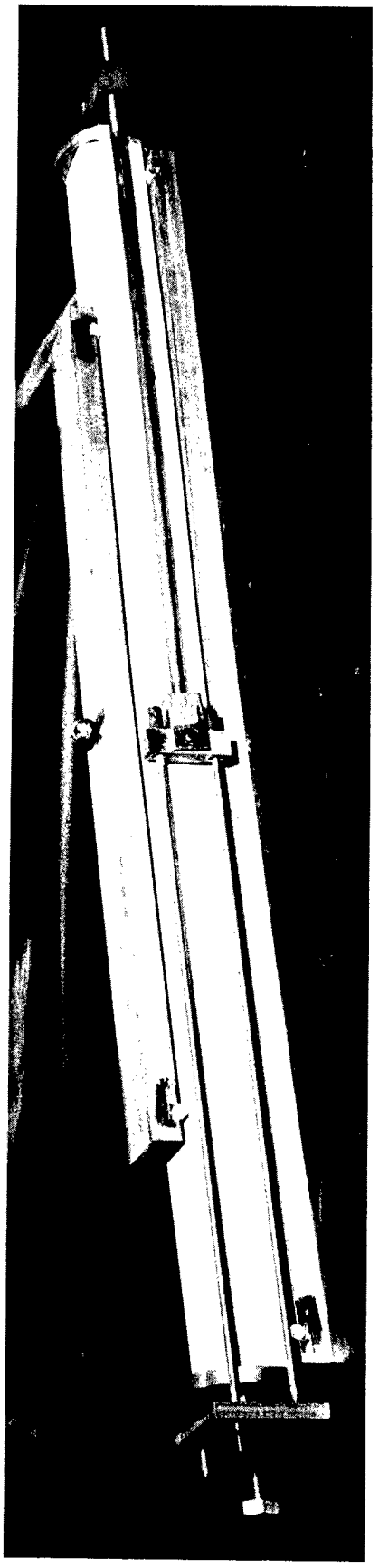

Figure 21 Prestressed Monolithic Plaster Beam

where V is the volume of a beam of length L, width b, and depth d; the maximum fiber stress $\sigma = 6M/bd^2$ is taken as the intensity level; ϕ is taken as 2y/d; and y is the coordinate through the beam depth measured from the neutral axis. For materials like Hydrostone that have low tensile strengths, it is common practice to attempt to fit their fracture data with a two parameter assumption, i.e., $\sigma_u = 0$. Then, Equation (39) simplifies to

$$B = \frac{V}{2(m+1)} \left(\sigma/\sigma_o\right)^m \tag{40}$$

or

$$B = \frac{1}{(m+1)} \left(\sigma/\sigma'_o\right)^m \tag{41}$$

where the volume has been incorporated into the scale parameter σ'_o.

The cumulative probability of failure curve for the unprestressed beams is shown in Figure 22 where the data have been ordered and the probability of failure at the stress associated with the i^{th} observation is estimated to be F = i/N+1 where N is the total number of observations. The maximum likelihood estimates of the parameters σ'_o and m are found from the solutions of (ref. 3):

$$\frac{N}{m} + \sum_{i=1}^{N} \log \sigma_i - N \frac{\sum_{i=1}^{N} \left(\sigma_i^m \log \sigma_i\right)}{\sum_{i=1}^{N} \sigma_i^m} = 0 \tag{42}$$

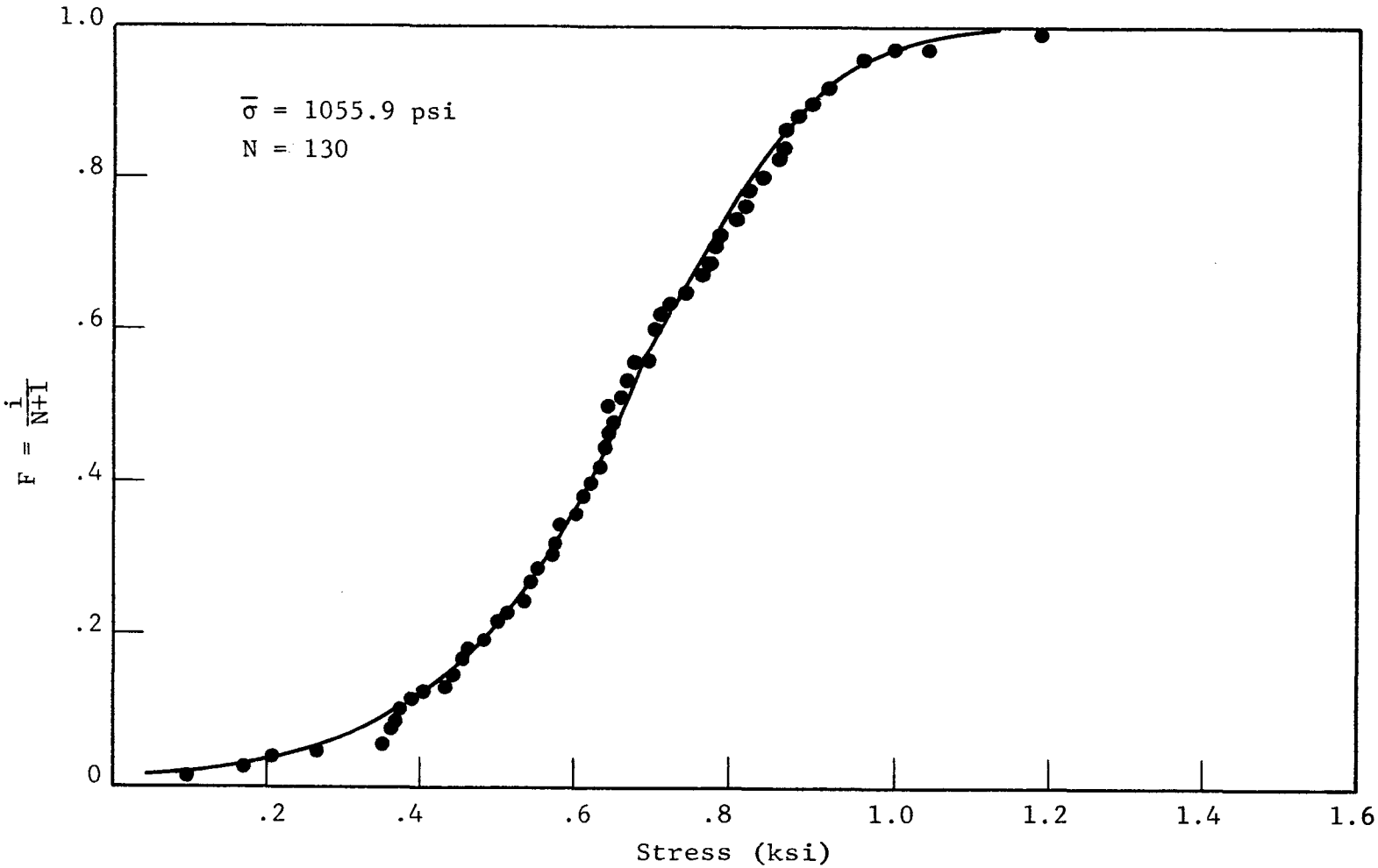

Figure 22 Failure Probabilities for Unprestressed Beams

and

$$(\sigma'_o)^m = \frac{1}{N(m+1)} \sum_{i=1}^{N} \sigma_i^m \qquad (43)$$

where the σ_i are the observed fiber stresses at fracture. When the results of Equation (42) and (43), σ'_o = 821 psi and m = 5.94, were checked by a Chi-squared test the response was at the fifty percent level, indicating a very good fit.

For the loading shown in Figure 20, the beam-column solution is (ref. 4).

$$y = \frac{Q \sin k\,c}{P\,k \sin k\,\ell} \left[\sin k\,x + \sin k\,(\ell - x)\right] - \frac{Q\,c}{P} \qquad (44)$$

where $k = \sqrt{P/EI}$. In order to verify the assertion about the linear behavior of the beam up to its cracking load, deflections were measured for one beam. The cracking load was observed to be 702 pounds accompanied by a center deflection of .183 inches. Substituting into Equation (44) the appropriate values:

Q = 702 pounds	$E = 2.8 \times 10^6$ psi
ℓ = 45 inches	$I = 3.26$ in^4
c = 7.5 inches	P = 10,000 pounds
$x = \ell/2 = 22.5$ inches	$k = .0321$ in^{-1}

we find y = .179 inches, a satisfactory agreement.

The bending stress in the outer fiber can be found by differentiating Equation (44).

$$\sigma = \frac{M(d/2)}{I} = \frac{d}{2I}\,(-EI\,y'') \qquad (45)$$

$$= \frac{Edk}{2P} \frac{\sin kc}{\sin k\ell} Q \left[\sin kx + \sin k(\ell - x)\right]$$

In a manner analogous to that used in developing Equation (39) one can find the risk of rupture to be

$$B = \frac{bd}{2(m+1)\sigma_o{}^m} \int_c^{\ell-c} \frac{\left[\sigma(x)-\sigma_p\right]^{m+1}}{\sigma(x)} \, dx \qquad (46)$$

Using the transformation $w = x-\ell/2$ and the symmetry about the centerline this can be written as

$$B = \frac{bd}{(m+1)} \left(\frac{\sigma_p}{\sigma_o}\right)^m \int_o^{\ell/2-c} \frac{(\sigma/\sigma_p-1)^{m+1}}{\sigma/\sigma_p} \, dw \qquad (47)$$

To normalize the integral we can use $z = (2/L)w$, leading to:

$$B = \frac{bdL}{2(m+1)} \left(\frac{\sigma_p}{\sigma_o}\right)^m \int_o^1 \frac{(\sigma/\sigma_p-1)^{m+1}}{\sigma/\sigma_p} \, dz \qquad (48)$$

or in the notation of Equation (42),

$$B = \frac{1}{(m+1)} \left(\frac{\sigma_p}{\sigma_o}\right)^m \int_o^1 \frac{(\sigma/\sigma_p-1)^{m+1}}{\sigma/\sigma_p} \, dz; \quad \sigma \geq \sigma_p \qquad (49)$$

Using Equation (45) to find the σ associated with any value of Q, Equation (49) can be evaluated numerically. Substitution into Equation (38) will give the probability of failure for any load Q. The results are shown in Figure 23 along with the test results. Bearing in mind that only 26 prestressed beam tests were run, the predicted failure probabilities are fairly well borne out.

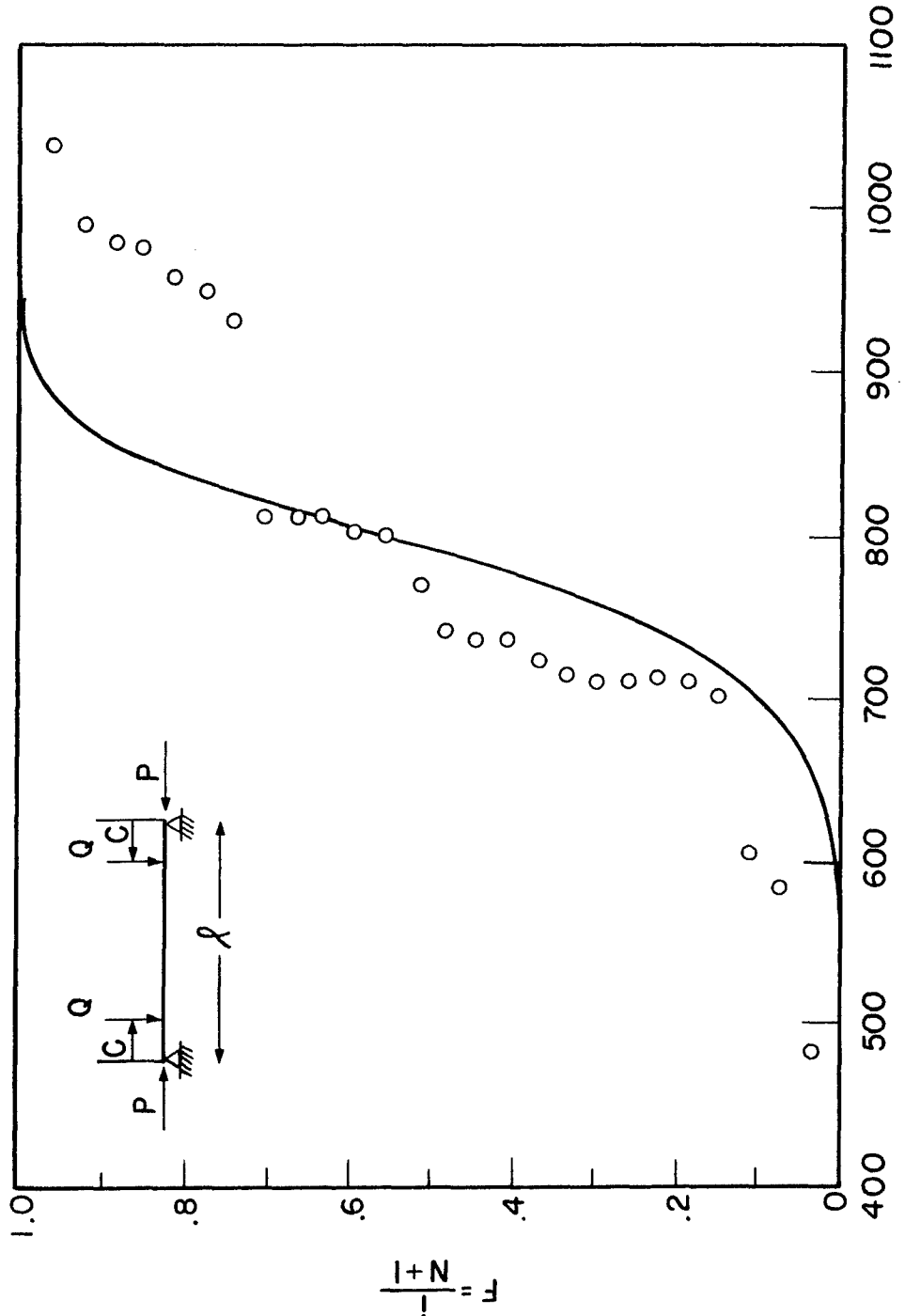

Figure 23 Probability of Failure for Prestressed Beams

III. SEGMENTED COLUMNS

The study of segmented columns in brittle materials is motivated in part by the enormous potential of ceramics for resisting buckling and compressive fracture and in part for the relationship that exists between column behavior and bending behavior. There are two intrinsic properties of segmented columns that demand special attention. First, the column has no tension resistance and, consequently, we must modify the classical formulation of the buckling problem. Second, the imperfect interface contract that exists between segments gives rise to statistical column behavior. Furthermore, rough interfaces cause uneven loading across the segments which induces tensile stresses in directions transverse to the axial compression. The problems of stability, statistics, and strength are studied in this chapter.

A. Buckling - Perfectly Flat Interfaces

For the particular case of a rectangular cross section with perfect contact between segments, a static buckling analysis of a segmented column will be developed. The column, illustrated in Figure 24, is assumed to be acted upon only by the steady (nonfollower) forces F a distance e from the column's original neutral axis. It is also assumed that the number of segments is very large and that the segment material is entirely linear elastic. Under these assumptions, solutions are found in this section for the static beam deflection equations describing the behavior of the segmented beam-column. It is observed that when

$$F \rightarrow F_b = \frac{4\ EI_o}{L^2}\left[\cos^{-1}\left(\frac{6e}{\sqrt{5}\ d}\right)\right]^2 \qquad (50)$$

the deflections become unbounded. Also it is observed that

$$\lim_{e \rightarrow 0} F_b = \frac{\pi^2\ EI_o}{L^2}$$

which is the classic Euler buckling load for a monolithic column.

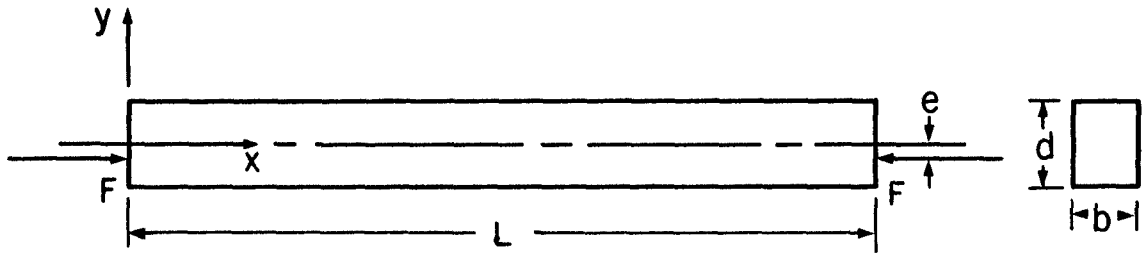

a) Column Geometry

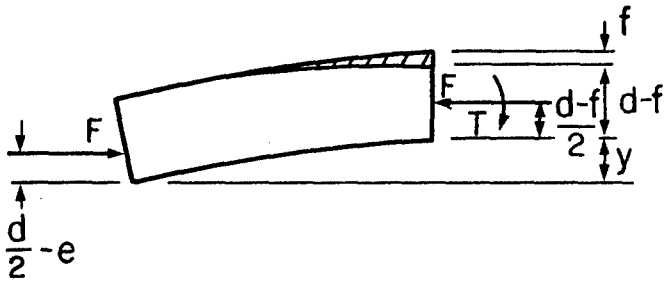

b) Free Body For Determination Of Resultant Moment T

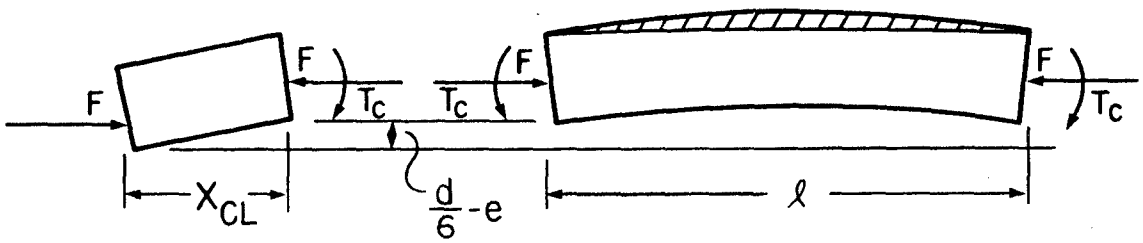

c) Free Body Diagrams For Cracked And Uncracked Regions

Figure 24 Eccentrically Loaded Segmented Column

The development of this solution will now be presented. Referring to Figure 24 , the resultant moment acting upon an arbitrary section of the column is found to be

$$T(x) = F\left[y(x) + e - \frac{1}{2} f(x)\right] \tag{51}$$

The governing differential equation for the deflection curve from elementary beam theory is

$$EI(x) \frac{d^2y}{dx^2} = - T(x) \tag{52}$$

The relationships for the crack penetration into a rectangular cross section apply in this case, thus

$$\begin{aligned} f(x) &= 0 && \text{for } T(x) \leq T_c \\ f(x) &= d - \frac{6T(x)}{F} && \text{for } T(x) \geq T_c \end{aligned} \tag{53}$$

where the resultant moment for incipient cracking, T_c, is given by

$$T_c = \frac{Fd}{6} \tag{54}$$

The local moment of inertia is given by

$$\begin{aligned} I(x) &= I_o = \frac{bd^3}{12} && \text{for } T(x) \geq T_c \\ I(x) &= 18b \left[\frac{T(x)}{F}\right]^3 && \text{for } T(x) \geq T_c \end{aligned} \tag{55}$$

Using Equation (51) and (54), Equation (53) may be expressed as

$$\begin{aligned} &\text{when } y < \frac{d}{6} - e \text{ then } T(x) < T_c \text{ and } f(x) = 0 \\ &\text{when } y = \frac{d}{6} - e \text{ then } T(x) = T_c \text{ and } f(x) = 0 \\ &\text{when } y > \frac{d}{6} - e \text{ then } T(x) > T_c \text{ and } f(x) > 0 \end{aligned} \tag{56}$$

Consequently, the analysis will depend upon which of the following two cases exists: (1) entire column uncracked, (2) portion of column cracked.

Case (1): $f(x) \equiv 0$

In this case the differential equation, Equation (52), reduces to

$$\frac{d^2y}{dx^2} + k^2y = - k^2e \tag{57}$$

where

$$k^2 = \frac{F}{EI_o} \tag{58}$$

The boundary conditions are simply

$$y(0) = y(L) = 0 \tag{59}$$

The solution to Equation (57) and (59) is readily found to be

$$y(x) = e \left[\frac{\cos k \left(x - \frac{L}{2}\right)}{\cos \frac{k L}{2}} - 1 \right] \tag{60}$$

Equation (60) will be valid as long as $y_{max} \leq \frac{d}{6} - e$. For $y_{max} = y\left(\frac{L}{2}\right) = \frac{d}{6} - e$, the limiting load is found to be

$$F = \frac{4 E I_o}{L^2} \left[\cos^{-1} \left(\frac{6e}{d} \right)\right]^2 \tag{61}$$

Case (2): $f(x) \not\equiv 0$

In this case solutions must be found in both the cracked and uncracked regions and forced to match displacements and slopes on the boundaries between the regions. Referring to Figure 24c, $x = x_{cL}$ locates the left boundary between the regions. Note that $T(x_{cL}) = T_c$ and $y(x_{cL}) = \frac{d}{6} - e$. By symmetry $x_{cR} = L - x_{cL}$ and thus $\ell = x_{cR} - x_{cL} = L - 2x_{cL}$.

In the uncracked region, $0 \leq x \leq x_{cL}$, the solution found in Case (1) still applies, thus

$$y(x) = e\left[\frac{\cos k\,(x - \frac{L}{2})}{\cos \frac{k\,L}{2}} - 1\right] \tag{62}$$

Using the fact that $y(x_{cL}) = \frac{d}{6} - e$, Equation (62) yields

$$\ell = \frac{2}{k} \cos^{-1}\left(\frac{d}{6e} \cos \frac{k\,L}{2}\right) \tag{63}$$

In the cracked central region ℓ it is readily shown that the differential equation, Equation (52), becomes

$$\frac{d^2y}{dx^2} = - h\,(y + e - \frac{d}{2})^{-2} \tag{64}$$

where

$$h = \frac{2\,F}{9\,b\,E} \tag{65}$$

Equation (64) may be integrated once to yield

$$\left(\frac{dy}{dx}\right)^2 = 2\,h\,(y + e - \frac{d}{2})^{-1} + c \tag{66}$$

The fact that it is known a priori that $y(x_{cL}) = \frac{d}{6} - e$ enables c to be determined at this point by matching slopes and displacements in Equation (62) and (66). Using this value for c and Equation (65) for ℓ, Equation (66) becomes

$$\left(\frac{dy}{dx}\right)^2 = k^2\,e^2\left[\left(\cos \frac{k\,L}{2}\right)^2 - \frac{d^2}{36e^2}\right] + 2\,h\left[(y + e - \frac{d}{2})^{-1} - \frac{3}{d}\right] \tag{67}$$

Using the fact that

$$y_{max} = y\left(\frac{L}{2}\right) \tag{68}$$

and

$$\left.\frac{dy}{dx}\right|_{x = \frac{L}{2}} = 0$$

Equation (67) may be solved for y_{max}, thus

$$y_{max} = y\left(\frac{L}{2}\right) = \frac{d}{2} - e + d\left\{\frac{15}{4} - 3\left[\frac{3e}{d\cos\frac{kL}{2}}\right]^2\right\}^{-1} \tag{69}$$

Inspection of Equation (69) reveals that y_{max} becomes unbounded when the term inside the braces approaches zero, i.e., when

$$k = \frac{2}{L}\cos^{-1}\left(\frac{6e}{\sqrt{5}\,d}\right)$$

or

$$F = F_b = \frac{4EI_o}{L^2}\left[\cos^{-1}\left(\frac{6e}{\sqrt{5}\,d}\right)\right]^2 \tag{70}$$

We observe that in the limit as the eccentricity vanishes, F_b approaches the Euler buckling load for monolithic columns, thus

$$\lim_{e\to 0} F_b = \frac{\pi^2 E I_o}{L^2}$$

B. Nonflat Interface Problem

1. Area and length scaling.- Ideally, we would like to fabricate segmented structures from segments with perfectly flat interfaces; however, it may not be possible to obtain sufficient smoothness on practical size cross sections. Even in the case of our tungsten carbide gage blocks (one-half light band out of flat), we can still detect nonlinearity in our column response at low loads. At reasonable temperatures we may be able to approach monolithic behavior through the use of grout or gaskets between the segments. At elevated temperatures, however, these fillers may have to be dispensed with. It is for these applications that we will try to improve our understanding of the contact problem.

From a practical point of view, the alternative to full scale testing of segmented columns is to develop a scaling procedure that will enable us to predict the compression stress-strain diagrams for columns of any length and area from information obtained from a single segmented column. We begin our search for such a scaling law by examining the effects of column length. Let us assume that all the interfaces have been drawn from the same population and that for a specified axial stress there exists a frequency distribution for the interface contact areas. It follows, then, that the deflection of each segment will be a random variable which also possesses a frequency distribution. Now, the total deflection of a multi-segment column will represent the sum of the random deflections of the constituent blocks. Therefore, the frequency distribution of the responses of many nominally identical columns represents the distribution of the sums of the random segment responses. From the Central Limit Theorem of Statistics we are assured that the sums of random variables are normally distributed regardless of the form of the distribution for the random variables themselves. Thus, we can hypothesize that the stiffness of segmented columns of a given length and under a specified load are normally distributed.

On the basis that the stiffness of a given size multisegment column is normally distributed, we can proceed from the following

theorem to describe the scaling rule for length. Theorem (ref. 5): "If x is normally distributed with mean μ and standard deviation σ and a random sample of size n is drawn, then the sample mean $\bar{x}$ will be normally distributed with mean μ and standard deviation $\sigma/\sqrt{n}$." Evidence will be presented in the next section which supports the hypothesis of normality and the scaling of the scatter.

It is considerably more difficult to get a handle on the "column area" scaling problem and, because of a poorly executed experiment, our efforts in this study can hardly shed any light on this matter. We do, however, have a hypothesis that we feel is worth exploring. Let us examine the assumption that the interface contact is controlled primarily by the highest asperities on the surface. If the maximum asperity was measured on each of many nominally identical surfaces we could construct their frequency distribution. The resulting frequency curve represents the distribution of largest values in a sample of size n (or rather area A). Methods for scaling such distributions to larger areas are treated quite systematically by the methods of extreme value statistics. Assuming that the stiffness is inversely proportional to the maximum asperity heights, the stiffness distribution $F(E_t)$ might scale as the distribution of smallest values, i.e.,

$$F_L(E_t) = 1 - [1 - F_S(E_t)]^n$$

where the subscripts L and S refer respectively to the large and small area columns, E_t is the tangent modulus, and $n \equiv A_L/A_S$. This hypothesis conforms to our past observations that smaller area columns are stiffer.

2. Test results and interpretation.-

a. Description of Experiments: The study of column area and length scaling requires a data base of compressive stress-strain curves which we attempted to establish using segmented glass columns. To be sure that all segments would be drawn from the same population, they were all cut from the central region of a single

sheet of 1/4-inch window glass. Diamond core drills were used to accurately produce fifty circular disks of each of the diameters, 1/2, 1, 1-1/2, 2 and 3 inches. To fabricate a particular column, the appropriate size disks were randomly selected from a rotating "lazy Susan" on which they were scattered. For ease in handling and alignment, the columns were sheathed in thin paper tubes. Compressometers were attached to tabs glued to the edges of the top and bottom disks in the column as shown in Figure 25. These top and bottom segments were reused for all column tests of their diameter. Polyethylene pads were placed on the top and bottom of the columns which were then tested in a Riehle Universal Testing Machine. The load-deflection diagrams for 10, 20 and 30 segment columns were automatically recorded.

Seven typical load-deflection diagrams are shown in Figure 26 for two-inch diameter columns with 10 segments. To eliminate errors at low loads due to backlash in the automatic plotting equipment, only unloading curves were considered. The highly individual behavior associated with columns with nonflat interfaces is clearly illustrated in this figure. Three hundred and ninety such curves were obtained and the hypothesized statistical relationship which relates them was investigated by selecting the particular tangent modulus associated with the 120 psi compression level. This stress was selected because it fell close to the knee in most of the curves. Several methods were studied for measuring the slope of such curves - two optical devices, a graphical technique, fitting a tangent by eye, and parabolic interpolation. All of the methods gave reasonable results; but, the latter method was finally selected since it produced the least scatter.

A simple computer program was used to fit the load-deflection curves with a parabola, to compute the slope at 120 psi, and to establish the mean and the standard deviation associated with each group of 30 tests representing a given column height and area. The tendency to buckle precluded testing of the 20 and 30 segment columns for the 1/2-inch diameter disks. The cumulative distribution curve for the tangent modulus of each size column was plotted

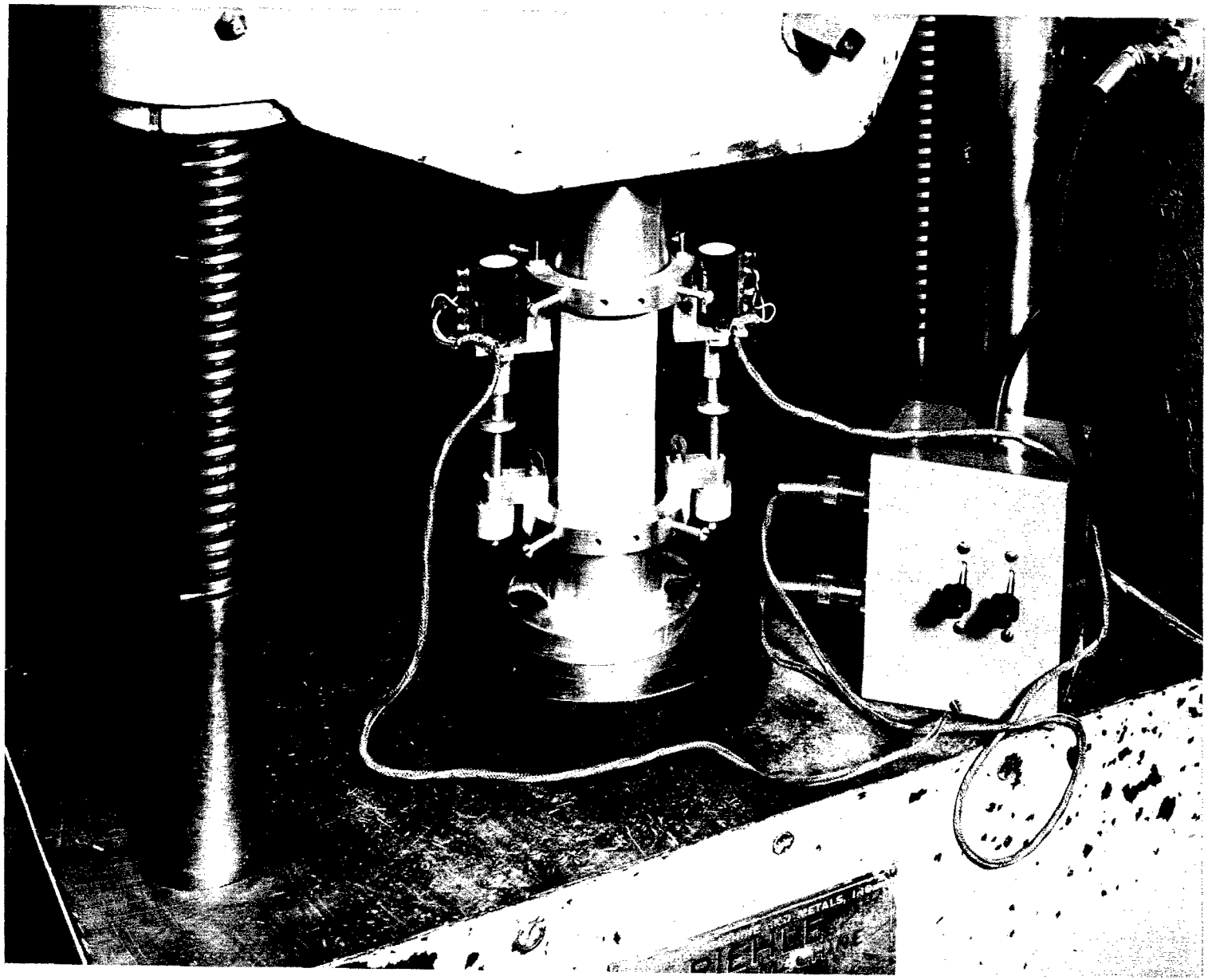

Figure 25 Segmented Glass Columns
(20 segment, 2 inch diameter)

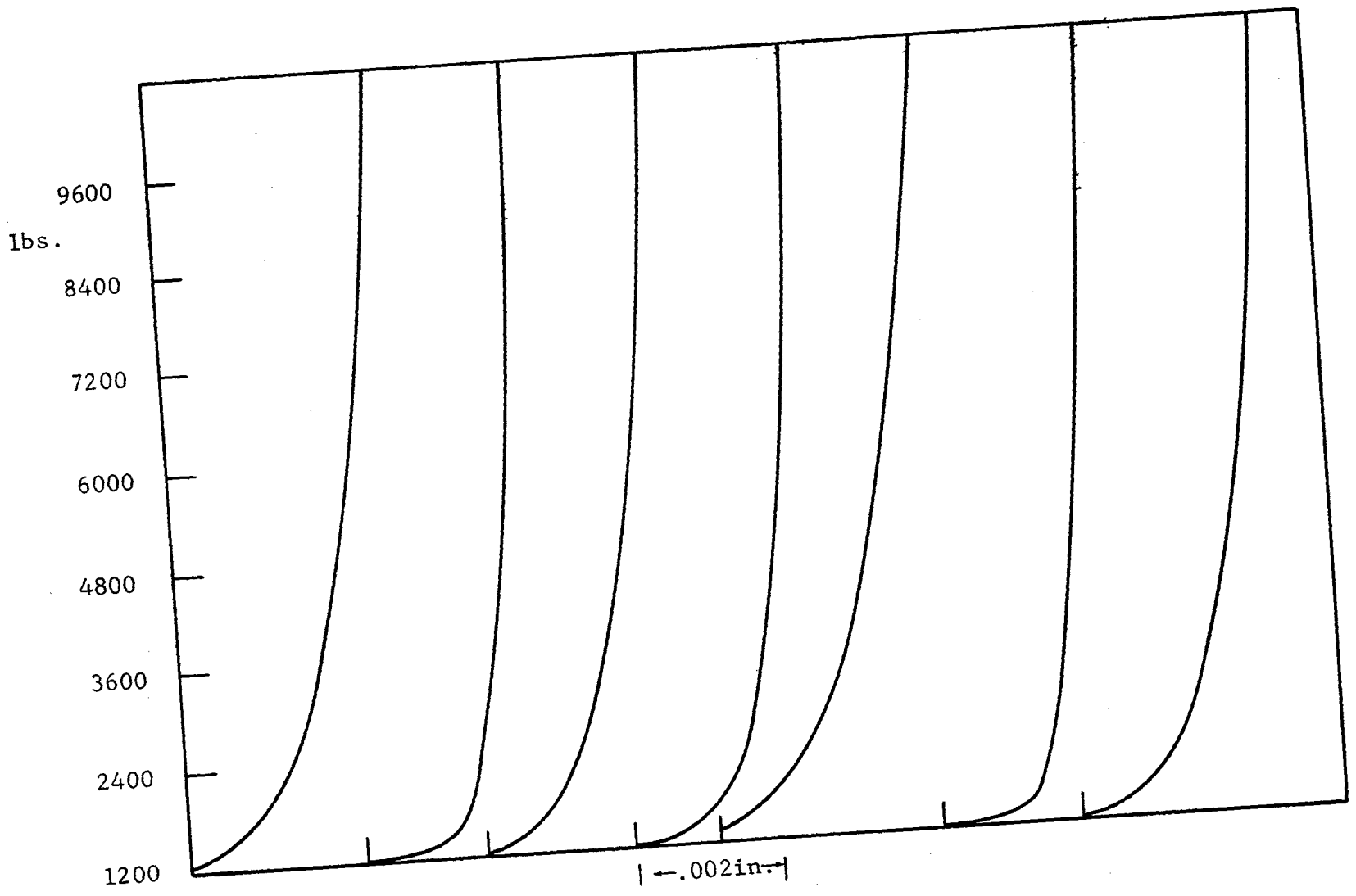

Figure 26 Load-Deflection Diagrams for Segmented Glass Columns (10 segments, 2 in. diameter)

on "Normal Probability Paper" and in every case a linear relationship was obtained which establishes the validity of our normality hypothesis. Typical distribution curves are shown in Figure 27 for the two-inch diameter column. The solid lines represent the normal curves generated from the computed mean and standard deviations of the data. Table 1 tabulates the means and the coefficients of variation (standard deviation ÷ mean) for each size column.

b. Interpretation of results: Referring all our remarks to Table 1, we first observe that no consistent pattern develops vertically for either the mean or the coefficient of variation. In view of the large scatter, as represented by the very high coefficients of variation, this unexpected result may have occurred by chance alone. On the other hand, the data may be in error. Examining the parameters in the horizontal direction reveals that the mean values consistently increase with increasing column height and, except for the three-inch column, the coefficients of variation uniformly decrease. Since we cannot attribute a consistent trend in 390 observations to chance, we must accept the possible presence of a systematic error.

Recalling that the entire column and not just the central portion, was used as the gage length, one suspects the influence of "end effects." In particular, since a properly run test would have a minimum of one diameter of segments outside of the gage length on the top and bottom, it seems reasonable to suggest that the Polyethylene pads that were used were too flexible. Furthermore, this flexibility is of a different character than we would experience with glass end segments. The influence of such pads should decrease with increasing column height and this should lead to increasing stiffness. This is, of course, exactly what we observe. Also, since the same Polyethylene pads and glass end disks were used for all columns of equal area, we would anticipate that the "end effect" would be reasonably constant for each of the five diameters.

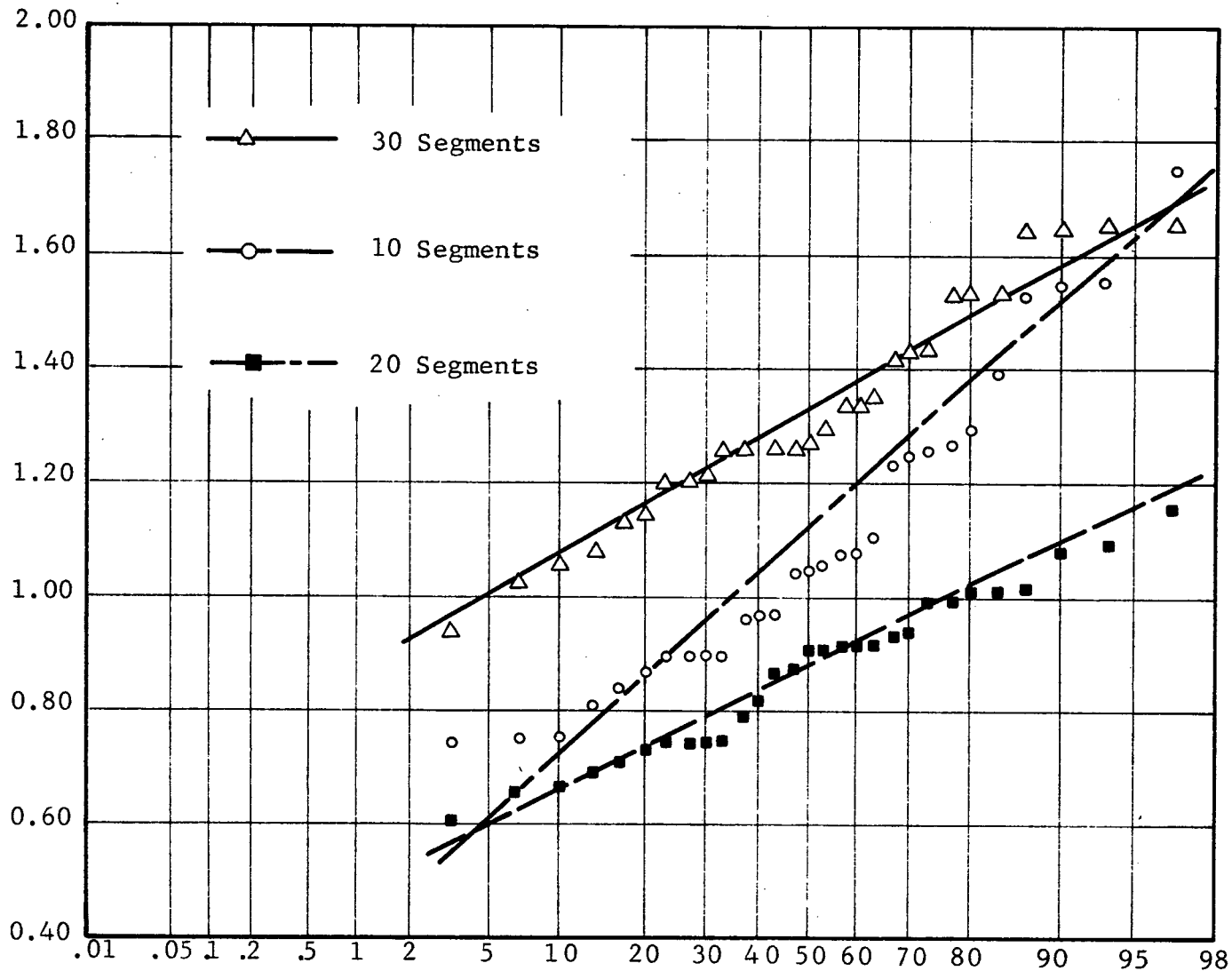

Figure 27 Tangent Modulus Distribution Plotted on Normal Probability Paper

TABLE 1

NORMAL DISTRIBUTION PARAMETERS FOR THE TANGENT MODULUS OF SEGMENTED GLASS COLUMNS AT 120 psi COMPRESSION

Diameter	Measure Quantity	Column Height (Number of Segments)		
		10	20	30
1/2"	mean, 10^6 psi coef. var.	0.92 28.0 %	Buckling	Buckling
1"	mean, 10^6 psi coef. var.	1.12 27.5 %	1.33 9.1 %	1.45 8.0 %
1-1/2"	mean, 10^6 psi coef. var.	0.63 21.0 %	0.96 14.1 %	1.12 12.0 %
2"	mean, 10^6 psi coef. var.	0.70 28.6 %	0.88 19.1 %	1.33 14.9 %
3"	mean, 10^6 psi coef. var.	0.93 10.7 %	0.93 10.8 %	1.12 13.2 %

Our contention that "end effects" influenced the behavior of the segmented columns was briefly examined by testing an aluminum rod using the identical procedures employed for the segmented glass columns. The rod was 10 inches in length with a two-inch diameter and the initial portion of its stress-strain curve turned out to be curvilinear. The proper result was recorded when the compressometer attachments were remote from the ends. Summarizing then, we feel that our measurements of the mean tangent modulus do not indicate the "pure" behavior of the segmented columns and that the standard deviations are fair approximations. On this basis we examined the possibility of scaling the coefficients of variations of various height columns and the results are tabulated in Table 2. According to our hypothesis, this quantity should scale as $1/\sqrt{n}$. Table 2 shows excellent agreement with this theory for the 1-1/2 and 2-inch diameter columns and for the average. This result together with the normality demonstration of Figure 27 tends to support our column height scaling hypothesis. Unfortunately, no conclusions can be drawn about the area scaling. Future experiments with segmented columns should incorporate the following improvements:

(1) Employ larger sample size in view of the large scatter observed.

(2) Compressometer attachments should be kept in the interior of the column.

(3) Digital output devices should be utilized.

C. Backbone Column

It was established in the first phase of this program that imperfect contact between the interface of a segmented column caused transverse stresses upon application of axial loads. These transverse stresses were compressive near the interfaces and tensile in the interior of the segment. Consequently, it appeared that if the lateral geometry of the segments could be appropriately altered, we might induce compression in the interior and tension near the interfaces of the segments. Thus, the two affects would tend to cancel

TABLE 2

MEASURED AND PREDICTED VALUES FOR THE COEFFICIENT OF VARIATION OF STIFFNESS FOR SEGMENTED GLASS COLUMNS

Diameter		Column Height (Number of Segments)		
		10	20	30
1"	Measured	27.5%	9.1%	8.0%
	Theory	27.5%	19.4%	15.9%
1-1/2"	Measured	21.0%	14.1%	12.0%
	Theory	21.0%	14.8%	12.1%
2"	Measured	28.6%	19.1%	14.9%
	Theory	28.6%	20.2%	16.5%
3"	Measured	10.7%	10.8%	13.2%
	Theory	10.7%	7.6%	6.2%
Average	Measured	22.0%	13.3%	12.0%
	Theory	22.0%	15.5%	12.7%

one another and thereby give rise to a segmented column with a higher strength to weight ratio than a prismatic column. The geometry selected for this experiment is shown in Figure 28, together with a cylindrical segment of the same height and interface area. This latter specimen was used to establish a group of control columns.

Using the procedures outlined in Appendix B, Hydrostone Gypsum specimens were cast in each of the shapes shown in Figure 28. With the simple setup shown in Figure 29, the ultimate compressive strength of 54 three-segment columns were obtained. The physical and mechanical properties of these columns are summarized in Table 3. It is of considerable interest that a number of columns tested developed longitudinal cracks through two or three of the segments. As shown in Figure 29, the cracks did not stop at the interfaces but passed into the next cylinder as if the column were continuous.

The backbone columns were tested in the same manner as the cylindrical columns as depicted in Figure 30. As indicated in Table 3 the strength-weight ratio of the backbone column is not significantly higher than the control column. Furthermore, the mode of failure casts doubt upon any possible superiority of the backbone specimen. Prior to ultimate fracture, the lips or flanges on the dogbone segments were stripped off leaving a prismatic column of smaller diameter. It would then appear that the higher strength-weight ratio is attributable to a size effect and not a geometry effect.

When stress concentrations appear in a compressive field it is possible to achieve "intelligent behavior" from materials which usually sustain no stress redistribution mechanism. In addition to the dogbone specimen, another example of such behavior was described to the author by H. A. Perry of the Naval Ordnance Laboratory. Glass spheres were fabricated from two hemispheres that were attached in such a way that a bead appeared around the equator on the inside. When the sphere was submerged in the ocean, the bead was stripped off and appeared as chips in the bottom of the sphere.

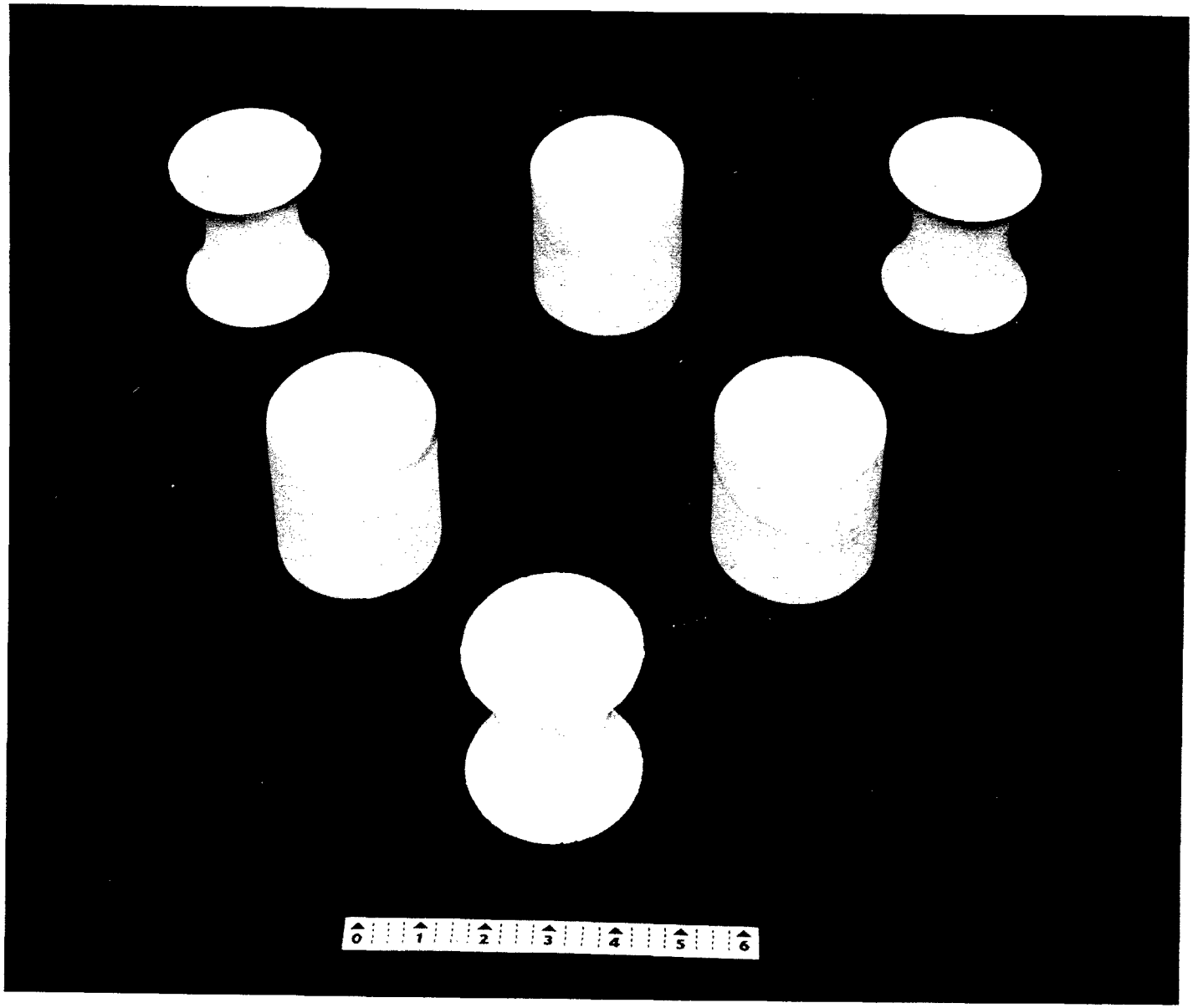

Figure 28 Example of Cylinder and Backbone Specimens

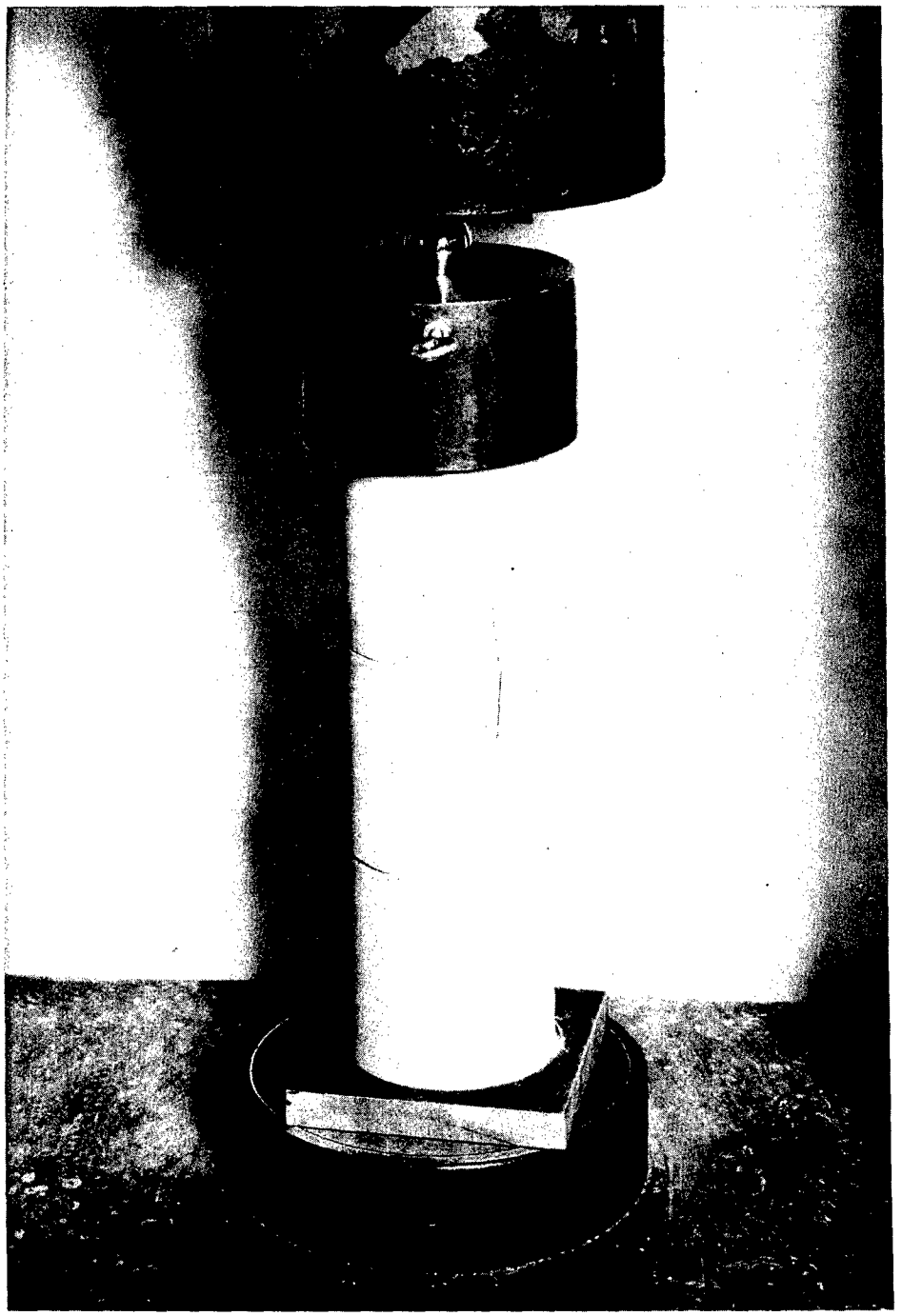

Figure 29 Test Setup for Cylindrical Columns

TABLE 3

PHYSICAL PROPERTIES OF CYLINDRICAL AND BACKBONE COLUMNS

Physical Properties	Cylindrical	Backbone
Interface Diameter	3 in	3 in
Segment Height	3 in	3 in
Segment Weight	593.6 gm	333.67 gm
Number of Segments	3	3
Avg. Ult. Compressive Strength	16989 lbs	9580 lbs
Avg.Strength-Weight Ratio	28.6 $\frac{\text{lbs}}{\text{gm}}$	38.7 $\frac{\text{lbs}}{\text{gm}}$
Material	Hydrostone	Hydrostone
Number of Columns Tested	54	46
Central Diameter	3 in	3 in

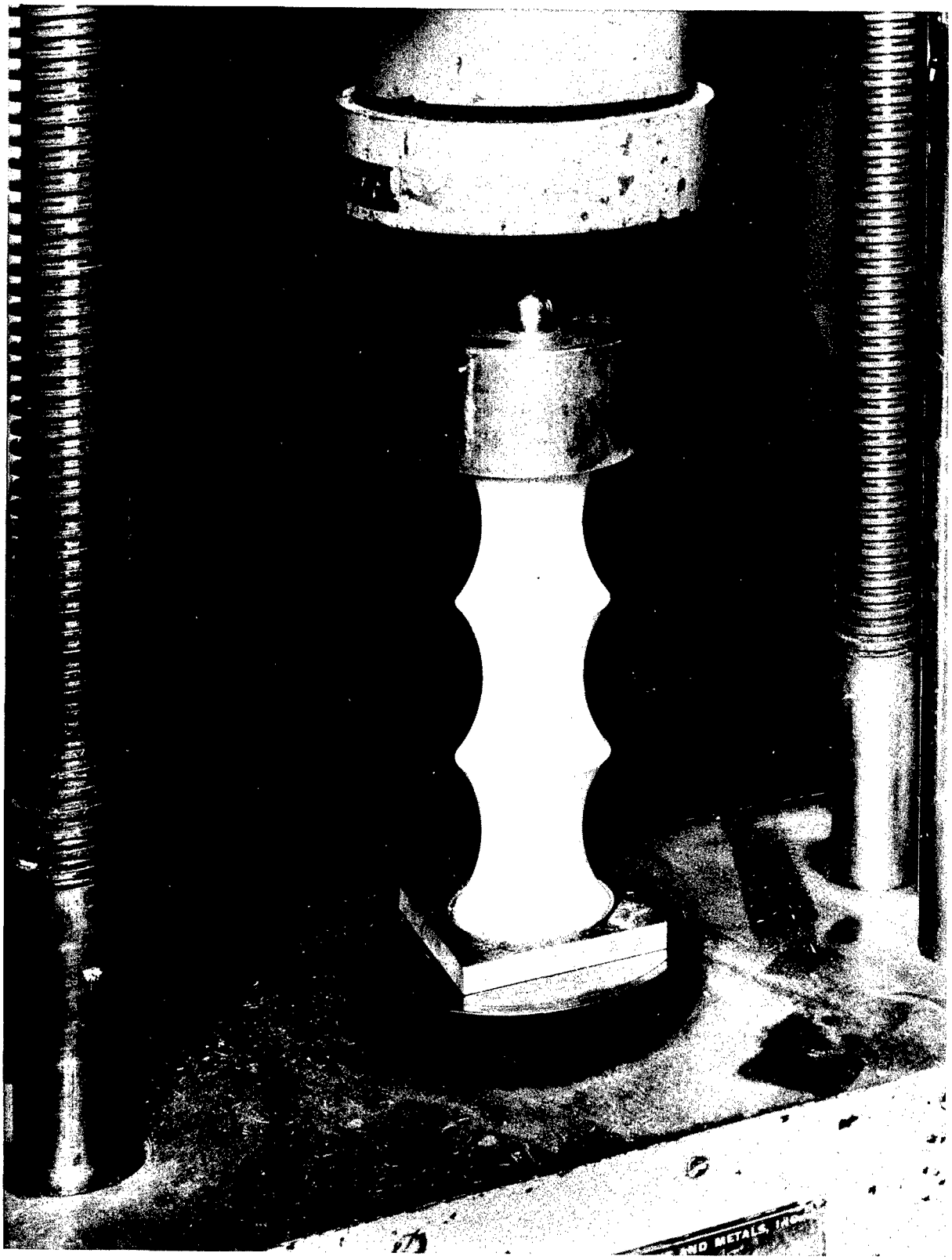

Figure 30 Test Setup for Backbone Columns

As a final observation concerning the backbone specimen we note that this shape makes it possible to apply a lateral prestress to a column using straps at a small number of locations. This idea is illustrated in Figure 31. Such structures may have advantages over jacketed or continuously wound columns. The bulkier prestressing tendons may be less fragile, easier to insulate, or require fewer attachments. A similar method of prestressing is briefly discussed in Section V for the ogive shell.

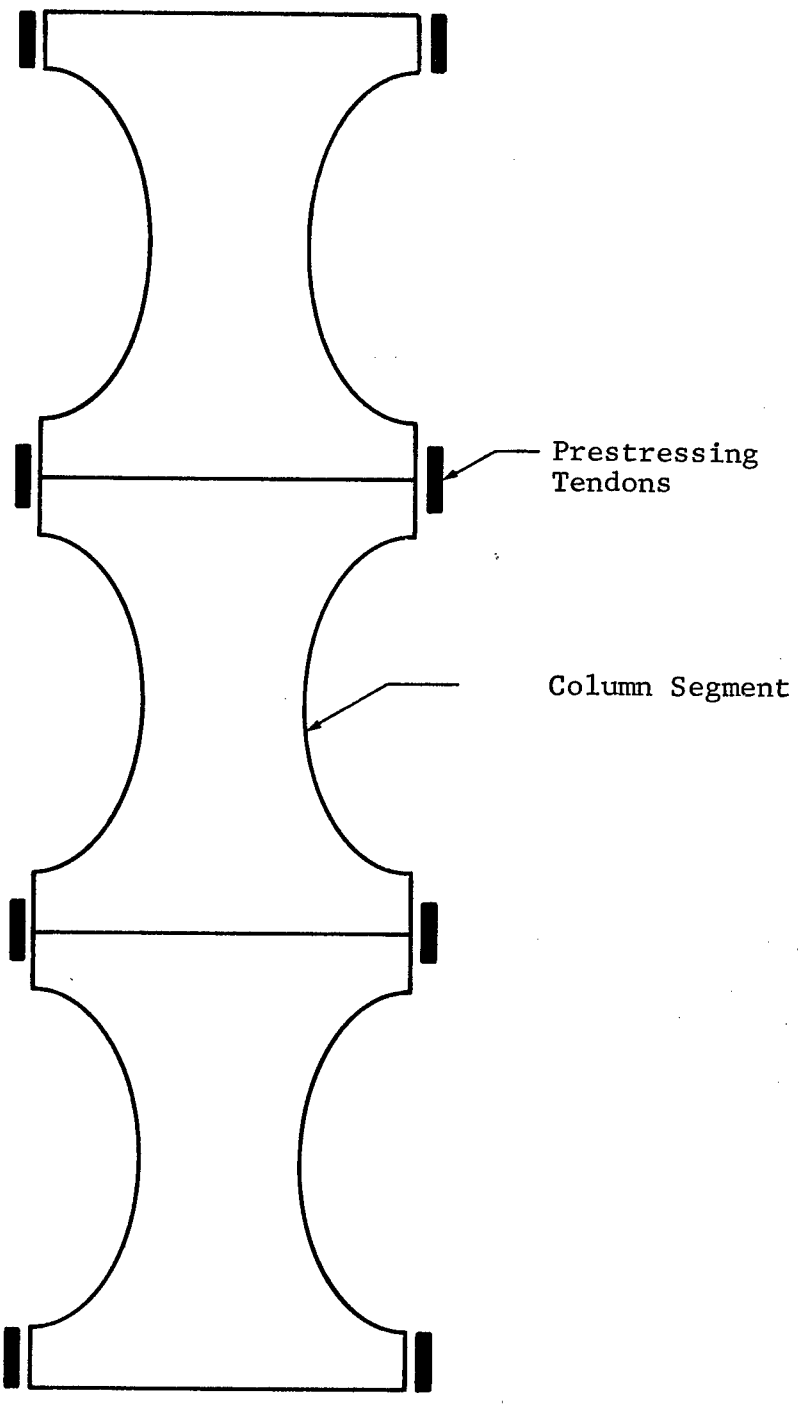

Figure 31 Laterally Prestressed Backbone Column

IV. PRESTRESSED PLATES

The similarity between prestressed segmented beam behavior and that of ductile bending made it possible to successfully apply the techniques of limit analysis to describe the ultimate load carrying capacity of prestressed segmented beams. The extension of these techniques to prestressed segmented plates is investigated in this section. Preliminary experiments are conducted using both monolithic and segmented circular plates.

A. Segmented Plates

If a circular plate is subjected to a uniform radial pressure around its periphery, a homogeneous isotropic state of plane compressive stress σ_o is introduced into the plate. Any and all cracks in such a plate will tend to close up, and in particular, the ultimate bending resistance along such cracks will be calculated in the same manner used for segmented beams. Referring to Figure 18 a, the limiting moment per unit length in a plate is simply

$$M_o = \frac{\sigma t^2}{2} \tag{71}$$

where σ is the stress acting normal to the crack interface and t is the plate thickness. We shall, of course, take σ as the prestress σ_p. This limiting moment capacity would not be effected by moments acting transverse to the crack which suggests the application of the square yield criterion shown in Figure 32 .

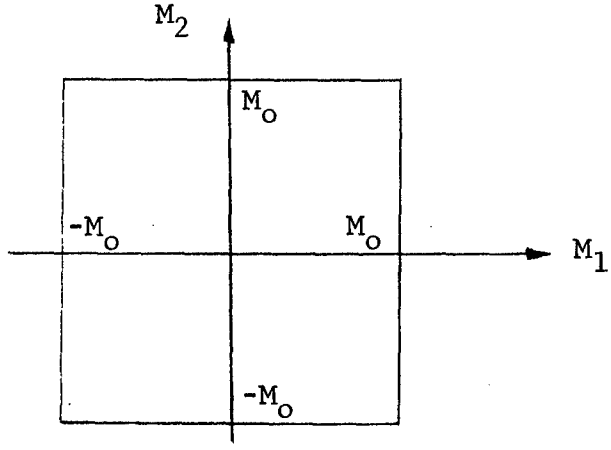

Figure 32 Square Yield Criterion

We shall use this criterion to analyze a circular plate of radius R which is simply supported on a circular ring of radius r and is subjected to a central load P brought onto the plate through a blunt circular rod of radius a. Assuming the yield (or crack) pattern shown in Figure 33, we observe that the loading die will ultimately contact the centerline of each segment at only one point a distance of a from the plate center. The loading at such points will be P/n where n is the number of segments. The virtual work done by these loads in the assumed displacement pattern is

$$n \left(\frac{P}{n} \right) \Delta \left(\frac{b-a}{b} \right)$$

The energy dissipated at the yield lines is given by

$$n R M_o 2\omega \sin \frac{\pi}{n}$$

Equating these virtual energies we obtain

$$n R \left(\frac{\sigma_p t^2}{2} \right) 2 \left(\frac{\Delta}{r \cos \frac{\pi}{n}} \right) \sin \frac{\pi}{n} = n \frac{P}{n} \Delta \left(1 - \frac{a}{r \cos \frac{\pi}{n}} \right)$$

or

$$P = \sigma_p t^2 n \tan \frac{\pi}{n} \left(\frac{R}{r - \frac{a}{\cos \frac{\pi}{n}}} \right) \qquad (72)$$

This load represents an upper bound on the true collapse load of the plate, and consequently, we should choose from among this class of collapse mechanisms the one which gives the lowest load. This occurs when $n \to \infty$, and hence,

$$P = \pi \sigma_p t^2 \left(\frac{R}{r-a} \right) \qquad n \to \infty \qquad (73)$$

The true collapse load is realized only when the correct yield pattern is chosen. In the present case, symmetry suggests that we have made the right choice.

We can cause yielding to occur along a finite number of radial lines by strengthening the material between them. We would expect

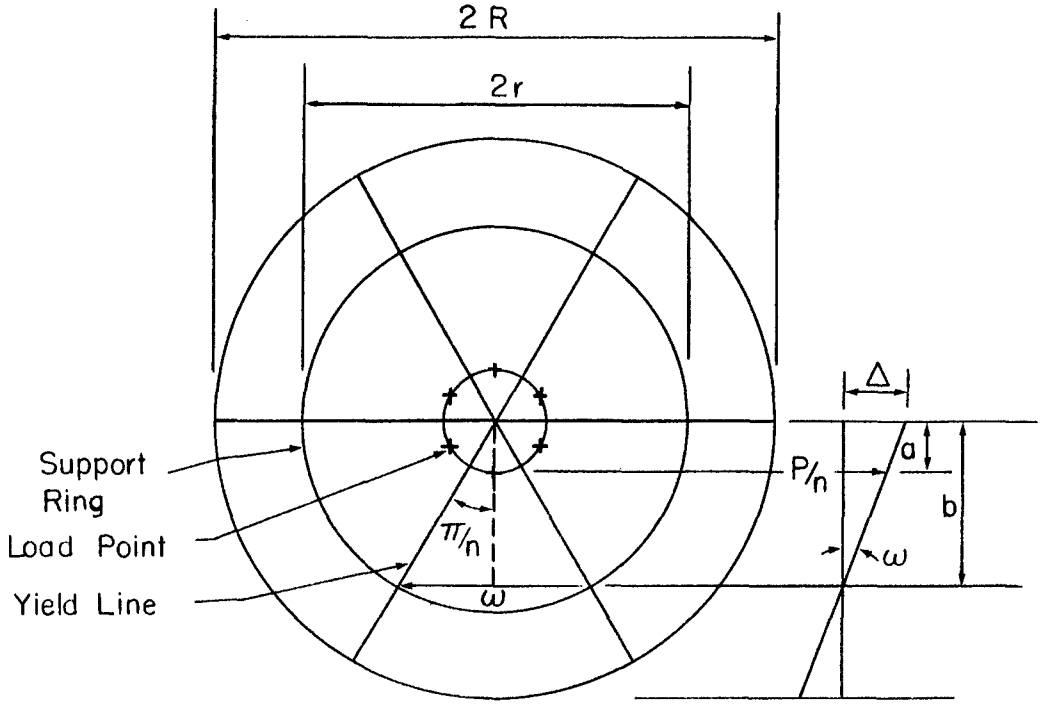

Deflection Of Load = $\Delta \left(\frac{b-a}{b}\right)$

Rotation $\omega = \frac{\Delta}{b} = \frac{\Delta}{r \cos \frac{\pi}{n}}$

Radial Rotation Component = $2\omega \sin \frac{\pi}{n}$

$b = r \cos \frac{\pi}{n}$

Figure 33 Collapse Pattern for a Circular Plate

the capacity of the plate to increase with such a procedure and this is exactly what Equation (72) predicts. As we force failure to occur along fewer and fewer lines, the required strength of the segments will correspondingly increase. As a rule, to avoid fracturing the elements in a segmented component we should select segment geometries that approximate the true yield patterns for the structure. An extensive treatment of limit analysis of plate structures can be found in Wood (ref. 6).

To establish the potential of the proposed analysis procedure, we constructed two segmented circular plates using eight Hydrostone plaster segments in each. The prestressing was accomplished by making a double wrap of steel strapping about the periphery of the plate as shown in Figure 34 , and tightening with a standard banding tool until yielding occurred near the grip. Seven monolithic plates and two segmented plates were prestressed in this way and the resulting strains in six of the plates were recorded by radially positioned electrical resistance foil strain gages. The strain gage readings and measured loads for these plates are tabulated in Table 4 . The support fixture and loading setup are shown in Figures 35 and 36 respectively. The load deflection diagrams for the segmented beams are shown in Figure 37 where we observe well defined horizontal regions. Upon unloading, we obtained complete deflection recovery with only occasional chipping at the segment edges.

As evidenced from Table 4 , the straps did not apply a uniform radial prestress; however, since care was taken to tighten the straps in the same way for all cases, it is felt that the average prestrains in the various plates were about the same. On this basis, the prestrain was taken as the average at sixteen gage readings, i.e., 49.4×10^{-6} inch/inch. Using this value together with the plate properties tabulated in Table 5 , Equation (72) predicts a yield load of $P = 309$ lb. This value differs from the measured values of 270 lb and 288 lb by 14.4 percent and 7.3 percent respectively.

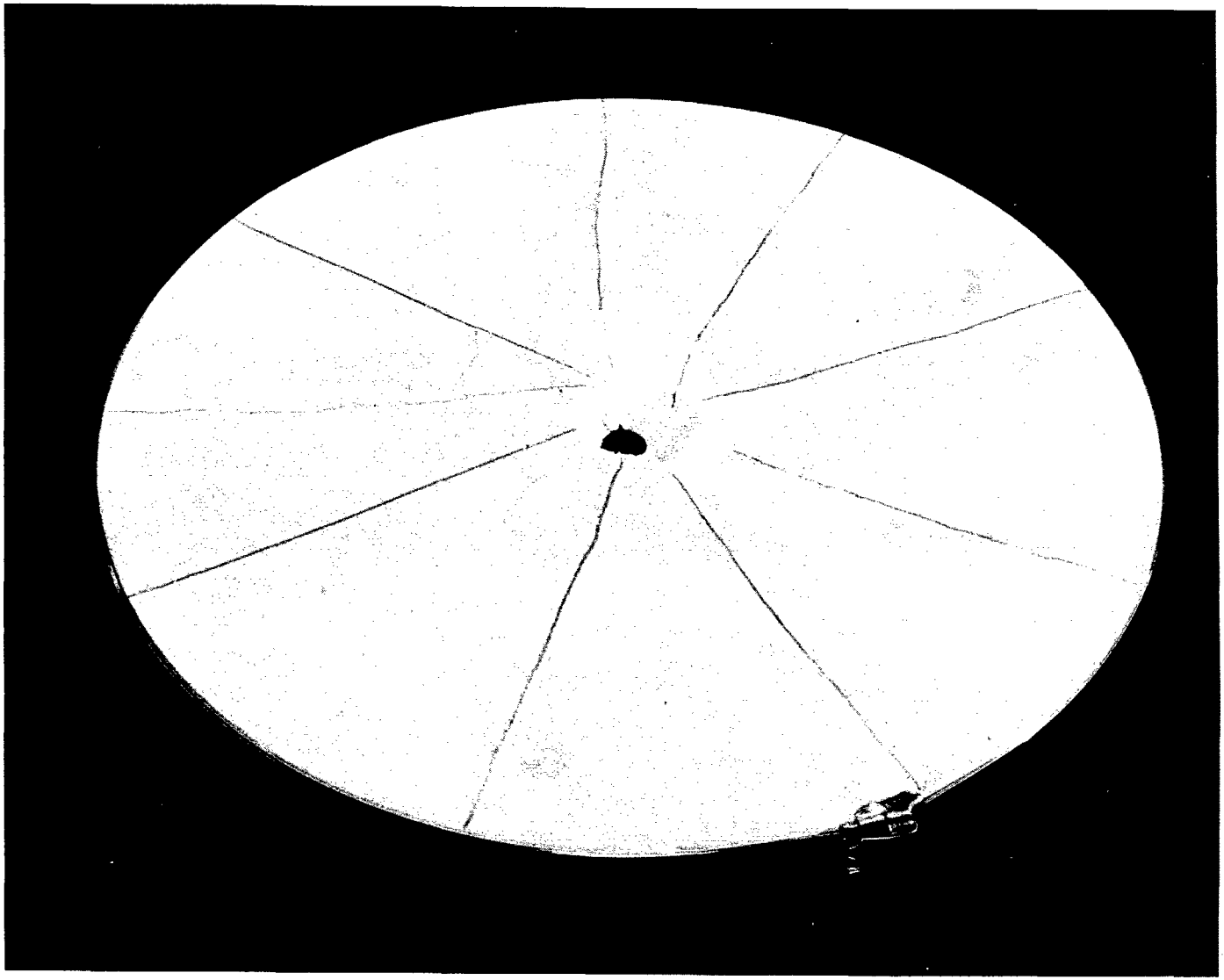

Figure 34 Prestressed Monolithic Circular Hydrostone Plaster Plate

TABLE 4

PRESTRESSED MONOLITHIC AND SEGMENTED CIRCULAR PLATE STRENGTHS

Plate Number	Strain x 10^{-6} in./in.			Yield Load (lb)	Ultimate Load (lb)
	a	b	c		
Monolithic 1	defect.	50	45	400	540
Monolithic 2	70	55	65	345	582
Monolithic 3	30	50	55	370	520
Monolithic 4	40	45	55	410	624
Monolithic 5	60	70	defect.	330	706
Monolithic 6	no gages			300	535
Monolithic 7	no gages			350	430
Segmented 1	50	40	10	270	---
Segmented 2	no gages			288	---

Average Strain Gage Reading: 49.4×10^{-6} in./in.

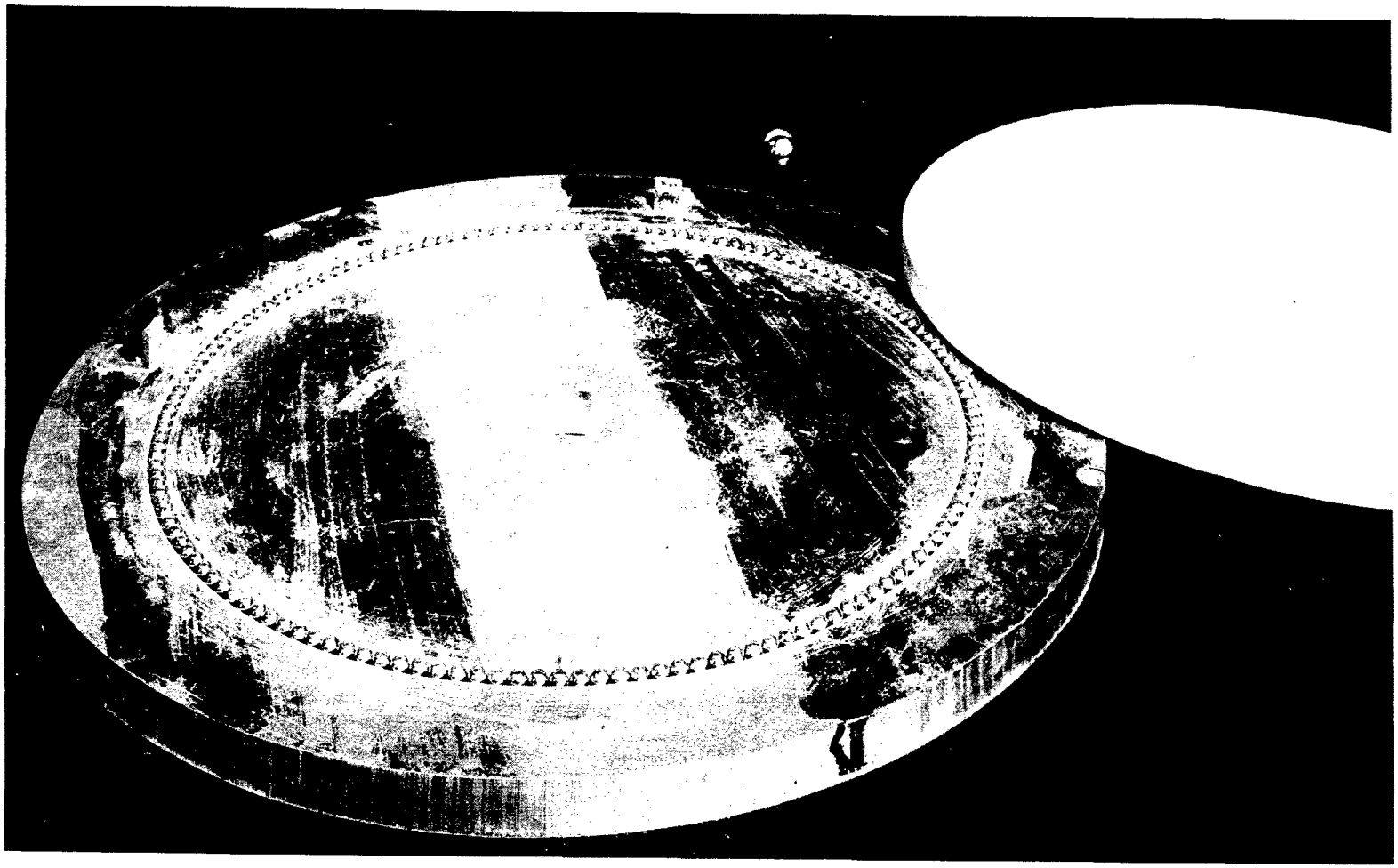

Figure 35 Ring Support for Circular Plates

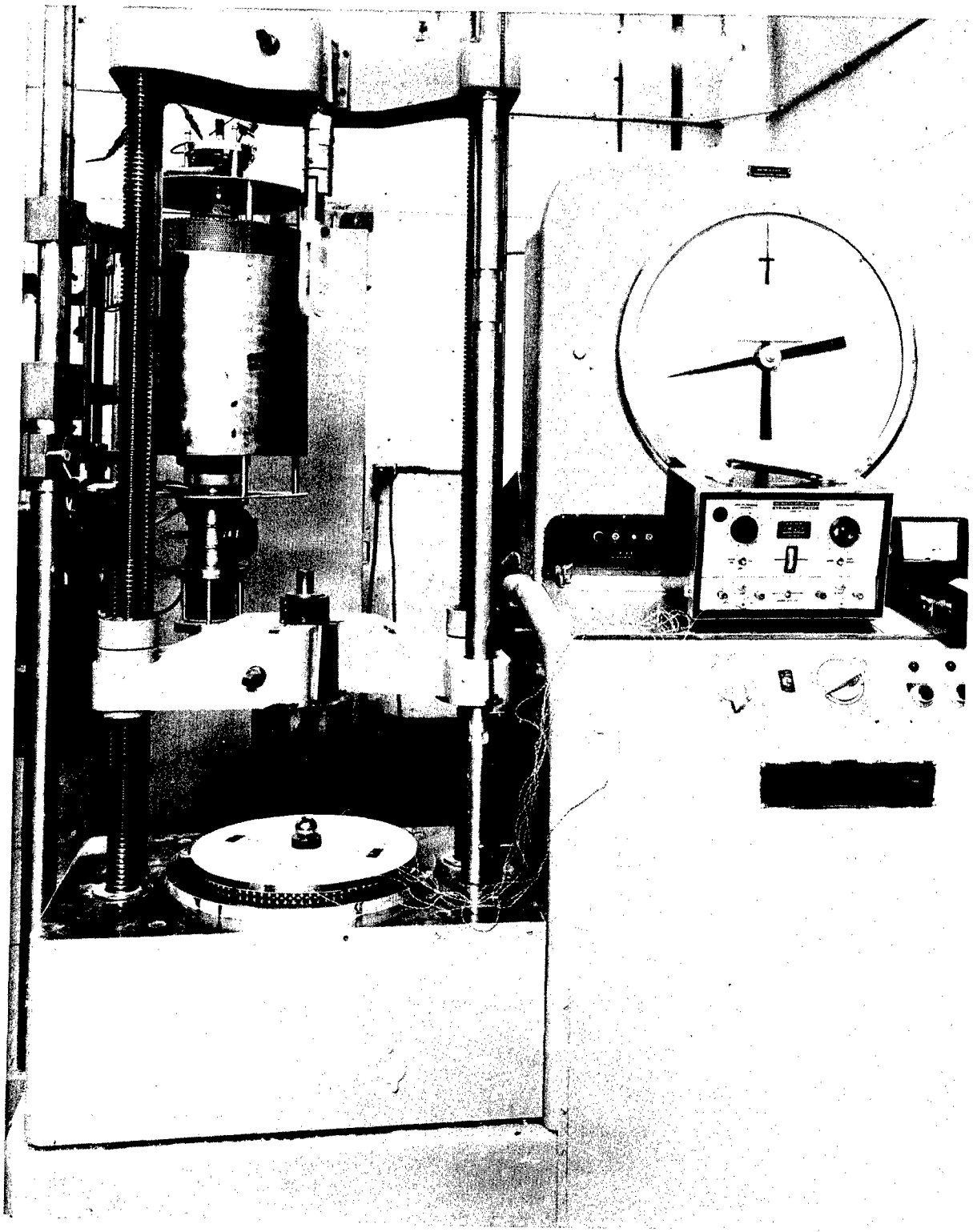

Figure 36 Test Setup for Loading Circular Plates

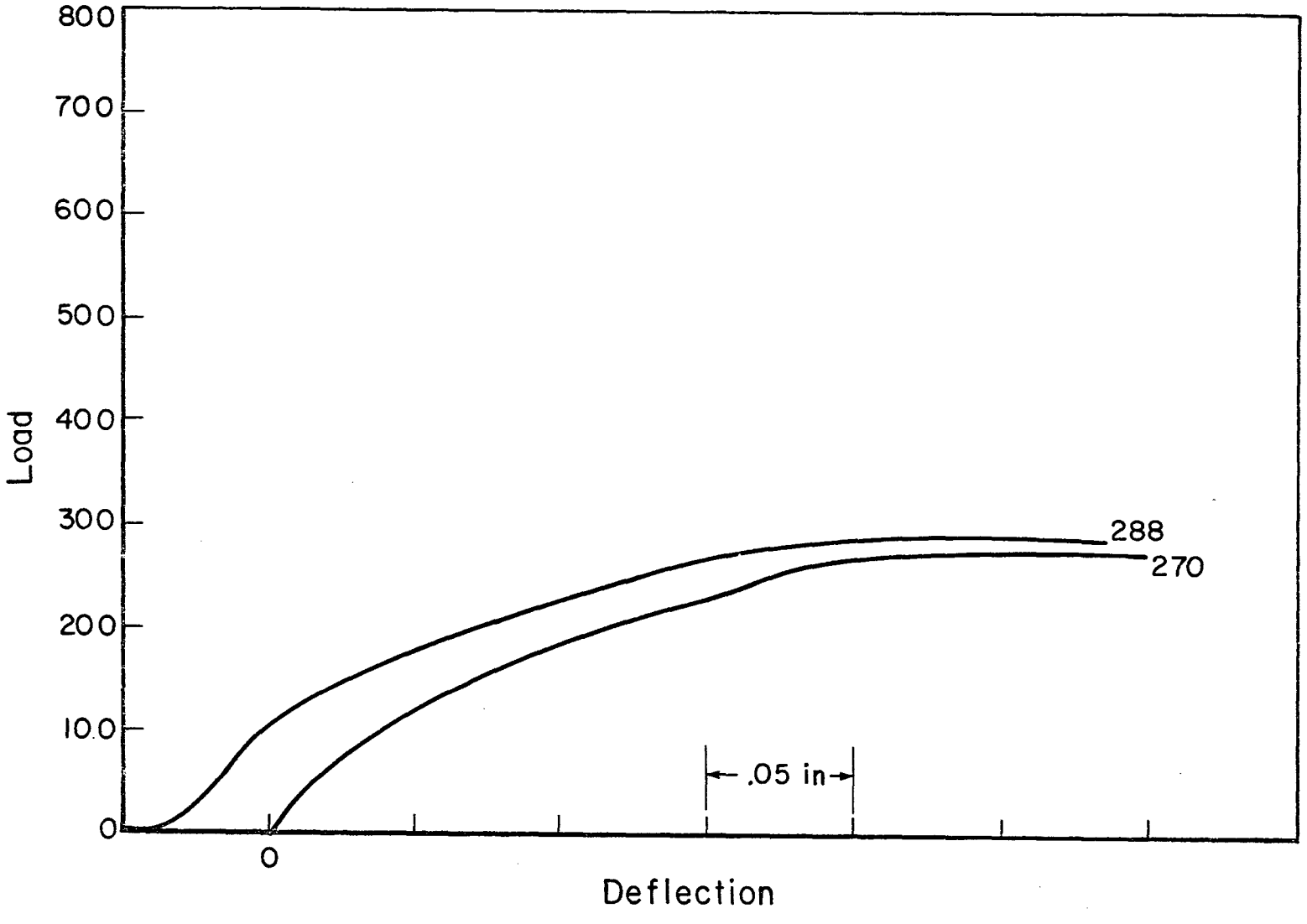

Figure 37 Central Load - Central Deflection Diagrams for Prestressed Segmented Circular Plates

TABLE 5

PHYSICAL PROPERTIES OF HYDROSTONE PLATES

Plate radius	R = 7.5 in.
Support ring radius	r = 6.75 in.
Central load die radius	a = 0.906 in.
Plate thickness	t = 5/8 in.
Average plate strain	$\varepsilon_p = 49.4 \times 10^{-6}$ in./in.
Modulus of elasticity of Hydrostone	$E = 2.79 \times 10^6$ psi
Poisson's Ratio for Hydrostone	$\nu = 1/4$
Average prestress level	$\sigma_p = \varepsilon_p \frac{E}{1-\nu} = 184$ psi
Number of segmented beam elements	= 8

B. Monolithic Plates

When a prestressed monolithic plate is slowly loaded, conventional elastic behavior is experienced until the net tensile stress at some point exceeds the material strength and a crack develops. In a constant strain rate machine, the load would fall off abruptly and then increase again as the strain continued to increase. This behavior is depicted in the central load-central deflection diagram shown in Figure 38 for the second monolithic plate referenced in Table 4. As we see, other cracks continue to form until the strength of the surviving material is sufficient to force unconstrained yielding in the existing crack pattern. The radial crack pattern (artificially darkened) shown in the top plate in Figure 34 is exactly what our limit analysis theory anticipates. The visible crushing at the center of this early plate test was caused by a steel ball that was used originally to load the plate. Subsequent tests employed a circular die to distribute the central load over a greater area.

Seven central load tests were conducted with monolithic plates and their yield and ultimate strengths are recorded in Table 4 . The average ultimate strength for these members is 562 pounds which represents a considerable increase in the average strength of monolithic plates without prestressing, 328 pounds. The distribution curve for the strength of these unprestressed control plates is shown in Figure 39 where we observe a considerable spread in the data. This implies that very low strength values will be present in a population of even a few hundred. Consequently, very "low strength" operating levels must be used to obtain reasonable reliability. For the prestressed plates, on the other hand, there is a built in fail-safe mechanism. Although the ultimate load is statistical and may be subject to wide variability, the yield load is bounded from below. We observe that the weakest plate is achieved when an infinite number of radial cracks develop in which case their yield load is computed from Equation (73). Real plates will crack in a finite number of places and will therefore be stronger. For our prestressed monolithic plates, Equation 73 predicts a yield load of 289 pounds and we observe from Table 4 that all of the

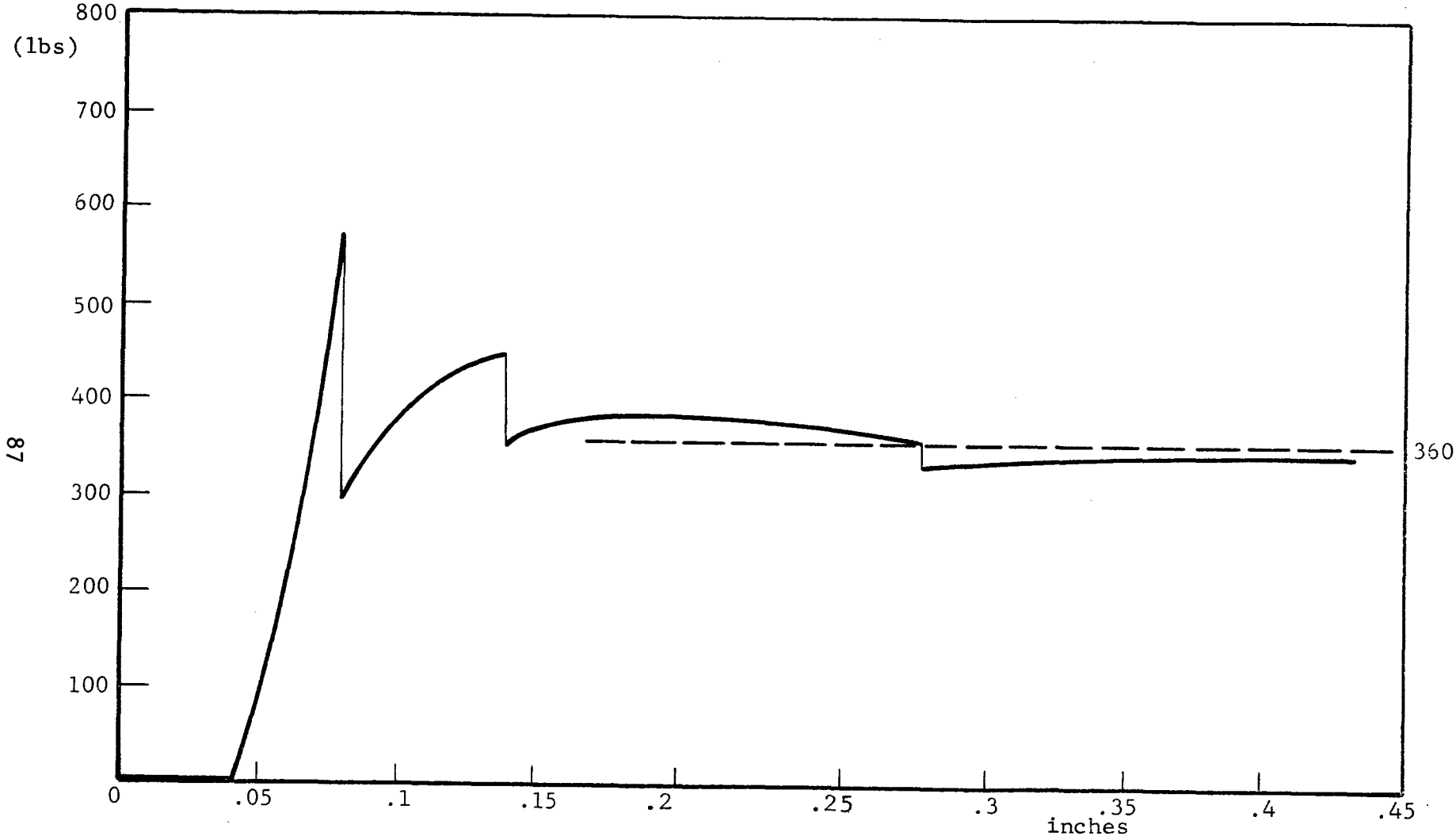

Figure 38 Central Load - Central Deflection Diagram of a Prestressed Monolithic Circular Hydrostone Plaster Plate

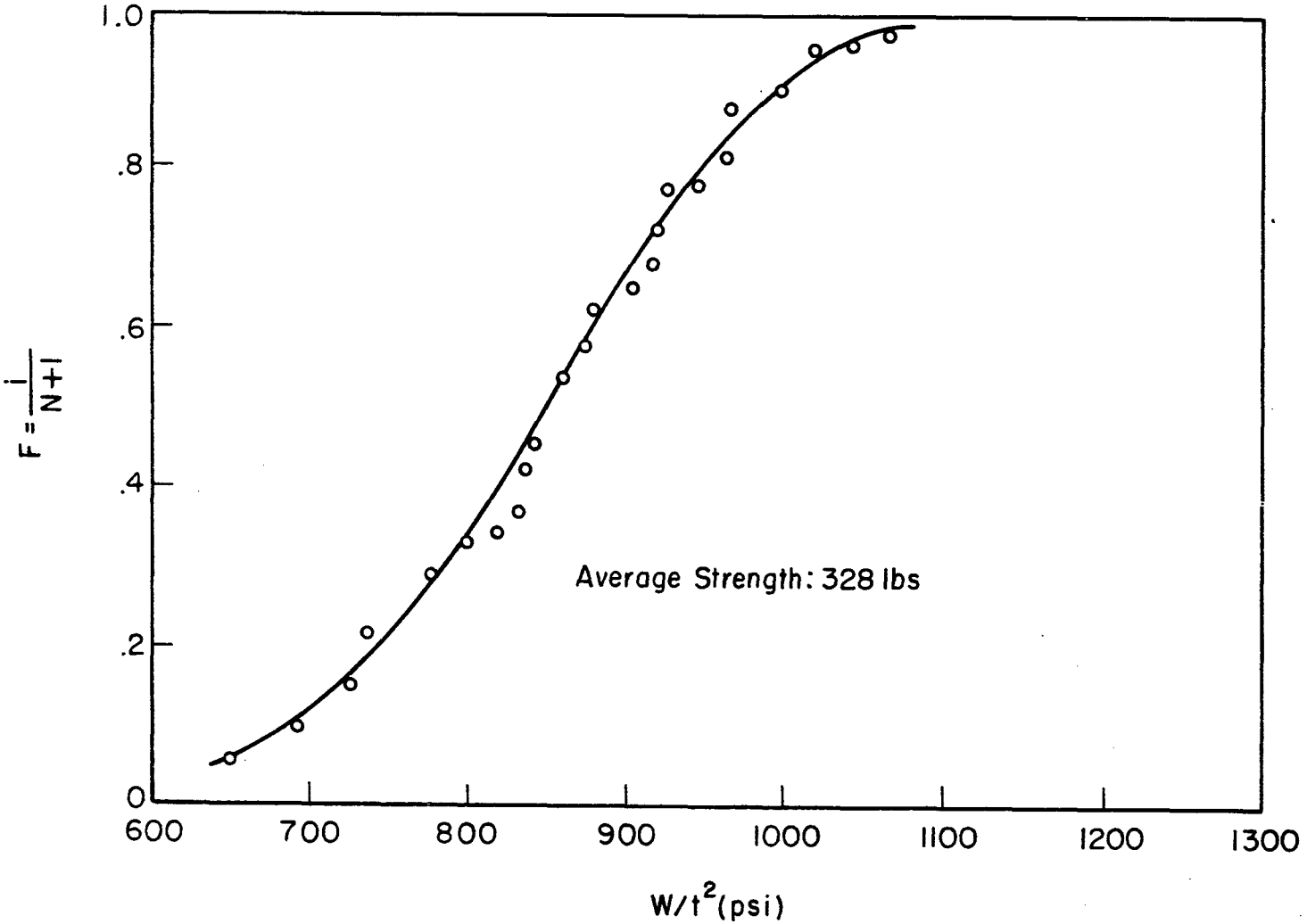

Figure 39 Failure Probabilities for Monolithic Circular Plates without Prestressing

yield strengths reported are higher than this value; the average load is 358 pounds.

We should point out that our two mathematical models for beams assume an infinite number of segments and should therefore predict a lower bound on the behavior of monolithic prestressed beams. In the exceptional case of a beam-column; however, we cannot make this statement since the resistance at a section can be lowered by virtue of the beam deflection. The distance from the outer compressive beam fibers to the centroid of the tendons decreases as the beam deflection increases. As a matter of fact, a point of instability is finally reached and the prestressing force participates in the catastrophic destruction of the beam. Finally, since a monolithic segment sustains no separation, it is stiffer than an equivalent length of several segments. Consequently, beams constructed with a finite number of elements will be stiffer than predicted from an infinite number of elements.

V. PRELIMINARY INVESTIGATIONS OF PRESTRESSED SHELLS

Fundamental studies of prestressed elements demand as a prerequisite that methods be available for applying, maintaining, and monitoring prestressing forces. In the case of shell structures, this may require a considerable amount of innovation and, perhaps, the elaborate development of special techniques. Since such efforts are beyond the scope of our present endeavors, a brief study has been undertaken to examine two conventional approaches to the problem of prestressing an ogive shell and a cylindrical shell.

A. Cylindrical Shell

For problems which require the continuous application of prestressing force over large areas, it is sometimes possible to utilize the technique of overwinding. Here, we visualize using a brittle component in place of a mandrel. Continuous filaments under high tension are then wound onto the components, and in this way, a jacket is formed permanently over the monolithic or segmented element which may prevent the leakage of liquids or gases and which could provide an energy absorbing layer that would protect the component from local impacts.

To investigate the potential of this technique, a three inch diameter alumina cylinder with a 0.2 inch wall thickness was overwrapped with preimpregnated 20 end glass roving. An electrical resistance strain gage was mounted on the inner wall of the cylinder to monitor the induced stress caused by the overwinding. Using an overwinding tension of 0.325 lbs/end to produce a tension force of 65 lb/in. along the cylinder axis, we obtained the relationship shown in Figure 40 between induced prestress and fiberglass layers.

The relationship between the induced prestress in a cylinder and the number of layers of overwound filaments was obtained where account is taken of the changes in filament stress that occur when additional filament layers are applied. The hoop stress σ_n is given by

$$\sigma_n = \frac{T}{t} \sum_{j=1}^{n} \frac{1}{1 + \left(\frac{\delta}{t}\right)\left(\frac{E_2}{E_1}\right)\frac{\left(r-\frac{t}{2}\right)\ (j-1)}{\left[r+(j-1)\ \frac{\delta}{2}\right]}}$$

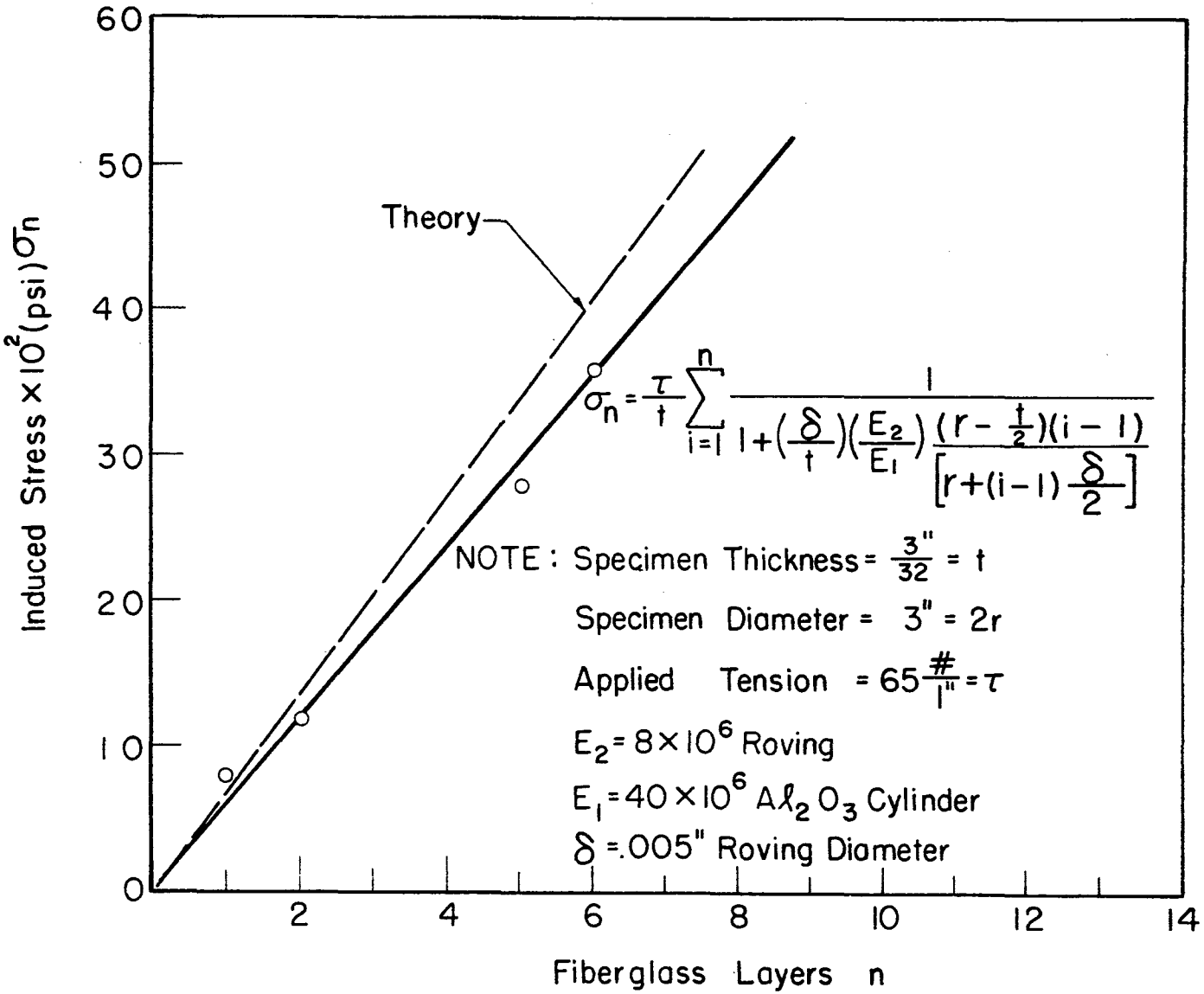

Figure 40 Relationship Between Cylinder Prestress and Layers of Overwound Fiberglass

where δ is the layer thickness, t is the wall thickness of the cylinder, r is the outside radius of the cylinder, T is the overwind tension per unit length in the direction of the axis of the cylinder, and E_1 and E_2 are the modulus of elasticity of the cylinder material and the filament material respectively. This theory assumes that we have perfect packing of rectangular fibers; however, for circular fibers without nesting we can modify the theory by replacing E_2 by $\pi E_2/4$. Using the following data, the theory is plotted in Figure :

$T = 65$ lb/in. $\quad t = 3/32$ in.
$\delta = 0.005$ in. $\quad E_1 = 40 \times 10^6$ psi
$r = 1.5$ in. $\quad E_2 = 8 \times 10^6$ psi.

Considering the preliminary nature of the experimental setup used, the agreement between the measured and predicted values is quite satisfactory. On this basis, calculations performed for ultra high strength overwinding materials such as high carbon steel wire and "S" fiberglass single end indicate that induced stresses exceeding 1000 psi/layer for a one inch wall thickness specimen are not unreasonable. This implies that for practical purposes any desired level of prestress can be obtained provided that winding on a geodesic path is possible.

B. Ogive Shell

If an axial compressive load is applied to the apex of an ogive shell, the membrane stresses in the shell wall are compressive in every direction. We see from this example that an effective state of initial stress can be accomplished by applying a prestressing force at a discrete point. Because the application and monitoring of such a force is exceptionally simple, the fabrication of ogive shells was attempted during this phase of the program.

Figure 41 illustrates one of several segmented Hydrostone plaster shells which were produced by cutting up monolithic shells before they completely cured. The interfaces of these shells tend to close up under compression; however, the thin sections near the

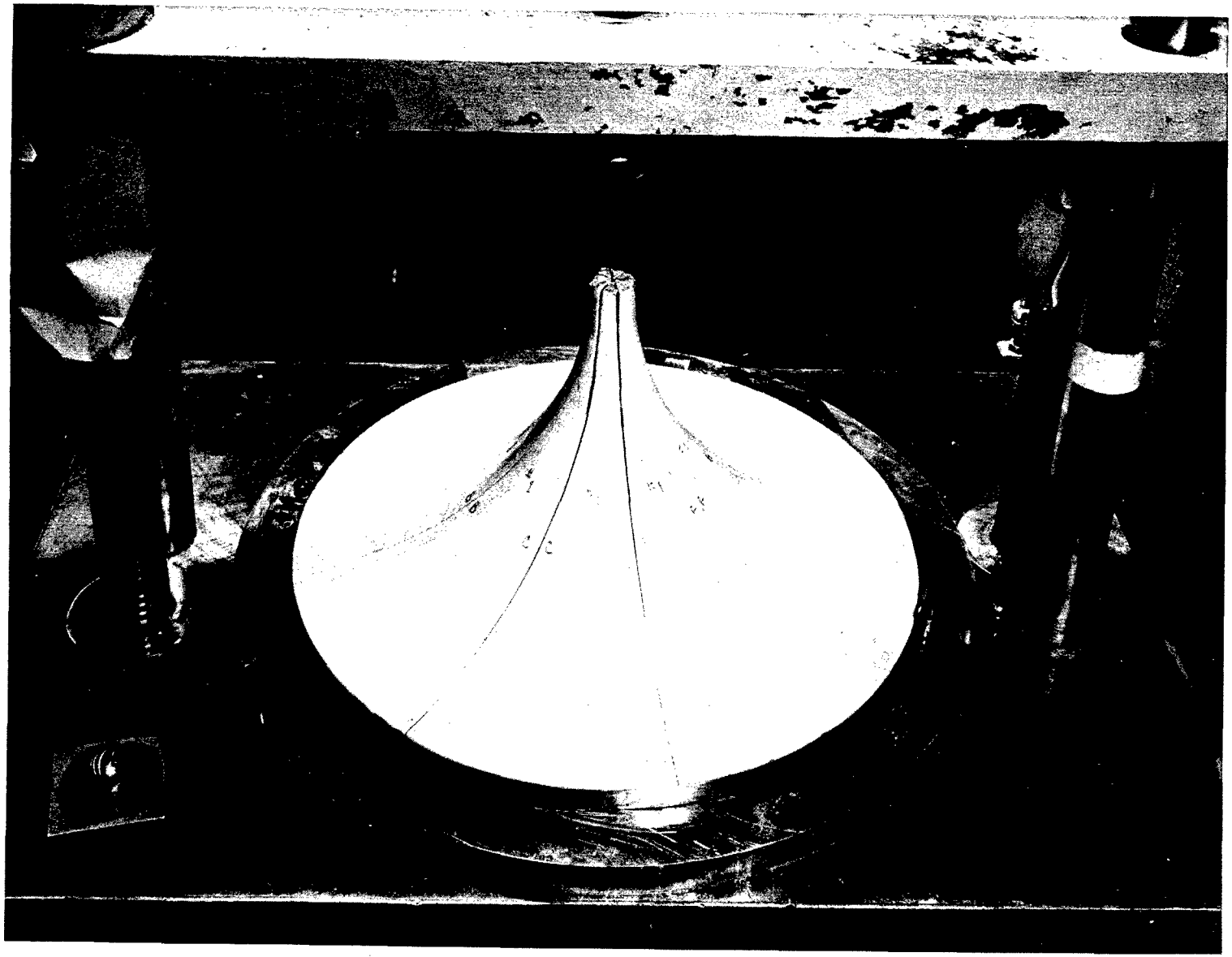

Figure 41 Segmented Ogive Shell Prestressed at it's Apex

apex are breaking under load. We attribute these failures to extremely rough interface conditions. Further studies with these shells should address themselves in this problem in addition to investigations of prestressed monolithic behavior.

APPENDIX A

I-BEAM COMPUTER PROGRAM

In this appendix, we shall present the computer program which was developed to perform the analysis of prestressed segmented I-beams with multiple elastic tendons. The program consists of a main program plus ten function subprograms. The main program essentially consists of those equations presented in the section on general relationships. Those relationships which depend explicitly upon the particular cross section being investigated have been isolated into individual function subprograms. The applied bending moment distribution, in normalized form, has also been isolated in its own function subprogram. Hence, only the appropriate subprogram(s) need be changed to permit the investigation of different cross sections and/or applied loadings.

Immediately following this introduction is a glossary of some of the important variables as they appear in the program along with their relationship to the variables used in the presentation of the analysis elsewhere in this report. Next after the glossary is a listing of the computer program as written in Fortran II for the IBM 7094. Finally, a sample input and corresponding output are presented.

The output has been designed to present as much relevant information as possible in a meaningful manner. The first page of output contains all the input data plus the results of a few preliminary calculations. Next is presented the table of W vs. f. The first differences in W are also given to illustrate whether the function is approximately linear between entries in the table as assumed by the linear interpolation scheme in the function subprogram FCP(W).

The remainder of the output consists of evaluating deflections, end rotations, etc. at the various selected values of the applied loading. The first value of the applied load is always zero and is followed by an intermediate value which leads to the value corresponding to incipient cracking. The program then truncates the cracking load to a specified number of figures and proceeds by adding specified increments in applied load until either the load exceeds the specified maximum or one of the counters exceeds its specified maximum. The final item in the output is a table of applied load versus central deflection, left end rotation, and right end rotation.

Partial listing of variables appearing in computer program:

AL ..... applied load, e.g. force, moment, etc.

ALDMBM ..... applied load divided by maximum bending moment, eg. P/(PL/4)

ALMAX ..... value of applied load which is not to be exceeded

AT ..... area of each tendon, A_t

CP ..... crack penetration, f

CPXD ..... crack penetration f at x_Δ

DAL ..... increment in applied load

DCENT ..... distance q from bottom of section to center of gravity

DELTA ..... deflection Δ at x_Δ

DIM1 = B ..... width of flange for I-beam, b

DIM2 = TW ..... thickness of web for I-beam, t_w

DIM3 = D ..... depth of web for I-beam, d

DIM4 = TF ..... thickness of flange for I-beam, t_f

DIM5, etc. = 0.. not used for I-beams

DISC(I) ..... distance from bottom of section to i^{th} discontinuity

DTOT ..... overall depth, d_{total}, of cross section

EB ..... elastic modulus of beam, E

EC ..... effective initial eccentricity of preload, e

ECT(I) ..... eccentricity of i^{th} tendon, e_i

ET ..... elastic modulus of tendon, E_t

F ..... total preload exerted by tendons, F

FO ..... initial preload exerted by tendons, F_o

FT(I) ..... force in the i^{th} tendon, F^i

FTO(I) ..... initial force in i^{th} tendon, F_o^i

IK ..... number of equally spaced points on beam at which deflections are to be found

IKK ..... if IKK = 2, then applied loading is symmetrical about x = L/2

K ..... number of increments used in numerical integrations

KFUDM1 ..... maximum number of applied load increment halvings

KFUDM2 ..... maximum number of occurrences of questionable output

KSMAX ..... maximum number of steps/loop in F and M_T directions in the solution of tendon equations

KTRYM ..... maximum number of loops in the solution of tendon equations

NIR(I) ..... number of entries in table of W vs. f between f = CP = DISC(I-1) and DISC(I)

NOREG ..... total number of regions cross section is divided into depthwise for table of W vs. f (three for I-beam)

NSF ..... number of significant figures for truncation of cracking load

NT ..... total number of tendons, n

PERMAX ..... maximum allowable percent in-out errot in the solution of the tendon equations

T ..... resultant bending moment applied to beam, T

TABAL(I) ..... i^{th} applied load for table at end of output

TABCD(I) ..... i^{th} central deflection for table at end of output

TABCP(I) ..... i^{th} crack penetration for table of W vs. f

TABTL(I) ..... i^{th} left end rotation for table at end of output

TABTR(I) ..... i^{th} right end rotation for table at end of output

TABW(I) ..... i^{th} value of W for table of W vs. f

THETAL ..... left end rotation, θ_L

THETAO ..... initial end rotation, θ_0

THETAR ..... right end rotation, θ_R

V ..... maximum value of W along the beam

W ..... variable, W = $(M-M_T)/F$, appearing in crack penetration equation

WCRACK ..... value of W corresponding to incipient cracking

X ..... coordinate, x, measured along the length of the beam

XD ..... location, x_Δ, where deflection is being determined

YL ..... lenth of segmented beam, L

YLT ..... length of tendons, L_t

YMB ..... maximum applied bending moment, M_{max}

YMT ..... tendon stiffness bending moment, M_T

PROGRAM LISTING

```
C     MAIN PROGRAM - PRESTRESSED SEGMENTED I BEAM WITH ELASTIC TENDONS,   PCH
      DIMENSION HOLLER(12),DIFX(200)
      DIMENSION FTO(10),ECT(10),FT(10),SIGMA(10),TABAL(100),TABTL(100),
     1TABTR(100),DISC(10),NIR(10),TABCP(200),TABW(200),TABCD(100)
      COMMON YMB,YMT,F,FO,YL,EB,XD,WCRACK,NI,IC,IBMD,IXS,DTOT,DCENT,DIM1
     1,DIM2,DIM3,DIM4,DIM5,DIM6,DIM7,DIM8,DIM9,DIM10,DISC,TABCP,TABW,EC
F     FDI
F     FTLI
F     FTRI
F     FBCI
   45 WRITE OUTPUT TAPE 6,50
   50 FORMAT(55H1PRESTRESSED SEGMENTED I BEAM WITH ELASTIC TENDONS, PCH)
      WRITE OUTPUT TAPE 6,55
   55 FORMAT(119HODIMENSIONS - LENGTHS ARE IN INCHES, LOADS ARE IN KIPS,
     1 BENDING MOMENTS ARE IN INCH-KIPS, STRESSES + MODULI ARE IN KSI )
  100 READ INPUT TAPE 5,101,HOLLER
  101 FORMAT(12A6)
      READ INPUT TAPE 5,105,YL,EB,YLT,ET,AT,PERMAX,K,NT,NOREG
  105 FORMAT(6F10.0,3I5)
      READ INPUT TAPE 5,110,(FTO(I),ECT(I),I=1,NT)
  110 FORMAT(2F10.0)
      READ INPUT TAPE 5,115,DTOT,DCENT,DIM1,DIM2,DIM3,DIM4
      READ INPUT TAPE 5,115,DIM5,DIM6,DIM7,DIM8,DIM9,DIM10
  115 FORMAT(6F10.0)
      READ INPUT TAPE 5,120,(DISC(I),NIR(I),I=1,NOREG)
  120 FORMAT (F10.6,I5)
      READ INPUT TAPE 5,127,IK,IKK,NSF,ALDMBM,ALMAX,DAL
  127 FORMAT(3I5,3F10.0)
      READ INPUT TAPE 5,128,KTRYM,KSMAX,KFUDM1,KFUDM2
  128 FORMAT(4I5)
      WRITE OUTPUT TAPE 6,130,HOLLER
  130 FORMAT(1H0,12A6)
      WRITE OUTPUT TAPE 6,135,YL,EB,YLT,ET,AT
  135 FORMAT(15HOBEAM LENGTH = ,F8.4,12H BEAM MOD = ,F10.2,17H TENDON LE
     1NGTH = ,F8.4,14H TENDON MOD = ,F10.2,19H AREA PER TENDON = ,F7.5)
      WRITE OUTPUT TAPE 6,140,PERMAX,K
  140 FORMAT(75HOPERCENT IN-OUT DIFFERENCE IN PRESTRESS AND TENDON MOMEN
     1T IS LESS THAN OR =,F6.4,33H NO. INCREMENTS IN INTEGRATIONS =,I4)
      WRITE OUTPUT TAPE 6,145,NT,NOREG
  145 FORMAT(18HONO. OF TENDONS = ,I2,18H NO. OF REGIONS = ,I2)
      WRITE OUTPUT TAPE 6,150,DTOT,DCENT,DIM1,DIM2,DIM3,DIM4
  150 FORMAT(15HOTOTAL DEPTH = ,F7.4,20H DIST TO CENTROID = ,F7.4,8H DIM
     11 = ,F7.4,8H DIM2 = ,F7.4,8H DIM3 = ,F7.4,8H DIM4 = ,F7.4)
      WRITE OUTPUT TAPE 6,155,DIM5,DIM6,DIM7,DIM8,DIM9,DIM10
  155 FORMAT(8HODIM5 = ,F7.4,8H DIM6 = ,F7.4,8H DIM7 = ,F7.4,8H DIM8 = ,
     1F7.4,8H DIM9 = ,F7.4,9H DIM10 = ,F7.4)
      WRITE OUTPUT TAPE 6,160,(I,DISC(I),I,NIR(I),I=1,NOREG)
  160 FORMAT(6H DISC(,I2,5H ) = ,F7.4,5H NIR(,I2,5H ) = ,I3)
      SUMECT=0.
```

```
      DO 165 I=1,NT
  165 SUMECT=SUMECT+ECT(I)
      ERRMAX=PERMAX/100.
      IXS=0
      IBMD=0
      WRITE = FM(0.0)
      WRITE = FI(0.0)
      IXS=1
      IBMD=1
      XNT=NT
      R=0.
      RM=0.
      DO 170 I=1,NT
      FT(I)=FTO(I)
      R=R+FTO(I)
  170 RM=RM+FTO(I)*ECT(I)
      FO=R
      EC=RM/R
      F=FO
      WRITE OUTPUT TAPE 6,175,ALDMBM,ALMAX,DAL
  175 FORMAT(35HO(APPLIED LOAD)/(MAX BEND MOMENT) =,F10.6,20H MAX APPLIE
     1D LOAD = ,F10.6,29H INCREMENT IN APPLIED LOAD = ,F10.6)
      WRITE OUTPUT TAPE 6,180,F,EC
  180 FORMAT(27HOINITIAL PRELOAD IN BEAM = ,F10.6,35H ECCENTRICITY OF IN
     1ITIAL PRELOAD = ,F10.6)
      WRITE OUTPUT TAPE 6,185,IK,NSF
  185 FORMAT(18HODEFLECTIONS AT 1/,I2,16H POINTS ON BEAM,,28H ROUND OFF
     1CRACKING LOAD TO ,I1,20H SIGNIFICANT FIGURES )
      IF(IKK-2)190,187,190
  187 WRITE OUTPUT TAPE 6,188
  188 FORMAT(40HOAPPLIED BENDING MOM DIST IS SYMMETRICAL )
  190 WRITE OUTPUT TAPE 6,195,KTRYM,KSMAX
  195 FORMAT(70HOFOR DETERMINATION OF PRELOAD AND TENDON MOMENT - MAX NO
     1. STEPS/LOOP = ,I2,16H MAX NO. LOOPS = ,I2,21H MAX NO. APPLIED LOA
     2D )
      WRITE OUTPUT TAPE 6,196,KFUDM1,KFUDM2
  196 FORMAT(21HOINCREMENT HALVINGS =,I2,44H MAX NO. OCCURENCES OF QUEST
     1IONABLE OUTPUT =,I2)
C     TABLE OF TABW VS TABCP (200 THRU 299)
  200 NIR1P1=NIR(1)+1
      DO 210 K2=1,NIR1P1
      TABCP(K2)=FLOATF(K2-1)*DISC(1)/FLOATF(NIR(1))
      X1=TABCP(K2)
  210 TABW(K2)=EC+X1-DCENT+FXB(X1)+FI(X1)/(FA(X1)*FXB(X1))
      WCRACK=TABW(1)
      NIRT=NIR(1)
      IF(NOREG-2) 240,215,215
  215 DO 230 K1=2,NOREG
```

```
      X2=DISC(K1)-DISC(K1-1)
      NNN=NIR(K1)+1
      DO 220 K2=1,NNN
      K3=NIRT+K2
      TABCP(K3)=DISC(K1-1)+FLOATF(K2-1)*X2/FLOATF(NIR(K1))
      X1=TABCP(K3)
      TABW(K3)=EC+X1-DCENT+FXB(X1)+FI(X1)/(FA(X1)*FXB(X1))
  220 CONTINUE
      NIRT=NIRT+NIR(K1)
  230 CONTINUE
  240 NI=NIRT
      WMAX=TABW(NI+1)
  245 WRITE OUTPUT TAPE 6,250,WCRACK
  250 FORMAT(9H1WCRACK =,F10.6)
      WRITE OUTPUT TAPE 6,255
  255 FORMAT(1H0,13X,6H TABCP,14X,5H TABW,12X,11H FIRST DIFF )
      DIFX(1)=0.0
      NIP2=NI+2
      DO 270 K4=2,NIP2
      DIFX(K4)=TABW(K4)-TABW(K4-1)
      K5=K4-1
      WRITE OUTPUT TAPE 6,260,K5,TABCP(K5),TABW(K5),DIFX(K5)
  260 FORMAT(I5,3F20.8)
  270 CONTINUE
      DO 280 I=1,NT
  280 FT(I)=FTO(I)
      CTEN=YLT/(AT*ET)
      V=0.
      YMT=0.
      MM=0
      YMB=0.
      XIK=IK
      IJK=IK/IKK
      KK=0
      KFUD=0
      X=0.
      TABTL(1)=FINT(FTLI,K)
      TABTR(1)=FINT(FTRI,K)
      TABAL(1)=0.
      THETAO=TABTL(1)
      THETAL=THETAO
      THETAR=THETAO
      WRITE OUTPUT TAPE 6,290
  290 FORMAT(1H1)
      WRITE OUTPUT TAPE 6,295,THETAO
  295 FORMAT(10H THETAO = ,F12.8)
      GO TO 400
C     ROUTINE FOR SELECTING APPLIED LOAD (300 THRU 399)
  300 KK=KK+1
```

```
      IF(KK-2) 310,320,330
  310 YMB=WCRACK*FO
      YMBOLD=YMB
      GO TO 400
  320 YMB=((FO*WCRACK)**2)/((2.*FO-F)*WCRACK-YMT)
      ID=XFIXF(.43429448*LOGF(YMB*ALDMBM))-NSF+1
      ALD=(10.**ID)*FLOATF(XFIXF(YMB*ALDMBM/(10.**ID)))
      SFYMB=ALD/ALDMBM
      GO TO 400
  330 YMB=SFYMB+DAL*FLOATF(KK-2)/ALDMBM
      AL=ALD+DAL*FLOATF(KK-2)
      IF(AL-ALMAX)400,400,340
  340 WRITE OUTPUT TAPE 6,345
  345 FORMAT(15H1  APPLIED LOAD,8X,12H CENTER DEFL,10X,11H THETA LEFT,8X
     1,12H THETA RIGHT)
      WRITE OUTPUT TAPE 6,350,(TABAL(N),TABCD(N),TABTL(N),TABTR(N),N=1,M
     1M)
  350 FORMAT(4F20.8)
      WRITE OUTPUT TAPE 6,355
  355 FORMAT (1H1)
      GO TO 45
C     ROUTINE FOR DETERMINING PRESTRESS FORCE AND MOMENT (400 THRU 499)
  400 AL=YMB*ALDMBM
      THETAL=FINT(FTLI,K)
      THETAR=FINT(FTRI,K)
      IF(ET*FLOATF(KK)) 410,500,410
C     ET=0. FOR ZERO STIFFNESS TENDONS
  410 CYMT=YMTOLD
      YMT=YMTOLD*YMB/YMBOLD
      F=FOLD*(YMB-YMT)/(YMBOLD-YMTOLD)
      DELF=(F-FOLD)/2.
      DELYMT=(YMT-YMTOLD)/2.
      KKFUD=0
      IF(ABSF(DELF/F)-ERRMAX)411,411,412
  411 DELF=2.*ERRMAX*F
  412 IF(ABSF(DELYMT)-ABSF(YMT*ERRMAX))413,413,414
  413 DELYMT=2.*ERRMAX*YMT
  414 SF=DELF
      SYMT=DELYMT
      KS=0
      WRITE OUTPUT TAPE 6,415,AL
  415 FORMAT(15HOAPPLIED LOAD =,F12.8)
  418 KTRY=0
      KALT=0
      WRITE OUTPUT TAPE 6,419,YMT
  419 FORMAT(14H HOLDING YMT =,F12.8)
      DFOLD=F
  425 FIN=F
      IF(KTRY-KTRYM)426,426,461
```

```
  426 WL=(YMB*FM(0.)-YMT)/F
      CPL=FCP(WL)
      WR=(YMB*FM(YL)-YMT)/F
      CPR=FCP(WR)
      THETAL=FINT(FTLI,K)
      IF(IKK-2) 428,427,428
C     IKK=2 FOR SYMMETRICAL LOADING, FM(X)=FM(L-X)
  427 THETAR=THETAL
      GO TO 429
  428 THETAR=FINT(FTRI,K)
  429 BCOMP=FINT(FBCI,K)
      YMTOUT=0.
      Z1=(SUMECT+XNT*(CPL-DCENT+FXB(CPL)))*(THETAL-THETAO)
      Z2=(SUMECT+XNT*(CPR-DCENT+FXB(CPR)))*(THETAR-THETAO)
      FOUT=FO+(Z1+Z2)/(CTEN+XNT*BCOMP)
      DO 430 I=1,NT
      ZZ1=(ECT(I)+CPL-DCENT+FXB(CPL))*(THETAL-THETAO)
      ZZ2=(ECT(I)+CPR-DCENT+FXB(CPR))*(THETAR-THETAO)
      FT(I)=FTO(I)+(ZZ1+ZZ2-(F-FO)*BCOMP)/CTEN
  430 YMTOUT=YMTOUT+FT(I)*(ECT(I)-EC)
      DF=FOUT-FIN
  435 VIN=(YMB-YMT)/FIN
      VOUT=(YMB-YMTOUT)/FOUT
      WRITE OUTPUT TAPE 6,438,FIN,VIN,FOUT,DF,YMTOUT,VOUT
  438 FORMAT(6H FIN =,F12.8,6H VIN =,F10.8,7H FOUT =,F12.8,5H DF =,F12.8
     1,9H YMTOUT =,F12.8,7H VOUT =,F10.8)
      IF(ABSF((FOUT-FIN)/FIN)-ERRMAX) 450,450,440
  440 IF(DFOLD*DF)445,450,442
  442 IF(ABSF(DFOLD)-ABSF(DF))443,448,448
  443 DELF=-.75*DELF
      GO TO 448
  445 DELF=-DELF/2.
  448 F=F-DELF
      DFOLD=DF
      KTRY=KTRY+1
      GO TO 425
  450 IF(KTRY-KTRYM/3)451,452,452
  451 SF=SF/2.
  452 DELF=SF
      IF(KS+KK-1)453,453,460
  453 DELYMT=YMTOUT/5.
      YMT=YMTOUT/(1.-2.*ERRMAX)
      GO TO 460
  455 IF(KTRY-KTRYM/3)456,456,457
  456 SYMT=SYMT/2.
  457 DELYMT=SYMT
      IF(KS+KK-2)458,458,460
  458 DELF=(FOUT-F)/5.
  460 KS=KS+1
      IF(KS-KSMAX)465,465,461
```

```
  461 IF(KFUD-KFUDM1)462,463,463
  462 DAL=0.5*DAL
      KK=2*(KK-1)-2
      KKFUD=1
  463 WRITE OUTPUT TAPE 6,464
  464 FORMAT(63HOTHE FOLLOWING OUTPUT FOR THIS LOAD IS OF QUESTIONABLE A
     1CCURACY)
      KFUD=KFUD+1
      IF(KFUD-KFUDM2)500,500,340
  465 IF(ABSF((F-FOUT)/F)-ERRMAX)466,466,470
  466 IF(YMT)467,470,467
  467 IF(ABSF((YMT-YMTOUT)/YMT)-ERRMAX)500,500,470
  470 IF(KALT)418,473,418
  473 KTRY=0
      KALT=1
      WRITE OUTPUT TAPE 6,474,F
  474 FORMAT(12H HOLDING F =,F12.8)
      DYMTO=YMB
  480 YMTIN=YMT
      IF(KTRY-KTRYM)481,481,461
  481 WL=(YMB*FM(0.)-YMT)/F
      CPL=FCP(WL)
      WR=(YMB*FM(YL)-YMT)/F
      CPR=FCP(WR)
      THETAL=FINT(FTLI,K)
      IF(IKK-2) 483,482,483
C     IKK=2 FOR SYMMETRICAL LOADING, FM(X)=FM(L-X)
  482 THETAR=THETAL
      GO TO 484
  483 THETAR=FINT(FTRI,K)
  484 BCOMP=FINT(FBCI,K)
      YMTOUT=0.
      Z1=(SUMECT+XNT*(CPL-DCENT+FXB(CPL)))*(THETAL-THETAO)
      Z2=(SUMECT+XNT*(CPR-DCENT+FXB(CPR)))*(THETAR-THETAO)
      FOUT=FO+(Z1+Z2)/(CTEN+XNT*BCOMP)
      DO 485 I=1,NT
      ZZ1=(ECT(I)+CPL-DCENT+FXB(CPL))*(THETAL-THETAO)
      ZZ2=(ECT(I)+CPR-DCENT+FXB(CPR))*(THETAR-THETAO)
      FT(I)=FTO(I)+(ZZ1+ZZ2-(F-FO)*BCOMP)/CTEN
  485 YMTOUT=YMTOUT+FT(I)*(ECT(I)-EC)
      DYMT=YMTOUT-YMTIN
  490 VIN=(YMB-YMTIN)/F
      VOUT=(YMB-YMTOUT)/FOUT
      WRITE OUTPUT TAPE 6,492,YMTIN,VIN,YMTOUT,DYMT,FOUT,VOUT
  492 FORMAT(8H YMTIN =,F12.8,6H VIN =,F10.8,9H YMTOUT =,F12.8,7H DYMT =
     1,F12.8,7H FOUT =,F12.8,7H VOUT =,F10.8)
      IF(ABSF((YMTOUT-YMTIN)/YMTIN)-ERRMAX) 455,455,493
  493 IF(DYMTO*DYMT)496,455,494
```

```
  494 IF(ABSF(DYMTO)-ABSF(DYMT))495,499,499
  495 DELYMT=-.75*DELYMT
      GO TO 499
  496 DELYMT=-DELYMT/2.
  499 YMT=YMT+DELYMT
      DYMTO=DYMT
      KTRY=KTRY+1
      GO TO 480
C     ROUTINE FOR DETERMINING TENDON STRESSES + BEAM DEFL. (500 TO 599)
  500 IF(KK-1)505,590,505
  505 AL=ALDMBM*YMB
      WRITE OUTPUT TAPE 6,510,AL,YMB,F
  510 FORMAT(16HOAPPLIED LOAD = ,F12.8,3X,24H MAX APPLIED BEND MOM = ,F1
     12.8,3X,25H TOTAL PRELOAD IN BEAM = ,F12.8)
      DF=F-FOUT
      DYMT=YMT-YMTOUT
      V=(YMB-YMT)/F
      WRITE OUTPUT TAPE 6,515,DF,YMT,DYMT,V
  515 FORMAT(7H DIFF =,F12.8,3X,21H TENDON BENDING MOM = ,F12.8,3X,7H DI
     1FF =,F12.8,3X,5H V = ,F12.8)
      WRITE OUTPUT TAPE 6,517,THETAL,THETAR
  517 FORMAT(20HOLEFT END ROTATION =,F12.8,21H RIGHT END ROTATION =,F12.
     18)
      WRITE OUTPUT TAPE 6,520
  520 FORMAT(30HOINITIAL TENDON ECCENTRICITY  ,13H TENDON FORCE,7X,14H T
     1ENDON STRESS)
      DO 530 I=1,NT
  530 SIGMA(I)=FT(I)/AT
      WRITE OUTPUT TAPE 6,540,(ECT(I),FT(I),SIGMA(I),I=1,NT)
  540 FORMAT(F20.8,7X,2F20.8)
      MM=MM+1
      TABAL(MM)=AL
      TABTL(MM)=THETAL
      TABTR(MM)=THETAR
      WRITE OUTPUT TAPE 6,550
  550 FORMAT(1HO,22X,6H XD/YL,8X,11H DEFLECTION,5X,17HCRACK PENETRATION)
      DO 570 IJ=1,IJK
      XIJ=IJ
      XD=YL*XIJ/XIK
      DELTA=FINT(FDI,K)
      WXD=(YMB*FM(XD)-YMT)/F
      CPXD=FCP(WXD)
      IF(XIJ/XIK-.5) 560,555,560
  555 TABCD(MM)=DELTA
  560 WRITE OUTPUT TAPE 6,565,IJ,IK,DELTA,CPXD
  565 FORMAT(23X,I2,2H /,I2,5X,1PE15.8,10X,0PF10.6)
  570 CONTINUE
      WRITE OUTPUT TAPE 6,580
  580 FORMAT(1H //////)
```

```
      IF(KKFUD-1)590,595,595
  590 FOLD=F
      YMTOLD=YMT
      YMBOLD=YMB
  595 IF(MM-100)300,340,340
      END
```

```
CFCP  CRACK PENETRATION AS A FUNCTION OF W USING TABULATED VALUES,    PCH
      FUNCTION FCP(W)
      DIMENSION FTO(10),ECT(10),FT(10),SIGMA(10),TABAL(100),TABTL(100),
     1 TABTR(100),DISC(10),NIR(10),TABCP(200),TABW(200),TABCD(100)
      COMMON YMB,YMT,F,FO,YL,EB,XD,WCRACK,NI,IC,IBMD,IXS,DTOT,DCENT,DIM1
     1,DIM2,DIM3,DIM4,DIM5,DIM6,DIM7,DIM8,DIM9,DIM10,DISC,TABCP,TABW,EC
      IF(W-WCRACK) 10,10,20
   10 FCP=0.
      GO TO 100
   20 KLOW=1
      KHIGH=NI+1
      IF(W-TABW(KHIGH))30,30,25
   25 FCP=DTOT
      WRITE OUTPUT TAPE 6,26
   26 FORMAT(38HOW GREATER THAN WMAX, SETTING FCP=DTOT , // )
      GO TO 100
   30 KMID=KLOW+(KHIGH-KLOW)/2
      IF(W-TABW(KMID)) 40,50,60
   40 KHIGH=KMID
      GO TO 70
   50 FCP=TABCP(KMID)
      GO TO 100
   60 KLOW=KMID
   70 IF(KHIGH-KLOW-1) 80,80,30
   80 SLOPE=(TABCP(KHIGH)-TABCP(KLOW))/(TABW(KHIGH)-TABW(KLOW))
      FCP=TABCP(KLOW)+(W-TABW(KLOW))*SLOPE
  100 RETURN
      END


CFA   I BEAM CROSS SECTIONAL AREA AS A FUNCTION OF CRACK PENETRATION,PCH
      FUNCTION FA(CP)
      DIMENSION FTO(10),ECT(10),FT(10),SIGMA(10),TABAL(100),TABTL(100),
     1 TABTR(100),DISC(10),NIR(10),TABCP(200),TABW(200),TABCD(100)
      COMMON YMB,YMT,F,FO,YL,EB,XD,WCRACK,NI,IC,IBMD,IXS,DTOT,DCENT,B,TW
     1,D,TF,DIM5,DIM6,DIM7,DIM8,DIM9,DIM10,DISC,TABCP,TABW,EC
      IF(CP-TF) 10,10,20
   10 FA=B*(TF-CP)+D*TW+B*TF
      GO TO 50
   20 IF(CP-TF-D) 30,30,40
   30 FA=(D+TF-CP)*TW+B*TF
      GO TO 50
   40 FA=(2.*TF+D-CP)*B
   50 IF(IXS) 70,60,70
   60 WRITE OUTPUT TAPE 6,65
   65 FORMAT (33HOI BEAM AREA FUNCTION IN PROGRAM )
   70 RETURN
      END
```

```
CFXB  I BEAM CENTROID DISTANCE FROM CRACK VS CRACK PENETRATION,      PCH
      FUNCTION FXB(CP)
      DIMENSION FTO(10),ECT(10),FT(10),SIGMA(10),TABAL(100),TABTL(100),
     1 TABTR(100),DISC(10),NIR(10),TABCP(200),TABW(200),TABCD(100)
      COMMON YMB,YMT,F,FO,YL,EB,XD,WCRACK,NI,IC,IBMD,IXS,DTOT,DCENT,B,TW
     1,D,TF,DIM5,DIM6,DIM7,DIM8,DIM9,DIM10,DISC,TABCP,TABW,EC
      IF(CP-TF) 10,10,20
   10 TOP=0.5*B*(TF-CP)**2+D*TW*(TF-CP+0.5*D)+B*TF*(1.5*TF-CP+D)
      FXB=TOP/FA(CP)
      GO TO 50
   20 IF (CP-TF-D) 30,30,40
   30 TOP=0.5*TW*(D+TF-CP)**2+B*TF*(D+1.5*TF-CP)
      FXB=TOP/FA(CP)
      GO TO 50
   40 FXB=(2.*TF+D-CP)/2.
   50 IF(IXS) 70,60,70
   60 WRITE OUTPUT TAPE 6,65
   65 FORMAT (37HOI BEAM CENTROID FUNCTION IN PROGRAM )
   70 RETURN
      END


CFI   I BEAM MOMENT OF INERTIA AS A FUNCTION OF CRACK PENETRATION,   PCH
      FUNCTION FI(CP)
      DIMENSION FTO(10),ECT(10),FT(10),SIGMA(10),TABAL(100),TABTL(100),
     1 TABTR(100),DISC(10),NIR(10),TABCP(200),TABW(200),TABCD(100)
      COMMON YMB,YMT,F,FO,YL,EB,XD,WCRACK,NI,IC,IBMD,IXS,DTOT,DCENT,B,TW
     1,D,TF,DIM5,DIM6,DIM7,DIM8,DIM9,DIM10,DISC,TABCP,TABW,EC
      IF(CP-TF) 10,10,20
   10 FI=(B*(TF-CP)**3+TW*D**3+B*TF**3)/12.+B*(TF-CP)*(FXB(CP)-0.5*(TF-
     1CP))**2+D*TW*(FXB(CP)-TF+CP-0.5*D)**2+B*TF*(D+1.5*TF-FXB(CP)-CP)**
     22
      GO TO 50
   20 IF(CP-TF-D) 30,30,40
   30 FI=(TW*(TF+D-CP)**3+B*TF**3)/12.+TW*(D+TF-CP)*(FXB(CP)-0.5*(D+TF-
     1CP))**2+B*TF*(D+1.5*TF-FXB(CP)-CP)**2
      GO TO 50
   40 FI=(B*(2.*TF+D-CP)**3)/12.
   50 IF(IXS) 80,60,80
   60 WRITE OUTPUT TAPE 6,65
   65 FORMAT (46HOI BEAM MOMENT OF INERTIA FUNCTION IN PROGRAM )
      WRITE OUTPUT TAPE 6,70,B,TF,D,TW
   70 FORMAT (16HOFLANGE WIDTH = ,F7.4,16H FLANGE THICK = ,F7.4,13H WEB
     1DEPTH = ,F7.4,13H WEB THICK = ,F7.4)
   80 RETURN
      END
```

```
CFINT SIMPSONS 1/3 RULE FOR NUMERICAL INTEGRATION                    PCH
      FUNCTION FINT(FDUM,K)
      DIMENSION FTO(10),ECT(10),FT(10),SIGMA(10),TABAL(100),TABTL(100),
     1 TABTR(100),DISC(10),NIR(10),TABCP(200),TABW(200),TABCD(100)
      COMMON YMB,YMT,F,FO,YL,EB,XD,WCRACK,NI,IC,IBMD,IXS,DTOT,DCENT,DIM1
     1,DIM2,DIM3,DIM4,DIM5,DIM6,DIM7,DIM8,DIM9,DIM10,DISC,TABCP,TABW,EC
      I1=K-1
      I2=K-2
      XK=K
      FINT1=0.
      FINT2=0.
      DO 10 I=1,I1,2
      XI=I
      X=XI*YL/XK
   10 FINT1=FINT1+FDUM(X)
      DO 20 I=2,I2,2
      XI=I
      X=XI*YL/XK
   20 FINT2=FINT2+FDUM(X)
      A1=FDUM(0.0)
      A2=FDUM(YL)
      FINT=(YL/(3.*XK))*(A1+4.*FINT1+2.*FINT2+A2)
      RETURN
      END

CFTLI FUNCTION FOR THETA LEFT INTEGRAL                               PCH
      FUNCTION FTLI(X)
      DIMENSION FTO(10),ECT(10),FT(10),SIGMA(10),TABAL(100),TABTL(100),
     1 TABTR(100),DISC(10),NIR(10),TABCP(200),TABW(200),TABCD(100)
      COMMON YMB,YMT,F,FO,YL,EB,XD,WCRACK,NI,IC,IBMD,IXS,DTOT,DCENT,DIM1
     1,DIM2,DIM3,DIM4,DIM5,DIM6,DIM7,DIM8,DIM9,DIM10,DISC,TABCP,TABW,EC
      W=(YMB*FM(X)-YMT)/F
      CP=FCP(W)
      T=F*(W-EC-CP+DCENT-FXB(CP))
      FTLI=T*(YL-X)/(YL*EB*FI(CP))
      RETURN
      END

CFTRI FUNCTION FOR THETA RIGHT INTEGRAL                              PCH
      FUNCTION FTRI(X)
      DIMENSION FTO(10),ECT(10),FT(10),SIGMA(10),TABAL(100),TABTL(100),
     1 TABTR(100),DISC(10),NIR(10),TABCP(200),TABW(200),TABCD(100)
      COMMON YMB,YMT,F,FO,YL,EB,XD,WCRACK,NI,IC,IBMD,IXS,DTOT,DCENT,DIM1
     1,DIM2,DIM3,DIM4,DIM5,DIM6,DIM7,DIM8,DIM9,DIM10,DISC,TABCP,TABW,EC
      W=(YMB*FM(X)-YMT)/F
      CP=FCP(W)
      T=F*(W-EC-CP+DCENT-FXB(CP))
      FTRI=T*X/(YL*EB*FI(CP))
      RETURN
      END
```

```
CFBCI FUNCTION FOR BEAM COMPRESSION INTEGRAL                          PCH
      FUNCTION FBCI(X)
      DIMENSION FTO(10),ECT(10),FT(10),SIGMA(10),TABAL(100),TABTL(100),
     1 TABTR(100),DISC(10),NIR(10),TABCP(200),TABW(200),TABCD(100)
      COMMON YMB,YMT,F,FO,YL,EB,XD,WCRACK,NI,IC,IBMD,IXS,DTOT,DCENT,DIM1
     1,DIM2,DIM3,DIM4,DIM5,DIM6,DIM7,DIM8,DIM9,DIM10,DISC,TABCP,TABW,EC
      W=(YMB*FM(X)-YMT)/F
      CP=FCP(W)
      FBCI=1./(EB*FA(CP))
      RETURN
      END


CFDI  FUNCTION FOR DEFLECTION (DELTA) INTEGRAL                        PCH
      FUNCTION FDI(X)
      DIMENSION FTO(10),ECT(10),FT(10),SIGMA(10),TABAL(100),TABTL(100),
     1 TABTR(100),DISC(10),NIR(10),TABCP(200),TABW(200),TABCD(100)
      COMMON YMB,YMT,F,FO,YL,EB,XD,WCRACK,NI,IC,IBMD,IXS,DTOT,DCENT,DIM1
     1,DIM2,DIM3,DIM4,DIM5,DIM6,DIM7,DIM8,DIM9,DIM10,DISC,TABCP,TABW,EC
      W=(YMB*FM(X)-YMT)/F
      CP=FCP(W)
      T=F*(W-EC-CP+DCENT-FXB(CP))
      G=T/(EB*FI(CP))
      IF(X-XD) 10,10,20
   10 FDI=G*X*(YL-XD)/YL
      GO TO 30
   20 FDI=G*XD*(YL-X)/YL
   30 RETURN
      END


CFM   UNIFORM BENDING MOMENT DISTRIBUTION                             PCH
      FUNCTION FM(X)
      DIMENSION FTO(10),ECT(10),FT(10),SIGMA(10),TABAL(100),TABTL(100),
     1 TABTR(100),DISC(10),NIR(10),TABCP(200),TABW(200),TABCD(100)
      COMMON YMB,YMT,F,FO,YL,EB,XD,WCRACK,NI,IC,IBMD,IXS,DTOT,DCENT,DIM1
     1,DIM2,DIM3,DIM4,DIM5,DIM6,DIM7,DIM8,DIM9,DIM10,DISC,TABCP,TABW,EC
      RULES=X
      FM=1.0
      IF(IBMD) 20,10,20
   10 WRITE OUTPUT TAPE 6,15
   15 FORMAT (38HOTERMINAL COUPLES, C , MAX MOMENT = C )
   20 RETURN
      END
```

SAMPLE INPUT

```
GLASS I BEAM WITH 6 ELASTIC TENDONS UNDER TERMINAL COUPLES,  PCH
   38.        10500.     38.        30000.     .0123        .1        50     6     3
    2.        1.33
    2.        1.33
    2.        0.
    2.        0.
    2.       -1.33
    2.       -1.33
    4.         2.         2.          .5       3.          .5
    0.         0.         0.         0.        0.          0.
     .5       30
    3.5       40
    4.        30
    4     2    3     1.         15.        .50
   25    10    5     5
```

SAMPLE OUTPUT

```
PRESTRESSED SEGMENTED I BEAM WITH ELASTIC TENDONS, PCH
DIMENSIONS - LENGTHS ARE IN INCHES, LOADS ARE IN KIPS, BENDING MOMENTS ARE IN INCH-KIPS, STRESSES + MODULI ARE IN KSI
GLASS I BEAM WITH 6 ELASTIC TENDONS UNDER TERMINAL COUPLES,  PCH
BEAM LENGTH =  38.0000 BEAM MOD =   10500.00 TENDON LENGTH =  38.0000 TENDON MOD =   30000.00 AREA PER TENDON = 0.01230
PERCENT IN-OUT DIFFERENCE IN PRESTRESS AND TENDON MOMENT IS LESS THAN OR =0.1000 NO. INCREMENTS IN INTEGRATIONS =  50
NO. OF TENDONS =  6 NO. OF REGIONS =  3
TOTAL DEPTH =  4.0000 DIST TO CENTROID =  2.0000 DIM1 =  2.0000 DIM2 =  0.5000 DIM3 =  3.0000 DIM4 =  0.5000
DIM5 =  0.     DIM6 =  0.     DIM7 =  0.     DIM8 =  0.     DIM9 =  0.     DIM10 =  0.
DISC( 1 ) =  0.5000 NIR( 1 ) =  30
DISC( 2 ) =  3.5000 NIR( 2 ) =  40
DISC( 3 ) =  4.0000 NIR( 3 ) =  30
TERMINAL COUPLES, C , MAX MOMENT = C
I BEAM AREA FUNCTION IN PROGRAM
I BEAM CENTROID FUNCTION IN PROGRAM
I BEAM MOMENT OF INERTIA FUNCTION IN PROGRAM
FLANGE WIDTH =  2.0000 FLANGE THICK =  0.5000 WEB DEPTH =  3.0000 WEB THICK =  0.5000
(APPLIED LOAD)/(MAX BEND MOMENT) =  1.000000 MAX APPLIED LOAD =  15.000000 INCREMENT IN APPLIED LOAD =  0.500000
INITIAL PRELOAD IN BEAM =  12.000000 ECCENTRICITY OF INITIAL PRELOAD =  -0.
DEFLECTIONS AT 1/ 4 POINTS ON BEAM, ROUND OFF CRACKING LOAD TO 3 SIGNIFICANT FIGURES
APPLIED BENDING MOM DIST IS SYMMETRICAL
FOR DETERMINATION OF PRELOAD AND TENDON MOMENT - MAX NO. STEPS/LOOP =25 MAX NO. LOOPS =10 MAX NO. APPLIED LOAD
INCREMENT HALVINGS = 5 MAX NO. OCCURENCES OF QUESTIONABLE OUTPUT = 5
```

WCRACK = 1.041667

	TABCP	TABW	FIRST DIFF
1	0.	1.04166666	0.
2	0.01666667	1.05029832	0.00863166
3	0.03333333	1.05883005	0.00853173
4	0.05000000	1.06725861	0.00842856
5	0.06666666	1.07558069	0.00832208
6	0.08333333	1.08379292	0.00821224
7	0.09999999	1.09189187	0.00809895
8	0.11666666	1.09987406	0.00798219
9	0.13333333	1.10773592	0.00786185
10	0.15000000	1.11547388	0.00773796
11	0.16666666	1.12308426	0.00761038
12	0.18333333	1.13056338	0.00747912
13	0.20000000	1.13790745	0.00734407
14	0.21666666	1.14511262	0.00720517
15	0.23333333	1.15217508	0.00706246
16	0.25000000	1.15909091	0.00691582
17	0.26666667	1.16585602	0.00676511
18	0.28333333	1.17246653	0.00661051
19	0.30000000	1.17891827	0.00645174
20	0.31666666	1.18520723	0.00628896
21	0.33333333	1.19132915	0.00612192
22	0.34999999	1.19727989	0.00595073
23	0.36666666	1.20305520	0.00577532
24	0.38333333	1.20865084	0.00559564
25	0.40000000	1.21406247	0.00541162
26	0.41666666	1.21928577	0.00522330
27	0.43333333	1.22431642	0.00503065
28	0.45000000	1.22914998	0.00483356
29	0.46666666	1.23378208	0.00463210
30	0.48333333	1.23820829	0.00442621
31	0.50000000	1.24242422	0.00421593
32	0.57500000	1.26084441	0.01842019
33	0.65000000	1.27911845	0.01827404
34	0.72499999	1.29724148	0.01812303
35	0.80000000	1.31520861	0.01796713
36	0.87500000	1.33301473	0.01780611
37	0.95000000	1.35065430	0.01763958
38	1.02499999	1.36812186	0.01746756
39	1.09999999	1.38541155	0.01728968
40	1.17500000	1.40251730	0.01710576
41	1.25000000	1.41943291	0.01691560
42	1.32499999	1.43615174	0.01671883
43	1.39999999	1.45266713	0.01651539
44	1.47499999	1.46897201	0.01630488
45	1.54999998	1.48505914	0.01608713
46	1.62500000	1.50092110	0.01586196
47	1.69999999	1.51655009	0.01562899
48	1.77499999	1.53193827	0.01538818
49	1.84999999	1.54707755	0.01513928
50	1.92499998	1.56195973	0.01488218

51	2.00000000	1.57657656	0.01461683
52	2.07499999	1.59091975	0.01434319
53	2.14999998	1.60498123	0.01406148
54	2.22499996	1.61875317	0.01377194
55	2.29999998	1.63222833	0.01347516
56	2.37500000	1.64540029	0.01317196
57	2.44999999	1.65826389	0.01286361
58	2.52499998	1.67081594	0.01255205
59	2.59999996	1.68305604	0.01224010
60	2.67499998	1.69498783	0.01193179
61	2.75000000	1.70662099	0.01163316
62	2.82499999	1.71797386	0.01135287
63	2.89999998	1.72907798	0.01110412
64	2.97499996	1.73998486	0.01090688
65	3.04999998	1.75077711	0.01079226
66	3.12500000	1.76158775	0.01081064
67	3.19999999	1.77263463	0.01104687
68	3.27499998	1.78428653	0.01165190
69	3.34999996	1.79720080	0.01291427
70	3.42499998	1.81264159	0.01544079
71	3.50000000	1.83333333	0.02069174
72	3.51666665	1.83888887	0.00555554
73	3.53333333	1.84444444	0.00555557
74	3.54999998	1.84999998	0.00555554
75	3.56666666	1.85555555	0.00555557
76	3.58333331	1.86111109	0.00555554
77	3.59999999	1.86666666	0.00555557
78	3.61666664	1.87222220	0.00555554
79	3.63333333	1.87777777	0.00555557
80	3.64999998	1.88333331	0.00555554
81	3.66666666	1.88888888	0.00555557
82	3.68333331	1.89444442	0.00555554
83	3.69999999	1.89999999	0.00555557
84	3.71666664	1.90555553	0.00555554
85	3.73333332	1.91111110	0.00555557
86	3.75000000	1.91666666	0.00555556
87	3.76666665	1.92222221	0.00555556
88	3.78333333	1.92777777	0.00555556
89	3.79999998	1.93333332	0.00555556
90	3.81666666	1.93888888	0.00555556
91	3.83333331	1.94444443	0.00555556
92	3.84999999	1.94999999	0.00555556
93	3.86666664	1.95555554	0.00555556
94	3.88333333	1.96111110	0.00555556
95	3.89999998	1.96666665	0.00555556
96	3.91666666	1.97222221	0.00555556
97	3.93333331	1.97777776	0.00555556
98	3.94999999	1.98333332	0.00555556
99	3.96666664	1.98888887	0.00555556
100	3.98333332	1.99444443	0.00555556
101	4.00000000	2.00000000	0.00555557

THETAO = -0.

APPLIED LOAD = 0. MAX APPLIED BEND MOM = 0. TOTAL PRELOAD IN BEAM = 12.00000000
DIFF = 12.00000000 TENDON BENDING MOM = 0. DIFF = 0. V = 0.

LEFT END ROTATION = -0. RIGHT END ROTATION = -0.

INITIAL TENDON ECCENTRICITY	TENDON FORCE	TENDON STRESS
1.33000000	2.00000000	162.60162544
1.33000000	2.00000000	162.60162544
0.	2.00000000	162.60162544
0.	2.00000000	162.60162544
-1.33000000	2.00000000	162.60162544
-1.33000000	2.00000000	162.60162544

XD/YL	DEFLECTION	CRACK PENETRATION
1 / 4	-0.	0.
2 / 4	-0.	0.

APPLIED LOAD = 12.49999988
HOLDING YMT = 0.
FIN = 12.00000000 VIN =1.04166666 FOUT = 12.00000000 DF = 0. YMTOUT = 0.42626876 VOUT =1.00614426
HOLDING F = 12.00000000
YMTIN = 0.42712300 VIN =1.00607306 YMTOUT = 0.41170317 DYMT = -0.01541983 FOUT = 12.00000000 VOUT =1.00735804
YMTIN = 0.38449612 VIN =1.00962530 YMTOUT = 0.41315681 DYMT = 0.02866068 FOUT = 12.00000000 VOUT =1.00723691
YMTIN = 0.40580956 VIN =1.00784919 YMTOUT = 0.41243005 DYMT = 0.00662048 FOUT = 12.00000000 VOUT =1.00729749
YMTIN = 0.42712300 VIN =1.00607306 YMTOUT = 0.41170317 DYMT = -0.01541983 FOUT = 12.00000000 VOUT =1.00735804
YMTIN = 0.41646627 VIN =1.00696112 YMTOUT = 0.41206664 DYMT = -0.00439963 FOUT = 12.00000000 VOUT =1.00732777
YMTIN = 0.40580955 VIN =1.00784919 YMTOUT = 0.41243005 DYMT = 0.00662049 FOUT = 12.00000000 VOUT =1.00729749
YMTIN = 0.41113791 VIN =1.00740516 YMTOUT = 0.41224831 DYMT = 0.00111040 FOUT = 12.00000000 VOUT =1.00731263
YMTIN = 0.41646627 VIN =1.00696112 YMTOUT = 0.41206664 DYMT = -0.00439963 FOUT = 12.00000000 VOUT =1.00732777
YMTIN = 0.41380209 VIN =1.00718313 YMTOUT = 0.41215742 DYMT = -0.00164467 FOUT = 12.00000000 VOUT =1.00732020
YMTIN = 0.41113790 VIN =1.00740516 YMTOUT = 0.41224831 DYMT = 0.00111040 FOUT = 12.00000000 VOUT =1.00731263
YMTIN = 0.41246999 VIN =1.00729415 YMTOUT = 0.41220295 DYMT = -0.00026704 FOUT = 12.00000000 VOUT =1.00731641

APPLIED LOAD = 12.92654479
HOLDING YMT = 0.42654495
FIN = 12.40948296 VIN =1.00729416 FOUT = 12.00000000 DF = -0.40948296 YMTOUT = 0.42626870 VOUT =1.04168966
FIN = 12.51185369 VIN =0.99905258 FOUT = 12.00000000 DF = -0.51185369 YMTOUT = 0.42626870 VOUT =1.04168966
FIN = 12.43507564 VIN =1.00522104 FOUT = 12.00000000 DF = -0.43507564 YMTOUT = 0.42626870 VOUT =1.04168966
FIN = 12.35829759 VIN =1.01146615 FOUT = 12.00000000 DF = -0.35829759 YMTOUT = 0.42626876 VOUT =1.04168966
FIN = 12.28151953 VIN =1.01778933 FOUT = 12.00000000 DF = -0.28151953 YMTOUT = 0.42626870 VOUT =1.04168966
FIN = 12.20474148 VIN =1.02419209 FOUT = 12.00000000 DF = -0.20474148 YMTOUT = 0.42626876 VOUT =1.04168966

```
FIN = 12.12796342 VIN =1.03067590 FOUT = 12.00000000 DF = -0.12796342 YMTOUT =  0.42626870 VOUT =1.04168966
FIN = 12.05118537 VIN =1.03724234 FOUT = 12.00000000 DF = -0.05118537 YMTOUT =  0.42626870 VOUT =1.04168966
FIN = 11.97440732 VIN =1.04389298 FOUT = 12.00167692 DF =  0.02726960 YMTOUT =  0.42627084 VOUT =1.04154395
FIN = 12.01279628 VIN =1.04055703 FOUT = 12.00000000 DF = -0.01279628 YMTOUT =  0.42626876 VOUT =1.04168966
FIN = 11.99360168 VIN =1.04222235 FOUT = 12.00041807 DF =  0.00681639 YMTOUT =  0.42626894 VOUT =1.04165335

APPLIED LOAD =  12.92654479    MAX APPLIED BEND MOM =  12.92654479    TOTAL PRELOAD IN BEAM =  11.99360168
DIFF = -0.00681639    TENDON BENDING MOM =  0.42654495    DIFF =  0.00027601    V =   1.04222235

LEFT END ROTATION =  0.00310203 RIGHT END ROTATION =  0.00310203

INITIAL TENDON ECCENTRICITY   TENDON FORCE        TENDON STRESS
         1.33000000                2.08026391       169.12714767
         1.33000000                2.08026391       169.12714767
         0.                        2.00013816       162.61285782
         0.                        2.00013816       162.61285782
        -1.33000000                1.92001244       156.09857178
        -1.33000000                1.92001244       156.09857178

                    XD/YL          DEFLECTION     CRACK PENETRATION
                    1 / 4      2.20981175E-02            0.001073
                    2 / 4      2.94851124E-02            0.001073
```



```
APPLIED LOAD = 13.39999986
HOLDING YMT =  0.44216783
FIN = 12.43288624 VIN =1.04222235 FOUT = 12.00043344 DF = -0.43245280 YMTOUT =  0.44188172 VOUT =1.07980417
FIN = 12.54270732 VIN =1.03309688 FOUT = 12.00000000 DF = -0.54270732 YMTOUT =  0.44188148 VOUT =1.07984319
FIN = 12.46034145 VIN =1.03992590 FOUT = 12.00000000 DF = -0.46034145 YMTOUT =  0.44188154 VOUT =1.07984319
FIN = 12.37797558 VIN =1.04684581 FOUT = 12.00405097 DF = -0.37392461 YMTOUT =  0.44189358 VOUT =1.07947777
FIN = 12.29560971 VIN =1.05385843 FOUT = 12.00960815 DF = -0.28600156 YMTOUT =  0.44194871 VOUT =1.07897367
FIN = 12.21324384 VIN =1.06096563 FOUT = 12.01534295 DF = -0.19790089 YMTOUT =  0.44205129 VOUT =1.07845016
FIN = 12.13087797 VIN =1.06816934 FOUT = 12.02126992 DF = -0.10960805 YMTOUT =  0.44220436 VOUT =1.07790570
FIN = 12.04851210 VIN =1.07547154 FOUT = 12.02740598 DF = -0.02110612 YMTOUT =  0.44241136 VOUT =1.07733858
FIN = 11.96614623 VIN =1.08287427 FOUT = 12.03377652 DF =  0.06763029 YMTOUT =  0.44267619 VOUT =1.07674624
FIN = 12.00732911 VIN =1.07916021 FOUT = 12.03057075 DF =  0.02324164 YMTOUT =  0.44253635 VOUT =1.07704479
FIN = 12.04851198 VIN =1.07547155 FOUT = 12.02740598 DF = -0.02110600 YMTOUT =  0.44241130 VOUT =1.07733858
FIN = 12.02792048 VIN =1.07731274 FOUT = 12.02898288 DF =  0.00106239 YMTOUT =  0.44247198 VOUT =1.07719231

APPLIED LOAD =  13.39999986    MAX APPLIED BEND MOM =  13.39999986    TOTAL PRELOAD IN BEAM =  12.02792048
DIFF = -0.00106239    TENDON BENDING MOM =  0.44216783    DIFF = -0.00030416    V =   1.07731274

LEFT END ROTATION =  0.00321995 RIGHT END ROTATION =  0.00321995

INITIAL TENDON ECCENTRICITY   TENDON FORCE        TENDON STRESS
```

1.33000000	2.08801302	169.75715637
1.33000000	2.08801302	169.75715637
0.	2.00484160	162.99525070
0.	2.00484160	162.99525070
-1.33000000	1.92167017	156.23334694
-1.33000000	1.92167017	156.23334694

XD/YL	DEFLECTION	CRACK PENETRATION
1 / 4	2.29380986E-02	0.070182
2 / 4	3.06058845E-02	0.070182

APPLIED LOAD = 13.89999986
HOLDING YMT = 0.45866662
FIN = 12.47672343 VIN =1.07731274 FOUT = 12.03006434 DF = -0.44665909 YMTOUT = 0.45898211 VOUT =1.11728559
FIN = 12.58892417 VIN =1.06771103 FOUT = 12.02166629 DF = -0.56725788 YMTOUT = 0.45869285 VOUT =1.11809017
FIN = 12.50477362 VIN =1.07489616 FOUT = 12.02792466 DF = -0.47684896 YMTOUT = 0.45890027 VOUT =1.11749116
FIN = 12.42062306 VIN =1.08217865 FOUT = 12.03441262 DF = -0.38621044 YMTOUT = 0.45916569 VOUT =1.11686665
FIN = 12.33647251 VIN =1.08956049 FOUT = 12.04114473 DF = -0.29532778 YMTOUT = 0.45949316 VOUT =1.11621502
FIN = 12.25232196 VIN =1.09704374 FOUT = 12.04814279 DF = -0.20417917 YMTOUT = 0.45988768 VOUT =1.11553393
FIN = 12.16817141 VIN =1.10463049 FOUT = 12.05543184 DF = -0.11273956 YMTOUT = 0.46035433 VOUT =1.11482073
FIN = 12.08402085 VIN =1.11232290 FOUT = 12.06303966 DF = -0.02098119 YMTOUT = 0.46089941 VOUT =1.11407246
FIN = 11.99987030 VIN =1.12012319 FOUT = 12.07099843 DF = 0.07112813 YMTOUT = 0.46152973 VOUT =1.11328571
FIN = 12.04194558 VIN =1.11620942 FOUT = 12.06696320 DF = 0.02501762 YMTOUT = 0.46120340 VOUT =1.11368503
FIN = 12.08402085 VIN =1.11232290 FOUT = 12.06303966 DF = -0.02098119 YMTOUT = 0.46089941 VOUT =1.11407246
FIN = 12.06298316 VIN =1.11426277 FOUT = 12.06498814 DF = 0.00200498 YMTOUT = 0.46104866 VOUT =1.11388017
HOLDING F = 12.06298316
YMTIN = 0.45866662 VIN =1.11426277 YMTOUT = 0.46104866 DYMT = 0.00238204 FOUT = 12.06498814 VOUT =1.11388017
YMTIN = 0.46691601 VIN =1.11357892 YMTOUT = 0.46071255 DYMT = -0.00620346 FOUT = 12.06426096 VOUT =1.11397518
YMTIN = 0.46279131 VIN =1.11392085 YMTOUT = 0.46088058 DYMT = -0.00191073 FOUT = 12.06462431 VOUT =1.11392769
YMTIN = 0.45866661 VIN =1.11426277 YMTOUT = 0.46104866 DYMT = 0.00238205 FOUT = 12.06498814 VOUT =1.11388017
YMTIN = 0.46072896 VIN =1.11409181 YMTOUT = 0.46096456 DYMT = 0.00023560 FOUT = 12.06480622 VOUT =1.11390394

APPLIED LOAD = 13.89999986 MAX APPLIED BEND MOM = 13.89999986 TOTAL PRELOAD IN BEAM = 12.06298316
DIFF = -0.00182307 TENDON BENDING MOM = 0.46072896 DIFF = -0.00023560 V = 1.11409181

LEFT END ROTATION = 0.00335453 RIGHT END-ROTATION = 0.00335453

INITIAL TENDON ECCENTRICITY	TENDON FORCE	TENDON STRESS
1.33000000	2.09746850	170.52589417
1.33000000	2.09746850	170.52589417
0.	2.01082101	163.48138237
0.	2.01082101	163.48138237
-1.33000000	1.92417353	156.43687248
-1.33000000	1.92417353	156.43687248

XD/YL	DEFLECTION	CRACK PENETRATION
1 / 4	2.38967717E-02	0.147023
2 / 4	3.18850246E-02	0.147023

APPLIED LOAD = 14.39999986
HOLDING YMT = 0.47730193
FIN = 12.49690342 VIN =1.11409181 FOUT = 12.06713736 DF = -0.42976606 YMTOUT = 0.47754610 VOUT =1.15374950
FIN = 12.60538340 VIN =1.10450411 FOUT = 12.05728960 DF = -0.54809380 YMTOUT = 0.47683203 VOUT =1.15475105
FIN = 12.52402329 VIN =1.11167933 FOUT = 12.06462932 DF = -0.45939398 YMTOUT = 0.47735506 VOUT =1.15400517
FIN = 12.44266319 VIN =1.11894839 FOUT = 12.07228291 DF = -0.37038028 YMTOUT = 0.47795451 VOUT =1.15322390
FIN = 12.36130309 VIN =1.12631312 FOUT = 12.08028138 DF = -0.28102171 YMTOUT = 0.47863674 VOUT =1.15240388
FIN = 12.27994299 VIN =1.13377544 FOUT = 12.08866036 DF = -0.19128263 YMTOUT = 0.47940940 VOUT =1.15154119
FIN = 12.19858289 VIN =1.14133731 FOUT = 12.09746087 DF = -0.10112202 YMTOUT = 0.48028111 VOUT =1.15063143
FIN = 12.11722279 VIN =1.14900073 FOUT = 12.10673010 DF = -0.01049268 YMTOUT = 0.48126179 VOUT =1.14966947
HOLDING F = 12.11722279
YMTIN = 0.47730193 VIN =1.14900073 YMTOUT = 0.48126179 DYMT = 0.00395985 FOUT = 12.10673010 VOUT =1.14966947
YMTIN = 0.48558842 VIN =1.14831688 YMTOUT = 0.48088384 DYMT = -0.00470459 FOUT = 12.10582471 VOUT =1.14978668
YMTIN = 0.48144518 VIN =1.14865880 YMTOUT = 0.48107272 DYMT = -0.00037245 FOUT = 12.10627711 VOUT =1.14972810

APPLIED LOAD = 14.39999986 MAX APPLIED BEND MOM = 14.39999986 TOTAL PRELOAD IN BEAM = 12.11722279
DIFF = 0.01094568 TENDON BENDING MOM = 0.48144518 DIFF = 0.00037245 V = 1.14865880

LEFT END ROTATION = 0.00350086 RIGHT END ROTATION = 0.00350086

INITIAL TENDON ECCENTRICITY	TENDON FORCE	TENDON STRESS
1.33000000	2.10801393	171.38324547
1.33000000	2.10801393	171.38324547
0.	2.01758671	164.03143883
0.	2.01758671	164.03143883
-1.33000000	1.92715952	156.67963600
-1.33000000	1.92715952	156.67963600

XD/YL	DEFLECTION	CRACK PENETRATION
1 / 4	2.49391910E-02	0.225035
2 / 4	3.32759058E-02	0.225035

APPLIED LOAD = 14.89999986

```
HOLDING YMT =  0.49816202
FIN = 12.53795946 VIN =1.14865883 FOUT = 12.10996723 DF = -0.42799222 YMTOUT =  0.49777663 VOUT =1.18928671
FIN = 12.64314353 VIN =1.13910261 FOUT = 12.09808016 DF = -0.54506338 YMTOUT =  0.49653322 VOUT =1.19055803
FIN = 12.56425536 VIN =1.14625478 FOUT = 12.10691321 DF = -0.45734215 YMTOUT =  0.49744850 VOUT =1.18961382
FIN = 12.48536718 VIN =1.15349734 FOUT = 12.11620677 DF = -0.36916041 YMTOUT =  0.49846965 VOUT =1.18861707
FIN = 12.40647900 VIN =1.16083199 FOUT = 12.12601435 DF = -0.28046465 YMTOUT =  0.49960750 VOUT =1.18756187
FIN = 12.32759082 VIN =1.16826053 FOUT = 12.13639903 DF = -0.19119179 YMTOUT =  0.50087529 VOUT =1.18644124
FIN = 12.24870265 VIN =1.17578475 FOUT = 12.14743459 DF = -0.10126805 YMTOUT =  0.50228852 VOUT =1.18524706
FIN = 12.16981447 VIN =1.18340652 FOUT = 12.15920901 DF = -0.01060545 YMTOUT =  0.50386596 VOUT =1.18396960
HOLDING F = 12.16981447
YMTIN =  0.49816202 VIN =1.18340652 YMTOUT =  0.50386596 DYMT =  0.00570393 FOUT = 12.15920901 VOUT =1.18396960
YMTIN =  0.50652044 VIN =1.18271969 YMTOUT =  0.50342512 DYMT = -0.00309531 FOUT = 12.15803313 VOUT =1.18412037
YMTIN =  0.50234122 VIN =1.18306310 YMTOUT =  0.50364536 DYMT =  0.00130414 FOUT = 12.15862060 VOUT =1.18404503
YMTIN =  0.50443082 VIN =1.18289140 YMTOUT =  0.50353521 DYMT = -0.00089561 FOUT = 12.15832675 VOUT =1.18408272
YMTIN =  0.50338601 VIN =1.18297726 YMTOUT =  0.50359023 DYMT =  0.00020421 FOUT = 12.15847361 VOUT =1.18406388

APPLIED LOAD =  14.89999986    MAX APPLIED BEND MOM =  14.89999986    TOTAL PRELOAD IN BEAM =  12.16981447
DIFF =  0.01134086    TENDON BENDING MOM =  0.50338601    DIFF = -0.00020421    V =  1.18297726

LEFT END ROTATION =  0.00366472 RIGHT END ROTATION =  0.00366472

INITIAL TENDON ECCENTRICITY   TENDON FORCE        TENDON STRESS
         1.33000000                2.12093362        172.43362808
         1.33000000                2.12093362        172.43362808
         0.                        2.02627382        164.73770905
         0.                        2.02627382        164.73770905
        -1.33000000                1.93161400        157.04178810
        -1.33000000                1.93161400        157.04178810

                    XD/YL          DEFLECTION     CRACK PENETRATION
                    1 / 4      2.61065182E-02              0.310757
                    2 / 4      3.48334488E-02              0.310757
```

APPLIED LOAD	CENTER DEFL	THETA LEFT	THETA RIGHT
0.	-0.	-0.	-0.
12.92654479	0.02948511	0.00310203	0.00310203
13.39999986	0.03060588	0.00321995	0.00321995
13.89999986	0.03188502	0.00335453	0.00335453
14.39999986	0.03327590	0.00350086	0.00350086
14.89999986	0.03483345	0.00366472	0.00366472

APPENDIX B
SELECTION OF A MODELING MATERIAL

Because a meaningful statistical treatment of test specimens demands a large number of replications, an inexpensive modeling material was required for this program. The Hydrocal gypsum cements seemed to possess all the brittle characteristics desired and could be obtained in large quantities of uniform material at a reasonable cost.

To minimize possible errors in the measurement of mechanical strength, the strongest member of the gypsum family was sought. Test specimens in the form of small rectangular beams (1/4x1/4x4 inches) were cast using the Hydrocal, Ultracal 30, and Hydrostone cements. The results of these tests are shown in Figure 42. The Hydrostone was selected as the modeling material because this group (batch A) of specimens had the highest average stress.

It was learned that the mill preparation of Hydrostone involved one ton lots only. Therefore, to achieve the desired uniformity in the base material it was arranged with the manufacturer to have the Hydrostone bagged in accordance with the following procedure.

(1) Hydrostone was processed in twelve one-ton lots.
(2) Each lot was kept separate in the plant.
(3) Two bags from each of the lots were then selected and blended to form a 2400 pound lot.
(4) This process was repeated to form ten such re-blended lots.

Following this procedure, the shipment of 230 bags of Hydrostone were rebagged and shipped to IITRI. In addition to the "A" batch, two more batches "B" and "C" were prepared from two

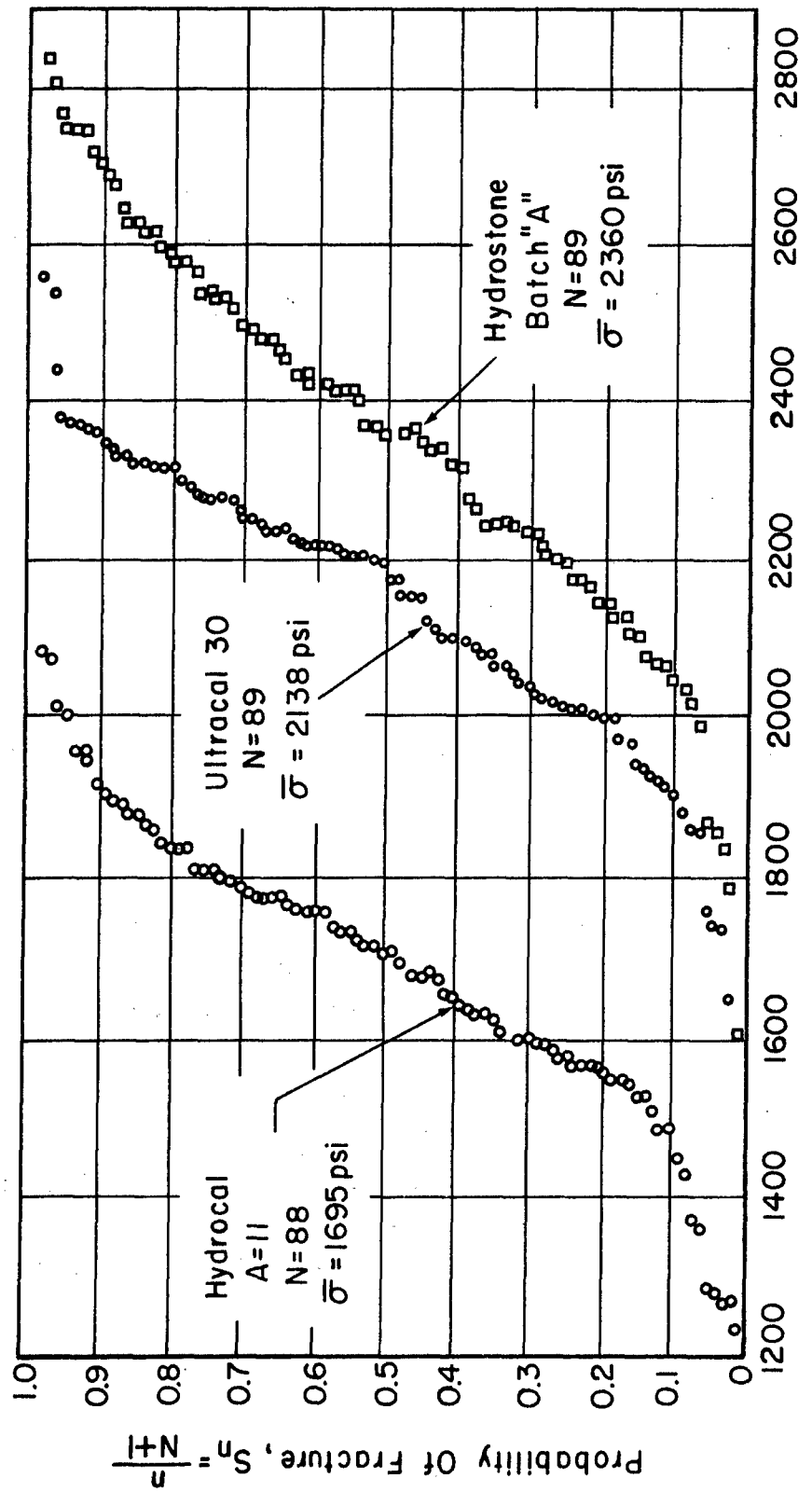

Figure 42 Distribution Curve of Fracture Stresses for 1/4 in. x 1/4 in. x 4 in. Bend Specimens of Three Gypsum Cements

different bags drawn from the Hydrostone supply. The distribution of fracture strength for these three batches are shown in Figure 43 . The small variability of fracture stress for these three batches indicate that the precautions taken to insure uniformity in the supply of Hydrostone were adequate.

The data illustrated in Figures 42 and 43 were obtained for materials mixed at maximum consistency which was desirable for strength purposes but somewhat unsatisfactory for molding purposes since the setting time was relatively short. For this reason, several mixtures of Hydrostone mixed at maximum consistency but with the addition of minute traces of sodate retarder were prepared. A wet mix working time of 1-1/2 hours was made possible by the following Hydrostone-water sodate retarder ratio:

Hydrostone (dry): water: retarder = 100:32:04. This formula was used uniformly throughout the course of all investigations reported herein.

Mold preparations and casting procedure for the Hydrostone specimens. - Various component shapes were required throughout the experimental effort. These shapes ranged from simple beams of square cross section to shapes of a somewhat more complicated geometry involving surfaces curved in two directions. The simple shapes such as the 2.5 inch x 2.5 inch x 40 inch beam and the 15 inch diameter by 5/8-inch thick plate were cast in one piece molds. The mold for the beams was constructed as a battery of five units. See Figures 44 and 45 . The complicated mold configurations as represented by the "backbone" and the ogive shell were obtained by first making master molds using wood and aluminum materials. The master molds were then used to prepare room-temperature vulcanizing rubber ship molds. These molds were in turn used as the production mold in casting the required quantity of the desired shape. See Figures 46 , 47 , and 41 .

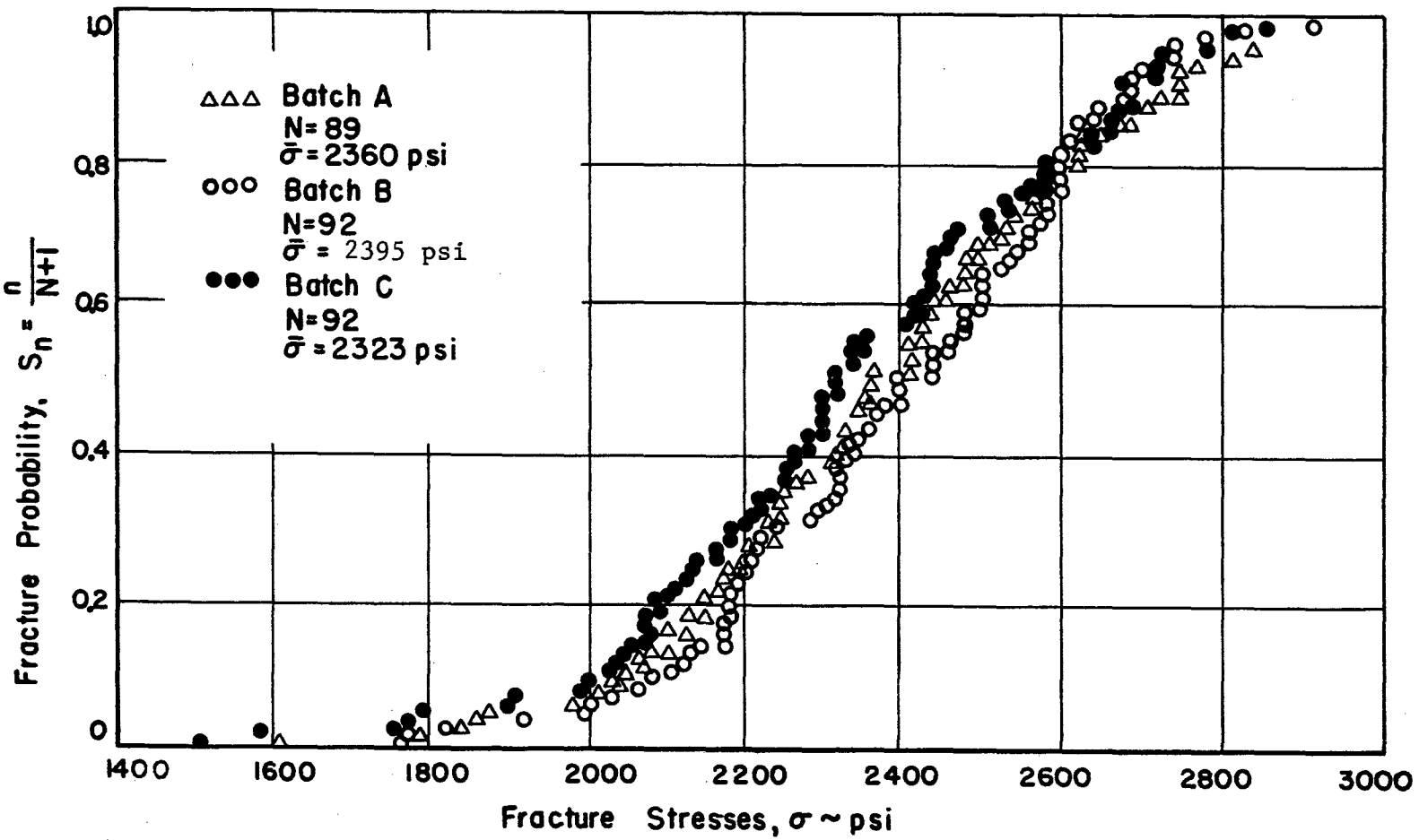

Figure 43 Distribution Curves of Fracture Stresses for Three Batches of Hydrostone Gypsum Cement

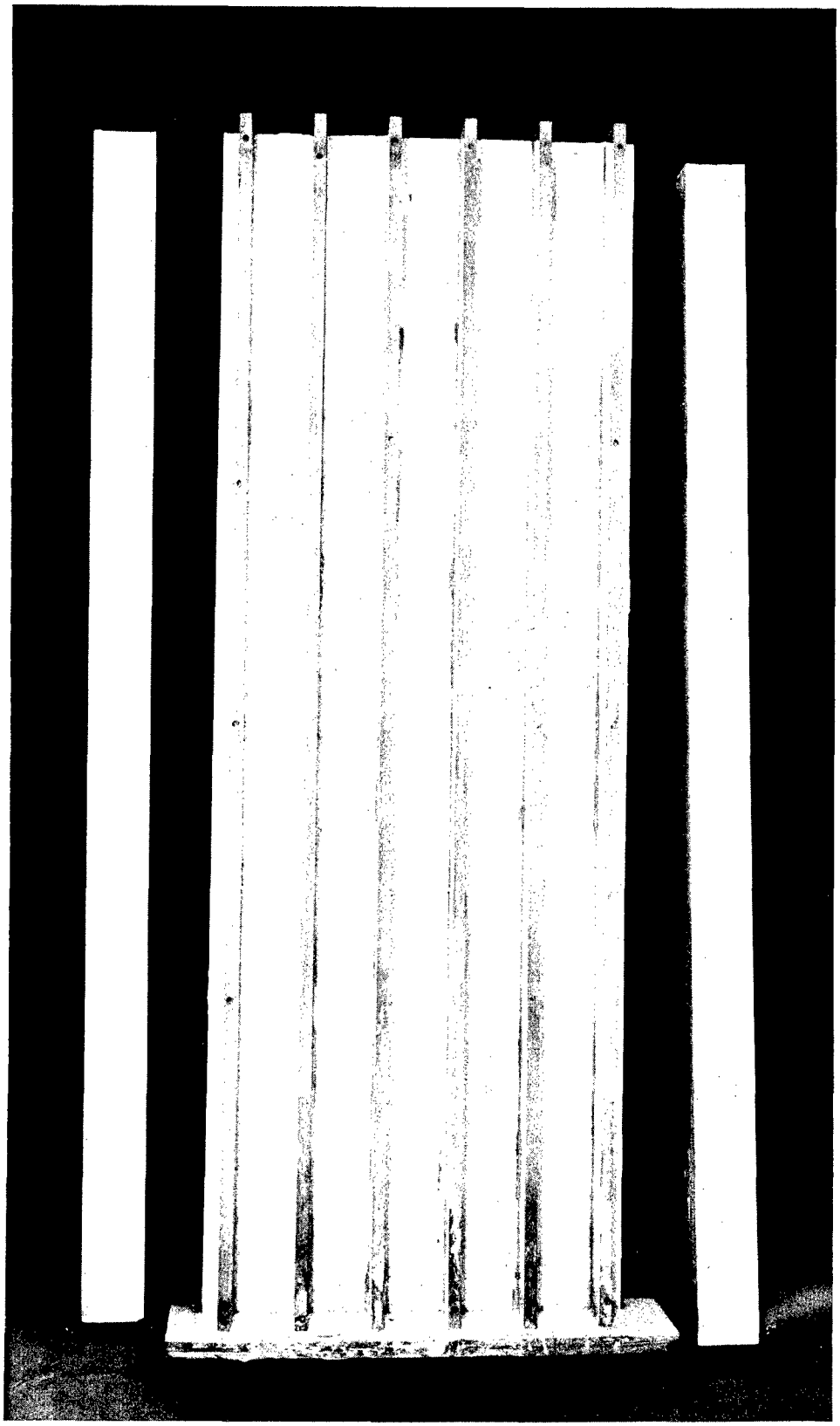

Figure 44 Example of Battery Mold for Casting Beams

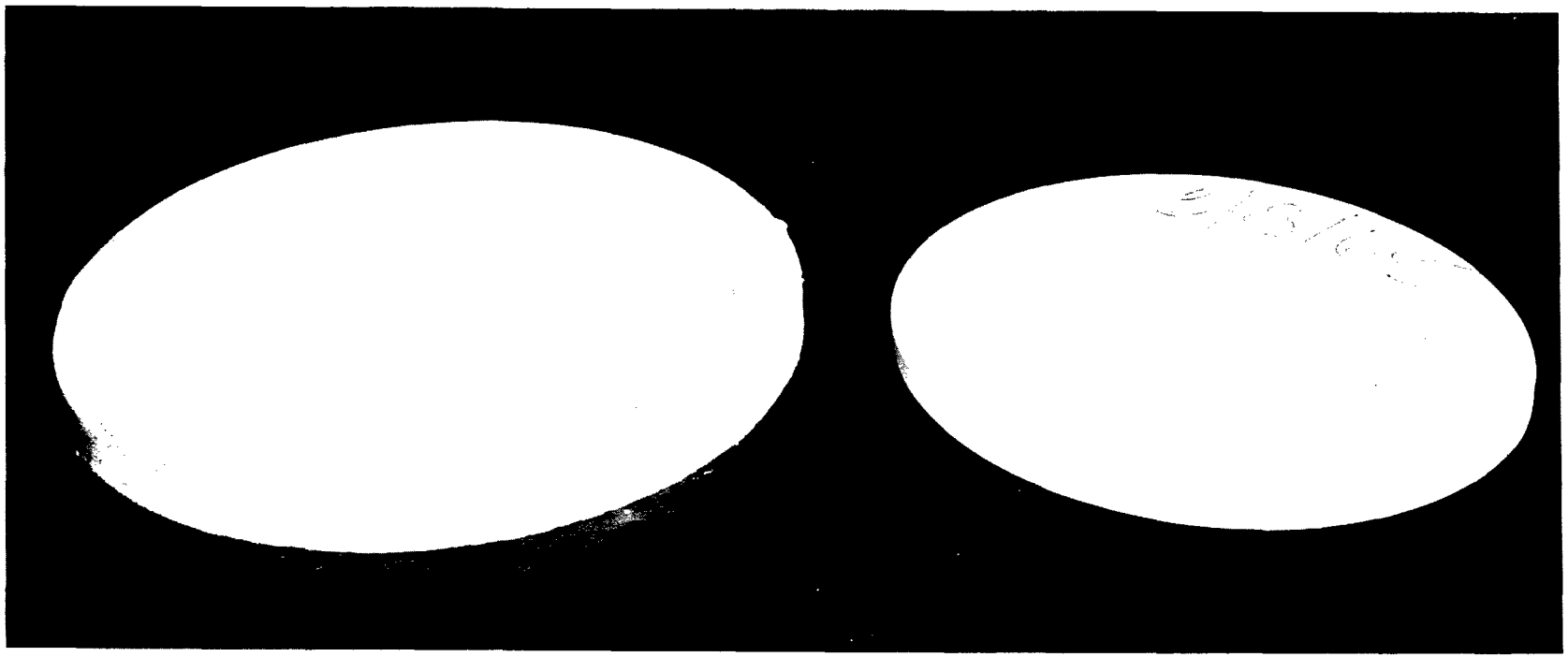

Figure 45 Example of Silastic Rubber Mold for Casting Plates

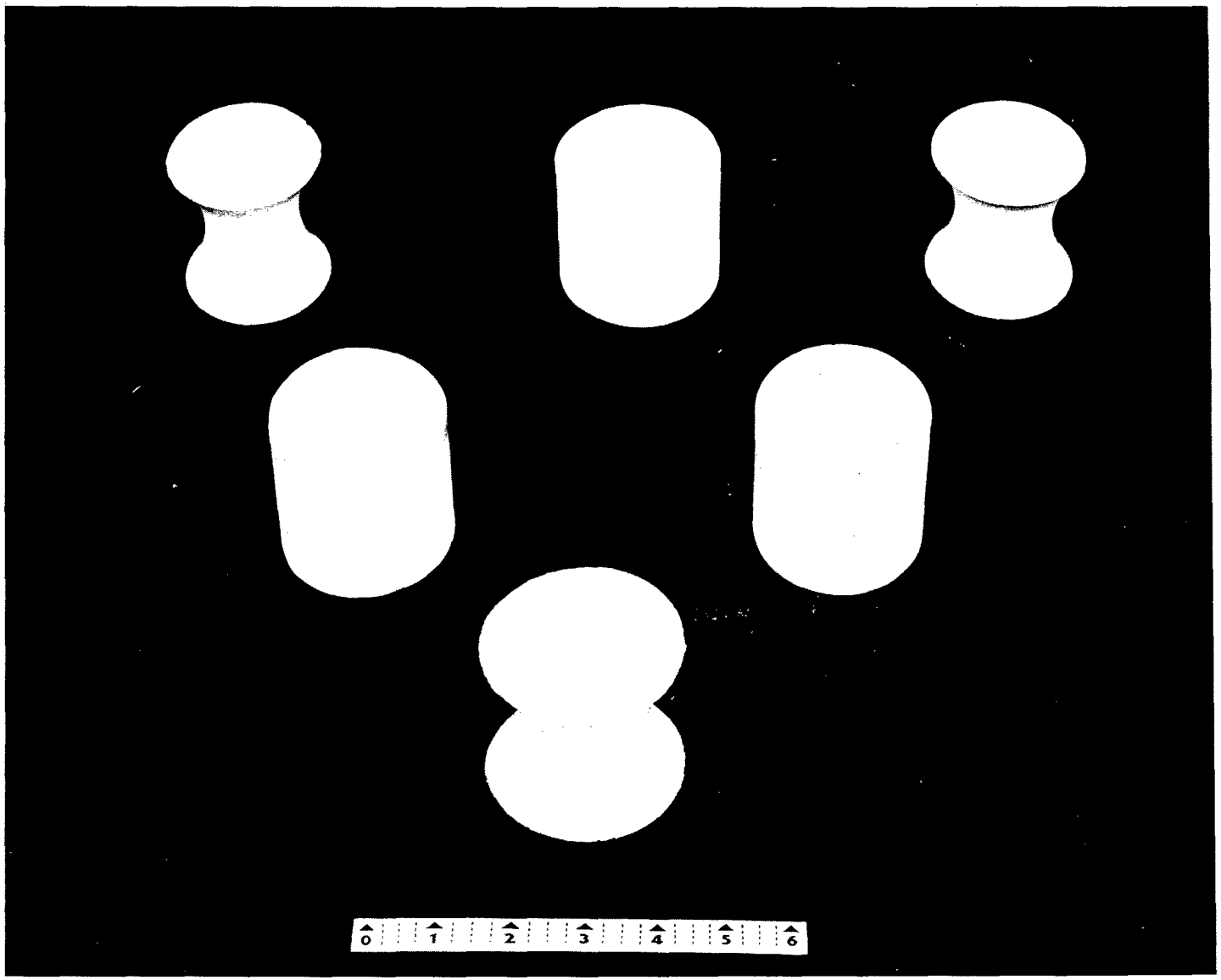

Figure 46 Example of Cylinder and Backbone Specimens

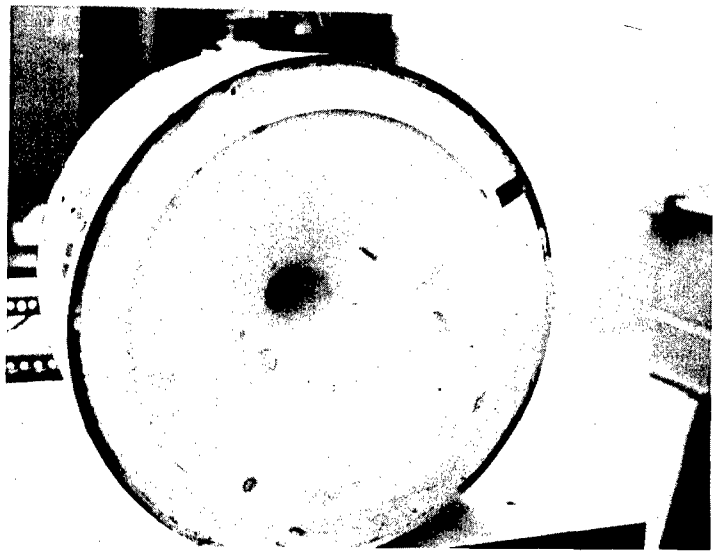

Figure 47 Ogive Shell Mold

The following casting process was used to produce consistent Hydrostone plaster test specimens; Hydrostone, water, and retarder were weighed out in the normal consistency proportions of 100:32:04. The gypsum was slowly sifted into the water and allowed to soak for about one minute. The mix was then stirred by hand for three to five minutes followed by mechanical mixing for three to four minutes. The mechanical mixing coalesced the smaller bubbles into larger bubbles which quickly came to the surface of the mix and dissipated into the air. The resulting castings were reasonably bubble free and fairly consistent in appearance from batch to batch.

Curing of Hydrostone specimens. - In order to insure uniformity among specimens with regard to strength, each specimen was cured by driving off the excess moisture in a drying oven. It was determined that in the case of the large volume beam specimens, ten hours of exposure at 104°F was sufficient to bring the specimens to constant weight. As an added margin, no specimen tested was subjected to less than 24 hours of drying time.

REFERENCES

1. Barnett, R., Hermann, P., and Costello, J., "Prestressed Monolithic and Segmented Brittle Structures," NASA Contractor Report NASA CR-113, October 1964.

2. Kooharian, A., "Limit Analysis of Voussoir (Segmental) and Concrete Arches," Jour. Am. Concrete Inst., Vol. 24, pp. 317-328, December 1952.

3. Barnett, R. L., Hofer, K. E., and Costello, J. F., "Utilization of Refractory Non-Metallic Materials in Future Aerospace Vehicles," Contract AF 33(615)-1494, Second Quarterly Report, July 1964.

4. Timoshenko, S. P., and Gere, J. M., "Theory of Elastic Stability," McGraw-Hill, 1961.

5. Hoel, P., "Introduction to Mathematical Statistics," John Wiley and Sons, Inc., New York, 2nd Ed., pp. 103, 1954.

6. Wood, R. H., "Plastic and Elastic Design of Slabs and Plates," The Ronald Press Co., New York, 1961.

NASA-Langley, 1966 CR-505